Supplementary Data

Mediterranean Marine Science
Indexed in WoS (Web of Science, ISI Thomson) and SCOPUS
www.hcmr.gr
DOI: https://doi.org/10.12681/mms.39523

Contribution to the Special Issue: Marine Animal Forest of the World (MAF WORLD)

Licence to predict – Investigating approaches to modelling low-occurrence deep-sea Irish Antipatharia with a new evaluation metric

Alexa PARIMBELLI, Mark P. JOHNSON, Kerry HOWELL, Claire LAGUIONIE MARCHAIS, and A. Louise ALLCOCK

Mediterranean Marine Science, 26, 2 (special issue) 2025

Section A

Data for species distribution modelling

Table S1. Details and source of the variable layers used in the study.

Environmental variable	Data source	Native cell size	Final resolution
Bathymetry	Data was available from Howell et al., 2022	See Table S1.1 of Howell *et al.*, 2022	200 m
Broad-scale and fine-scale bathymetric position indexes, curvature, plan and profile curvature, terrain rugosity and slope	Data was derived from bathymetry and available from Howell et al., 2022		200 m
Salinity, bottom temperature	Data was available from Howell et al., 2022	See Table S2.1 of Howell *et al.*, 2022	200 m
Ocean current velocity (horizontal and vertical components)	Data was available from Marine Institute Regional Ocean Modelling System (ROMS) 2020 annual averages (Nagy et al. 2020)	1.9 km	200 m - Resampled with nearest neighbour algorithm

Table S2. Summary of RV Celtic Explorer surveys.

Survey Name	Survey Location	ROV Dives	Depth range (m)	Survey dates
CE13008 – Biodiscovery and Ecosystem Function of Canyons	North Porcupine Bank, Whittard Canyon	16	654 – 2560	30/05/2013 – 21/06/2013
CE14009 – Ecosystem functioning and biodiscovery at Whittard Canyon	Whittard Canyon	15	605 – 2710	05/06/2014 – 21/06/2014
CE16006 – Submarine Canyon Ecosystem Services	Whittard Canyon	28	702 – 2100	29/05/2016 – 15/06/2016
CE17008 – Exploiting and Conserving Deep-Sea Genetic Resources: SFI cruise I	Hovland Mound, Gollum Channel, Belgica Mound, Whittard Canyon,	22	790 – 1830	24/05/2017 – 05/06/2017
CE18012 – Exploiting and conserving deep-sea genetic resources: SFI cruise II	North Porcupine Bank	17	960 – 2280	11/08/2018 – 23/08/2018

Table S3. Description of the morphospecies modelled in this study. The morphospecies name coincides with or contains a species/genus name because of the morphological similarity with the original species description. As the data was collected only from videos, it was impossible to confirm the taxonomy of each colony observed, making it important to underline how morphospecies, and not species, were modelled. The SMID column refers to the OTU number(s) for each morphospecies in SMarTaR-ID (Howell *et al.,* 2019).

Morphospecies	Picture	Description	SMID
Antipathes dichotoma (AD)		Has one main branch, from which whip-like secondary branches split. Branches are slightly curved towards the ends. The polyps on the branch become denser and bigger in the stem.	SM144
Bathypathes m2 (B2)		Has an upright main stem, with bilateral pinnules that are progressively shorter from the base to the top of the colony, giving it an overall oval shape. The tissue is red, the polyps have thick tentacles.	SM139
Leiopathes m1 (L1)	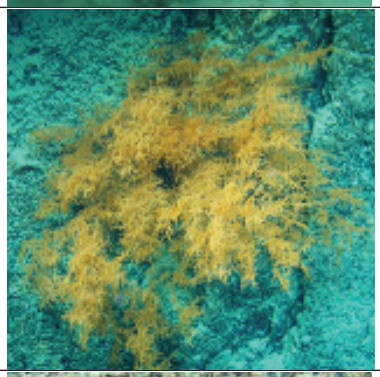	Tree-shaped coral, no pinnulation. Has very characteristic orange polyps, and the black skeleton is often visible on the main branches.	SM136 SM141 SM155
Parantipathes hirondelle (PH)		Bottlebrush coral. It has one main stem with perpendicular pinnules. The pinnules are all the same length, giving the coral a bottlebrush shape. Polyps are pink-red and grow on the pinnules.	SM133 SM181

Continued

Table 3 continued

Morphospecies	Picture	Description	SMID
Cladopathes plumosa (CP)		Similar to *P. hirondelle* but branching. The branches are straight and have a "broken" look.	SM134
Stauropathes arctica (SA)		Main branch with pinnules splitting from them with an angle of at least 70°. The branches are very close and can be fused together to form a net. The coral has an overall curved-fan shape, but some branches can be sur-imposed and give a bushy effect.	SM167
Stichopathes gravieri (SG)		Whip coral with one single line of thick, yellow polyps all oriented in one direction. The tentacles look longer than in *Antipathes dichotoma*. The main stem is coiled, giving the coral a spring-like shape.	SM130
Stichopathes m1 (S1)		Whip-like coral, straight and slightly bent at the end of the stem. The orange polyps grow in a single line; they look thin, with very little tissue covering the corallum.	SM157 SM183
Stichopathes m3 (S3)		Whip-like coral, loosely curled. The polyps are thicker than in *Stichopathes* m1, and more tissue is covering the skeleton.	SM157 SM183

Variable selection

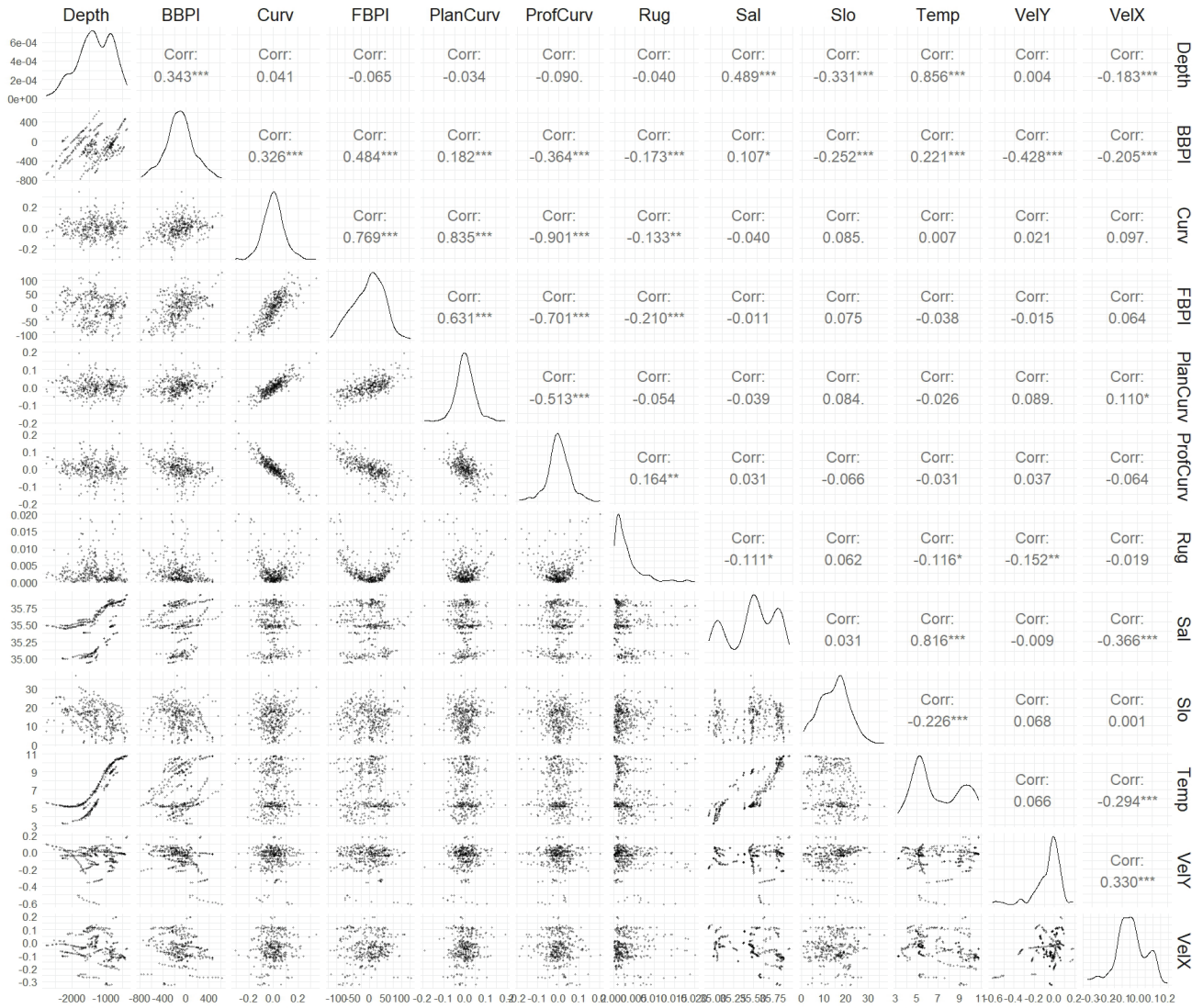

***Fig. S1**: Correlation between the environmental predictors used in the study. The asterisks indicate the statistical significance of the correlation (* $p < 0.05$; ** $p < 0.01$; *** $p < 0.001$). Highly correlated variables ($|r| > 0.7$) are highlighted in red.*

Table S4. Initial 'starting combinations' used in the models. To be able to test the contribution of all the variables in the model, all the possible combinations of non-correlated variables were created. Being temperature a more important driver than bathymetry for global cold-water coral distribution, only the combinations containing temperature were tested in the study.

	Var 1	**Var 2**	**Var 3**	**Var 4**	**Var 5**	**Var 6**	**Var7**	**Var8**
TC	BBPI	Curv	Rug	Slo	Temp	VelX	VelY	
TFP	BBPI	FBPI	PlanCurv	Rug	Slo	Temp	VelX	VelY
TPP	BBPI	PlanCurv	ProfCurv	Rug	Slo	Temp	VelX	VelY

Examples of finding the 'best' variable combination (i.e. the array of predictors that minimizes AICc) in MaxEnt and GBM models. In MaxEnt models, jackknife test of variable importance was used to identify the variable that, when used in isolation, produced the model with the lowest gain. The variable was then removed from the array, and a new model was constructed (Howell et al. 2022). The process was iterated until the model AICc did not decrease further.

In the case presented, for the model for Bathypathes m2, the Temperature-FBPI-PlanCurv combination was selected as optimal starting combination as it yields the lowest AICc. Then, rugosity, vertical velocity, horizontal velocity, temperature and slope were iteratively removed from the predictor array. Because the AICc of the model increased after removing slope, the variable was maintained in the final variable array. The variables were removing according to the gain of the model when the single predictor was used (Figure S2).

Table S5. Example of finding the best variable combination in the parsimonious MaxEnt model built for Bathypathes m2.

Variable combination	Presence	Coeff.	Log Likelihood	AIC	AICc	Variables
TC	42	31	-211.65	485.30	683.70	BBPI, Curv, Rug, Slo, Temp, VelX, VelY
TFP	42	30	-210.81	481.63	650.72	BBPI, FBPI, PlanCurv, Rug, Slo, Temp, VelX, VelY
TPP	42	35	-210.78	491.56	911.56	BBPI, PlanCurv, ProfCurv, Rug, Slo, Temp, VelX, VelY
No Rug	42	27	-212.09	478.17	586.17	BBPI, FBPI, PlanCurv, Slo, Temp, VelX, VelY
No VelY	42	22	-220.11	484.21	537.48	BBPI, FBPI, PlanCurv, Slo, Temp, VelX
No VelX	42	21	-220.22	482.44	528.64	BBPI, FBPI, PlanCurv, Slo, Temp
No Temp	42	11	-228.87	479.74	488.54	BBPI, FBPI, PlanCurv, Slo
No Slo	42	10	-234.45	484.90	489.27	BBPI, FBPI, PlanCurv

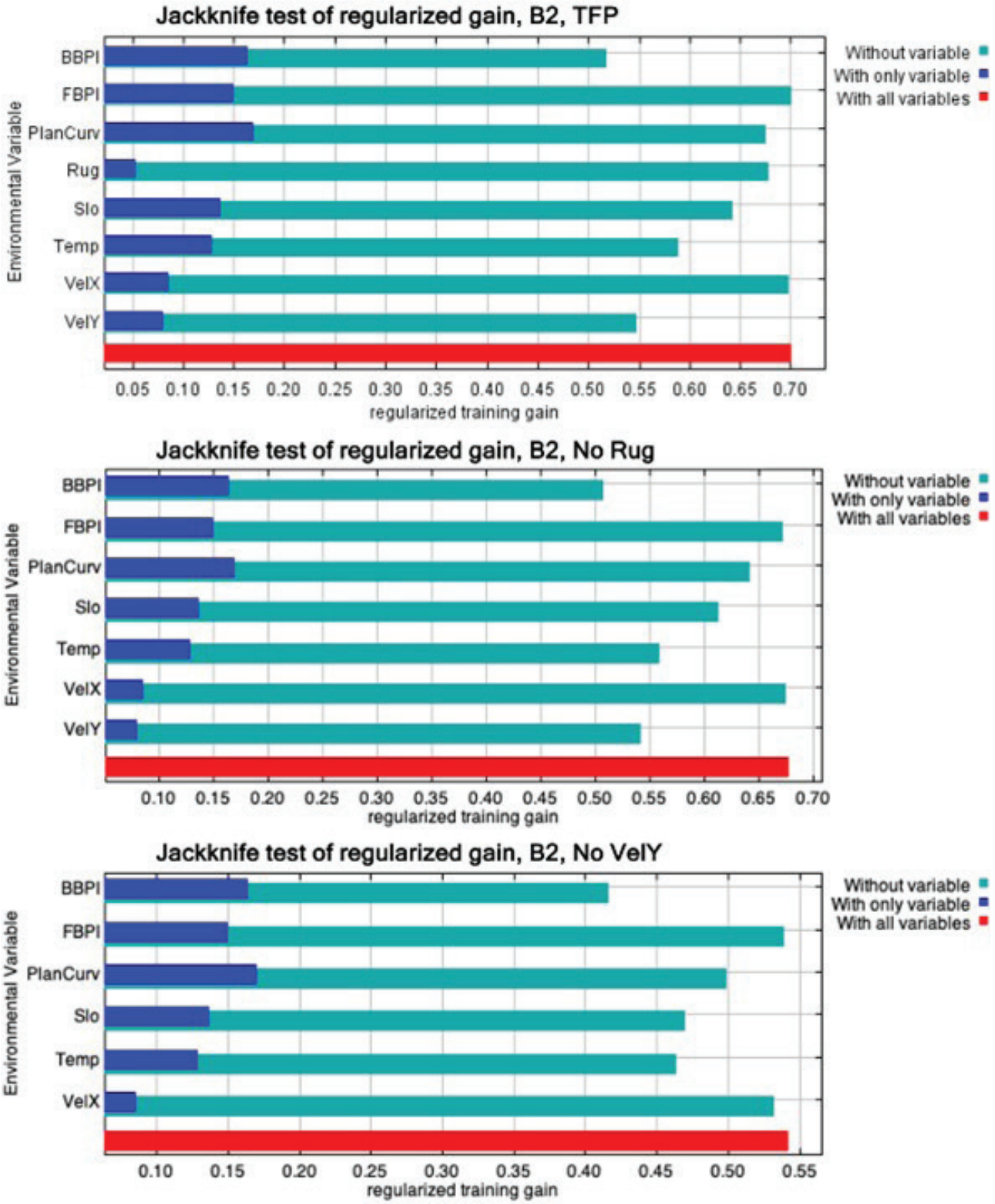

Fig. S2.1*:* Jackknife test of variable importance for each variable combination shown in Table S5.1.2. The variable to discard is the one whose individual model scores the lowest gain (dark blue line).

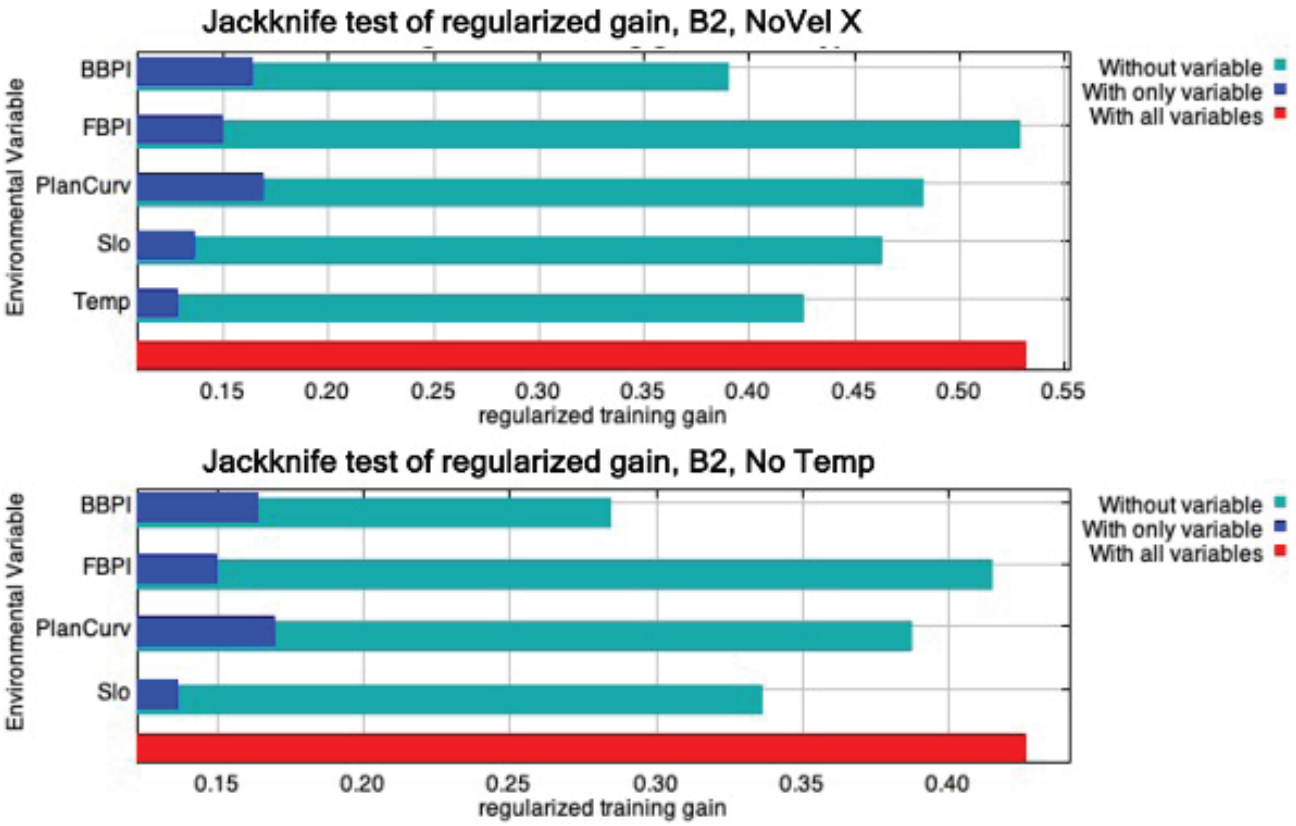

Fig. S2.2*:* Continue.

A similar method was employed for GBM models. Here, the variable importance was retrieved with the rel.inf() function of 'gbm', accessed through summary(). The value represents the relative influence of each variable, measured as the loss of model gain when the predictor is randomly permuted. In the case presented, TPP was identified as optimal starting combination. Rugosity was the variable with the smallest relative influence, therefore it was removed from the model. A second model was built, but it scored a higher AICc. Hence, all the variables in the 'TPP' combination were retained for model building.

Table S6. Example of finding the best variable combination in the parsimonious MaxEnt model built for Bathypathes m2. TC = tree complexity; Param. = number of parameters.

Variable Combination	Number of observations	Number of trees	TC	Param.	Log likelihood	AIC	AICc
TC	393	1200	2	3600	-1302.41	9804.82	1722.77
TFP	393	1000	2	3000	-1251.06	8502.13	1597.99
TPP	393	900	2	2700	-1208.37	7816.73	1497.23
No Rugosity	393	1000	2	3000	1224.867	8449.73	1545.59

Table S7. Variable importance the GBM models of table S5.1.2. Importance is defined as the gain of the model when it is built using only the variable in the Var. column.

Variable	Relative influence
Vertical velocity	18.811308
Temperature	17.915754
Plan curvature	16.765265
Slope	12.948907
Profile Curvature	11.284953
BBPI	10.316554
Horizontal velocity	6.530007
Rugosity	5.427252

Model tuning

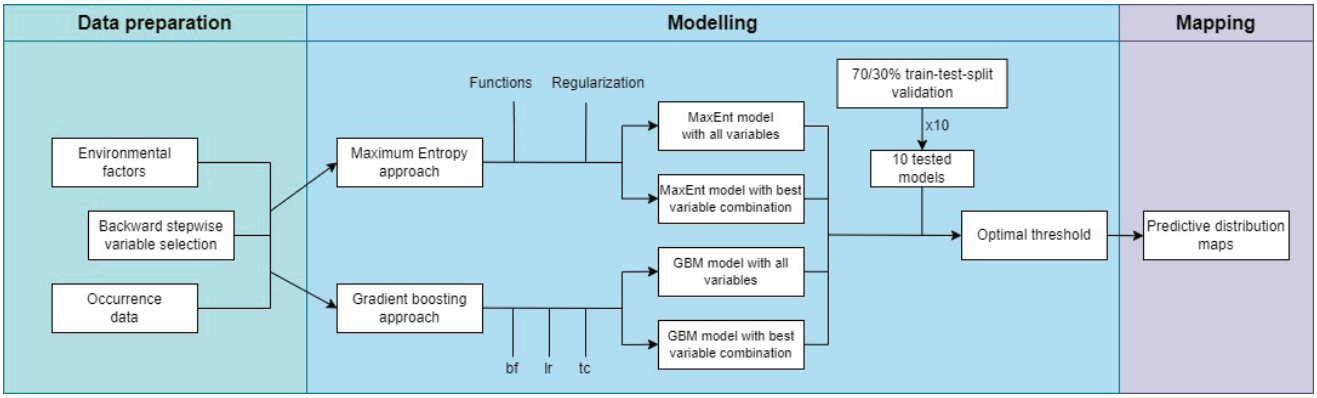

Fig. S3: Flow chart of the model building process.

To build the "best" MaxEnt model, all the possible combinations of function arrays were tested and AICc was calculated. The label "autofeature" indicates whether the features were set by the algorithm (on) or manually (off); the "no threshold" and "no hinge" labels refer to whether these functions were not included in the feature array. The 'best' feature combination was the one with the lowest absolute AICc (Table S6). When two feature combinations yielded the same AICc, the one using less features were kept.

Table S8. Example of feature tuning in MaxEnt for the morphospecies *Bathypathes* m2.

	Features	Occ.	Coefficients	Sum of logs	AIC	AICc
Auto features on	All	42	11	-228.871428	479.742857	488.542857
	No hinge	42	7	-230.956439	475.912878	479.206996
	No threshold	42	11	-228.871428	479.742857	488.542857
	No hinge, No threshold	42	7	-230.956439	475.912878	479.206996
Auto features off	All	42	15	-226.879911	483.759823	502.221361
	No hinge	42	11	-227.613437	477.226873	486.026873
	No threshold	42	17	-228.047852	490.095703	515.595703
	No hinge, No threshold	42	7	-231.457265	476.91453	480.208648

To find the optimal regularization value, we first tested the following values: 0.001, 0.01, 0.1, 1 (default), 3, 5, 7, 10 (Howell *et al.* 2022). Then, we identified the two models with the lowest AICc value, and we tested the middle regularization value. The process was iterated until the model with the lowest AICc value was found. As a rule of thumb, we decided to use maximum three decimal points.

Table S9. Example of regularization tuning in MaxEnt for the morphospecies *Bathypathes* m2.

Regularization	Presences	Coefficients	Sum of Logs	AIC	AICc
R0.001	42	8	-230.57661	477.15322	481.516856
R0.01	42	8	-230.57685	477.15369	481.517326
R0.1	42	8	-230.59653	477.193054	481.556691
R1	42	7	-231.45727	476.91453	480.208648
R3	42	5	-232.65172	475.303436	476.970103
R3.5	42	4	-232.81916	473.638323	474.719404
R4	42	4	-233.01332	474.026643	475.107724
R4.5	42	4	-233.234	474.468007	475.549088
R5	42	4	-233.48188	474.963763	476.044844
R5.5	42	3	-233.75729	473.514585	474.146164
R5.625	42	4	-233.8305	475.661005	476.742086
R5.75	42	4	-233.90542	475.810847	476.891928
R5.875	42	4	-233.98211	475.964219	477.0453
R5.938	42	4	-234.02142	476.042846	477.123927
R6	42	2	-234.06055	472.121096	472.428788
R6.063	42	4	-234.10075	476.201496	477.282577
R6.125	42	4	-234.14075	476.281495	477.362576
R6.25	42	4	-234.22271	476.445425	477.526506
R6.375	42	4	-234.30644	476.612887	477.693968
R6.5	42	2	-234.39195	472.783903	473.091596
R7	42	4	-234.7518	477.503591	478.584672
R10	42	4	-237.5231	483.046189	484.12727

Table S10. Example of modelling in GBM for the morphospecies *Antipathes dichotoma*.

Learning rate	Number of trees	Tree complexity	Bag fraction	Number of parameters	Log likelihood	AIC	AICc	Deviance	AUC	RMSE
LR_0.01	300	2	0.568	900	1240.222	4280.44	1087.92	0.334	0.959	0.223
LR_0.005	500	2	0.568	1500	1200.622	5401.24	1337.16	0.349	0.955	0.228
LR_0.001	3350	2	0.568	10050	1270.741	22641.48	1723.58	0.324	0.960	0.220
LR_0.007	500	2	0.568	1500	1285.121	5570.24	1506.16	0.321	0.961	0.219
LR_0.008	300	2	0.568	900	1184.092	4168.18	975.66	0.356	0.951	0.230
LR_0.009	350	2	0.568	1050	1256.661	4613.32	1259.07	0.331	0.958	0.222
LR_0.011	250	2	0.568	750	1233.072	3966.14	819.50	0.339	0.956	0.225
LR_0.012	250	2	0.568	750	1229.507	3959.01	812.37	0.336	0.958	0.224
LR_0.013	200	2	0.568	600	1213.183	3626.37	159.06	0.344	0.954	0.226
LR_0.014	250	2	0.568	750	1271.997	4043.99	897.35	0.322	0.963	0.219

To build the "best" model when using GBM, we selected the optimal bag fraction with gbm.bfcheck() from the 'gbm.auto' package v. 1.5.0 (Dedman *et al.*, 2017). We used gbm.step() from the 'gbm' package v.2.1.8.1 (Ridgeway, 2007) to find the optimal learning rate and number of tree combination. We tested a set array of learning rate values (0.1, 0.05, 0.01, 0.005, 0.001), identified the two models with the lowest AICc value, and tested the middle learning rate value between the two. The process was iterated until the model with the lowest AICc was found. Usually, learning rates of 0.01 and 0.05 were too high to obtain a model. In that case, if the model giving the lowest AICc was the one with learning rate of 0.01, higher learning rates were explored until it was possible to build the model and resume the iterative process. As a rule of thumb, we decided to use maximum three decimal points.

Model results and evaluation

Optimal models used in the study

Following is a list of tuned parameters for each model presented in the study. For MaxEnt models, feature selection and regularization parameter were optimised (Table 11.1); for GBM models, bag fraction, learning rate and number of trees were optimised (Table 11.2). Response curves for each optimal model are shown in figures

Table S11.1. Summary of the feature combinations and regularization parameters for MaxEnt models.

Morphospecies	Without variable selection		With variable selection	
	Feature selection	**R**	**Feature selection**	**R**
Antipathes dichotoma	autofeatures on no threshold, no hinge	10	autofeatures on no threshold, no hinge	9.875
Bathypathes m2	autofeatures on no threshold, no hinge	3	autofeatures on no threshold, no hinge	6
Leiopathes m1	autofeatures on no threshold, no hinge	5	autofeatures on no threshold	0.1
Parantipathes hirondelle	autofeatures off no threshold	0.5	autofeatures on no threshold, no hinge	2.75
Cladopathes plumosa	autofeatures off	1.25	autofeatures off	0.875
Stauropathes arctica	autofeatures on no threshold	1.188	autofeatures off no threshold	1
Stichopathes gravieri	autofeatures on no threshold, no hinge	10	autofeatures on no threshold, no hinge	6
Stichopathes m1	autofeatures off	1	autofeatures on no threshold, no hinge	6
Stichopathes m3	autofeatures on no threshold, no hinge	4.5	autofeatures on no threshold, no hinge	2.625

Table 11.2. Summary of tree complexity (tc), learning rate (lr), bag fraction (bf) and number of trees for GBM models.

Morphotypes	Without variable selection				With variable selection			
	tc	lr	bf	number of trees	tc	lr	bf	number of trees
Antipathes dichotoma	2	0.013	0.568	200	2	0.016	0.568	200
Bathypathes m2	2	0.026	0.5	200	2	0.015	0.5	350
Leiopathes m1	2	0.009	0.362	450	2	0.013	0.362	350
Parantipathes hirondelle	2	0.009	0.6	600	2	0.015	0.6	200
Cladopathes plumosa	2	0.007	1	700	2	0.01	1	600
Stauropathes arctica	2	0.016	0.778	250	2	0.018	0.778	200
Stichopathes gravieri	2	0.002	0.328	2000	2	0.037	0.328	200
Stichopathes m1	2	0.005	0.75	1300	2	0.013	0.75	750
Stichopathes m3	2	0.020	0.467	200	2	0.005	0.467	1200

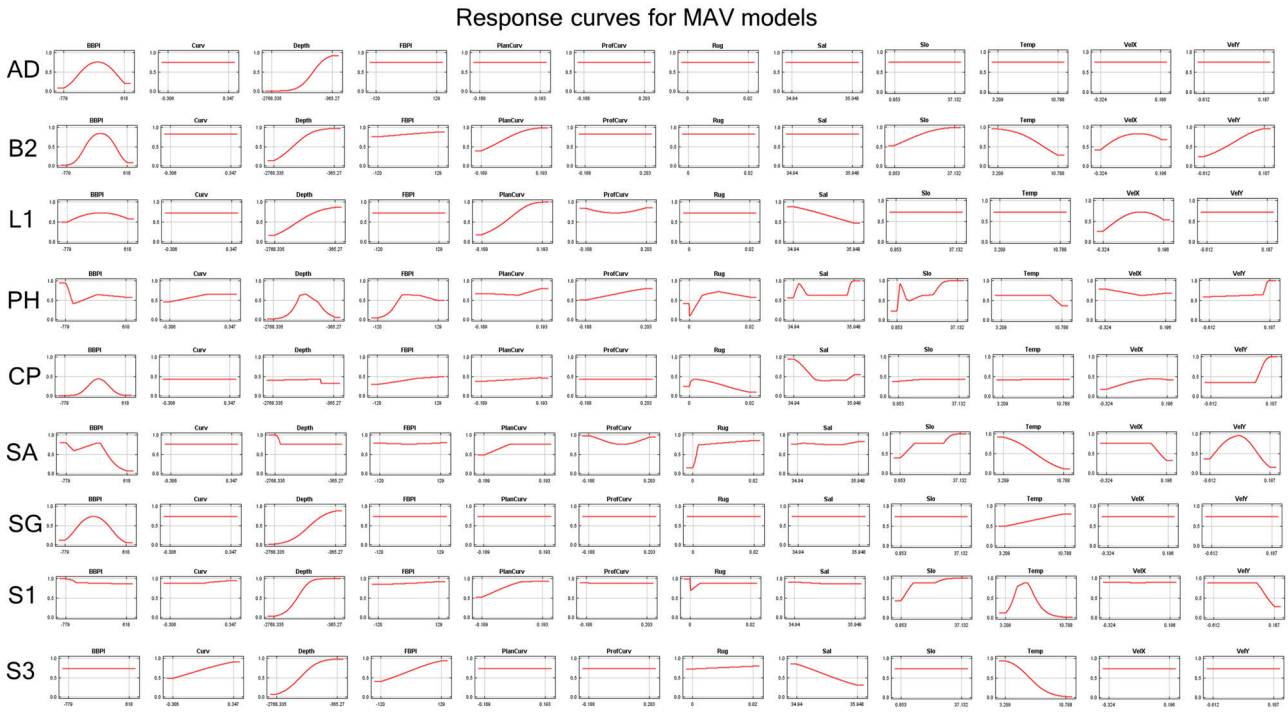

Fig. S4.1: Response curves of the optimal MaxEnt models, built using all the available predictors.

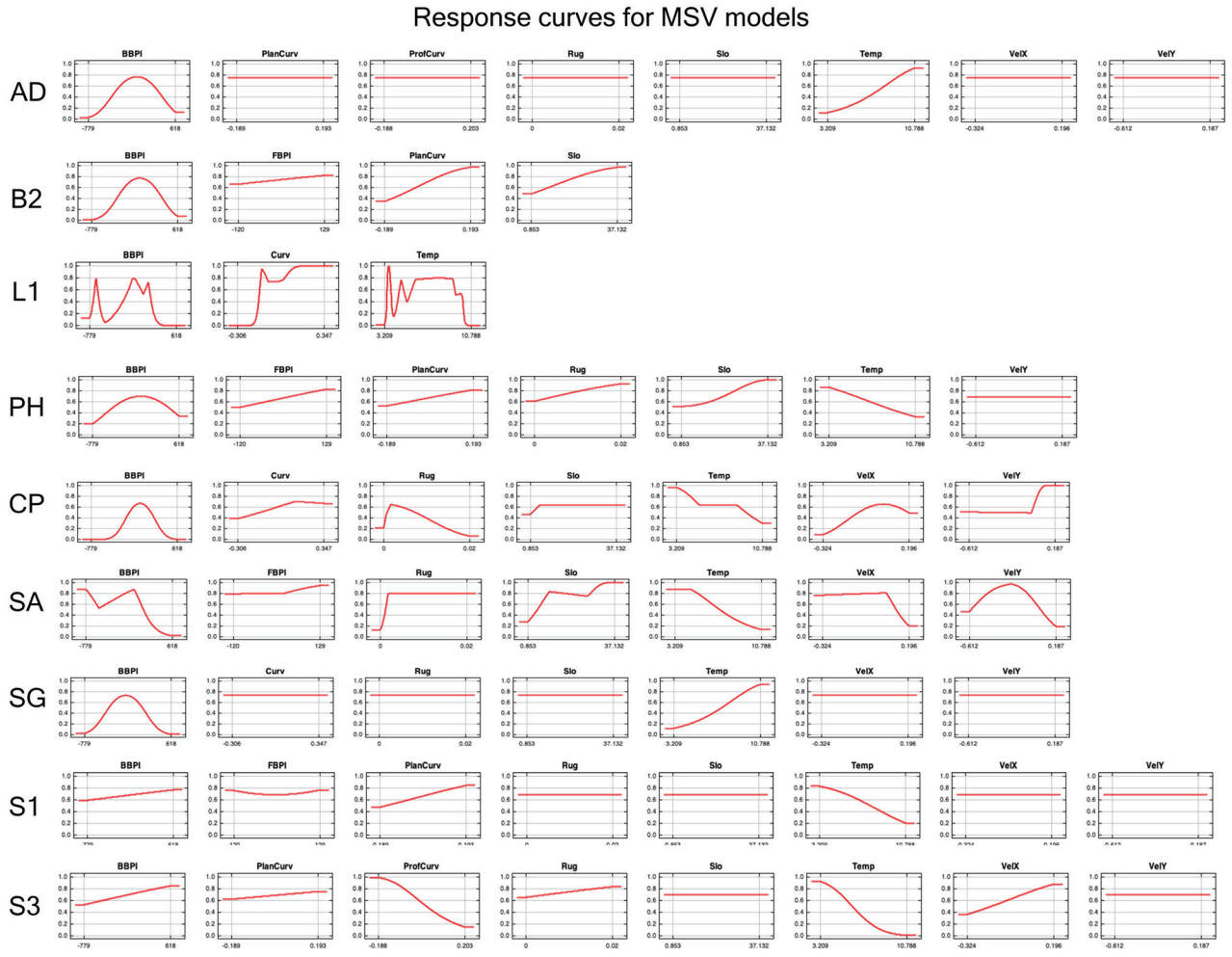

Fig. S4.2: Response curves of the optimal MaxEnt models, built using backwards stepwise pre-selected predictors.

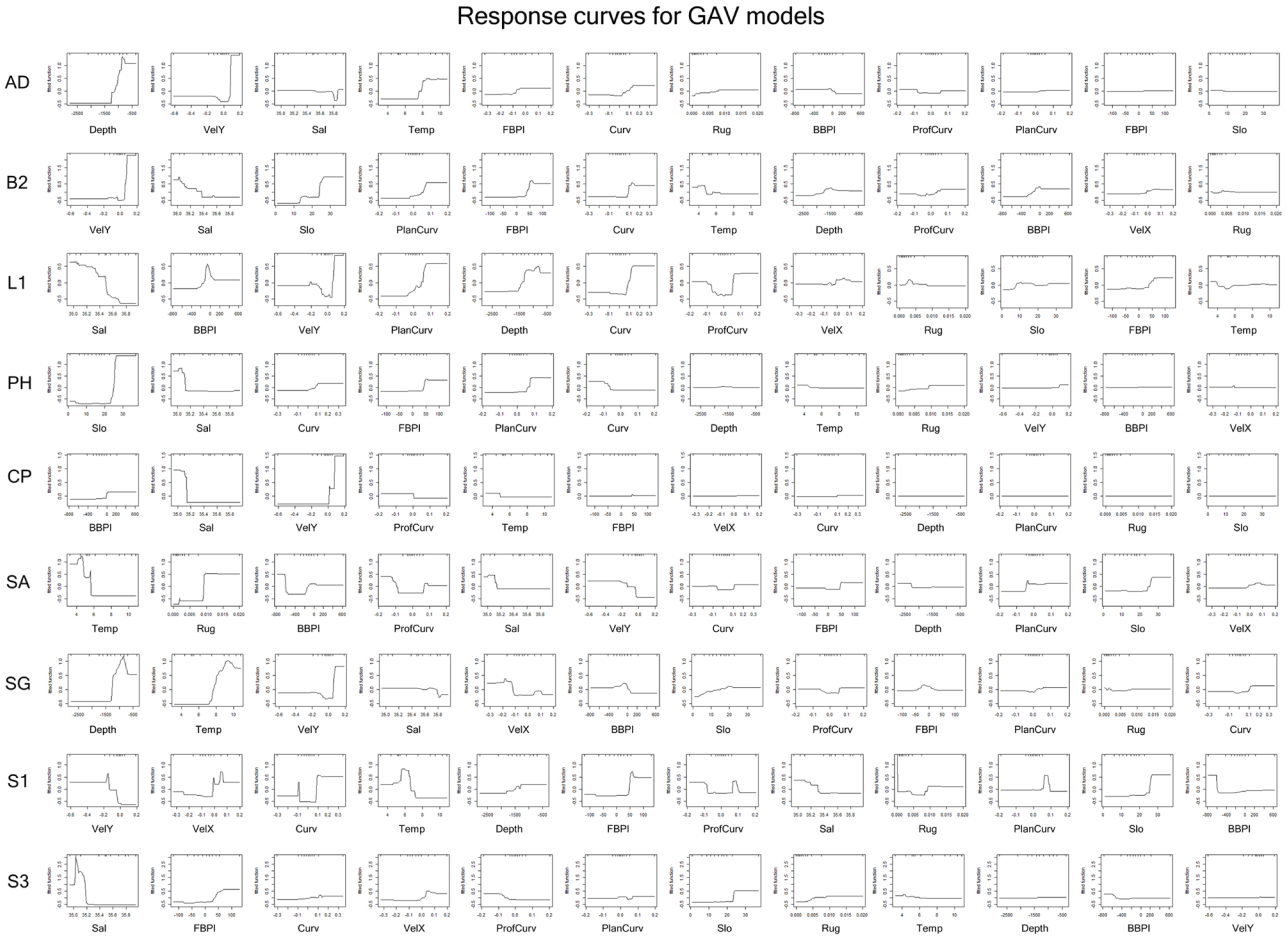

Fig. S4.3: Response curves of the optimal gradient boosting models, built using all the available predictors.

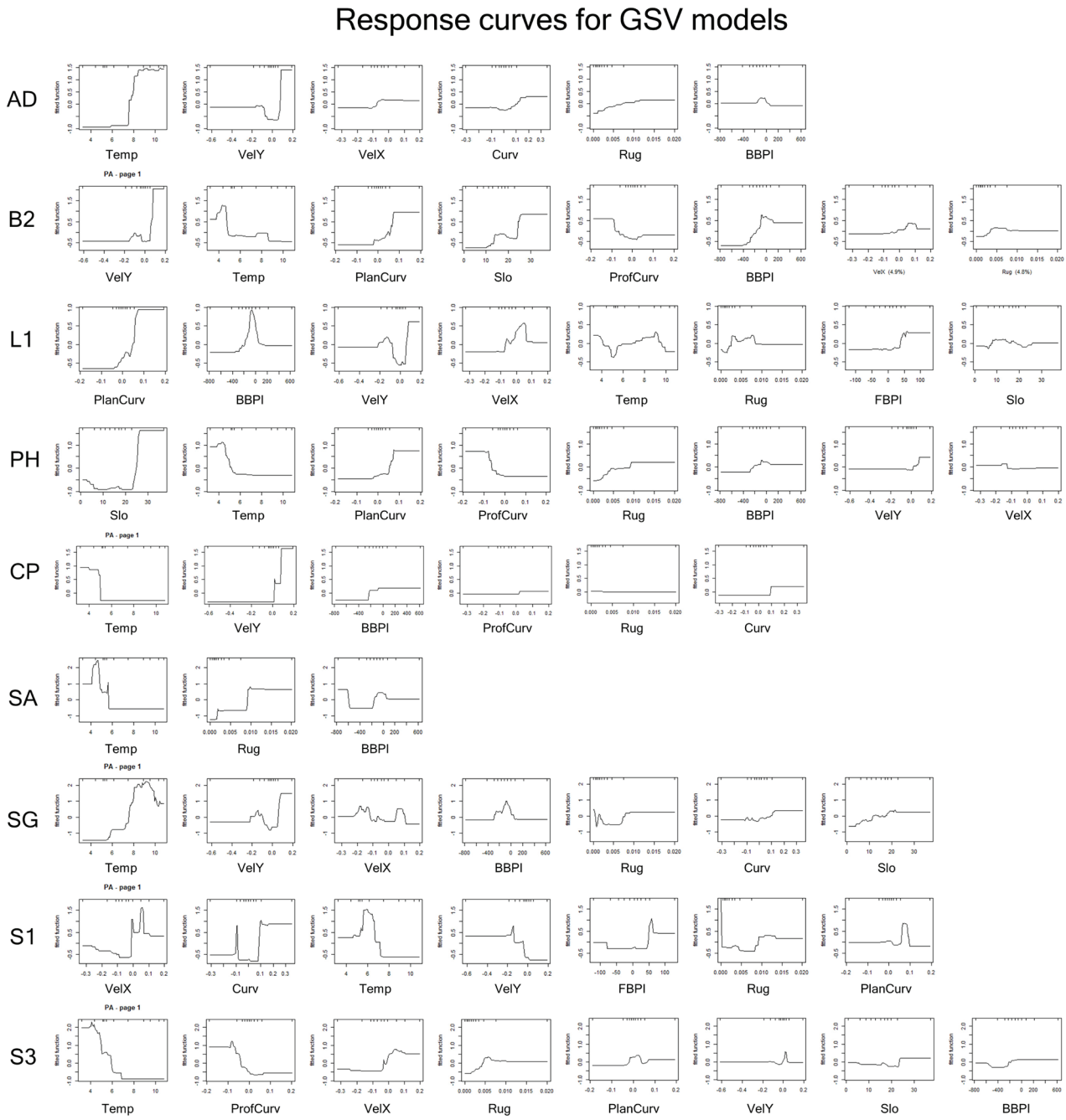

Fig. S4.4: Response curves of the optimal gradient boosting models, built using backwards stepwise pre-selected predictors.

Choosing the optimal thresholding methods

Maximization of sensitivity-specificity sum was selected as the optimal thresholding method in eighteen out of 36 models (Table S12), followed by maximization of kappa statistics (fifteen models, selected together with predicted-observed prevalence equality for the GBM model with no variable preselection of *Stichopathes* m1), and predicted-observed prevalence equality (three models).

Threshold for MaxEnt models ranged from 0.49 to 0.77. while thresholds for GBM models ranged from 0.02 to 0.47. This discrepancy is likely due to the distribution of the predicted probability of species occurrence, which tended to be lower in GBM than in MaxEnt (see Figure S5).

Table S12. Thresholding methods and threshold values selected for the nine morphotypes for the different species distribution model methods. MaxKappa: maximization of kappa statistics; MaxSensSpec: maximization of sensitivity-specificity sum; PredPrev=Obs: predicted-observed prevalence equality. The values used in the study are selected.

Morphospecies	MAV	MSV	GAV	GSV
Antipathes dichotoma	0.70 MaxKappa	0.41 MaxSensSpec	0.12 MaxSensSpec	0.19 MaxSensSpec
Bathypathes m2	0.71 MaxSensSpec	0.76 MaxKappa	0.31 PredPrev=Obs	0.18 MaxSensSpec
Leiopathes m1	0.72 MaxKappa	0.64 MaxKappa	0.29 PredPrev=Obs	0.305 MaxKappa
Parantipathes hirondelle	0.39 MaxSensSpec	0.75 MaxKappa	0.12 MaxSensSpec	0.245 MaxKappa
Cladopathes plumosa	0.77 MaxKappa	0.57 MaxSensSpec	0.13 MaxKappa	0.07 MaxSensSpec
Stauropathes arctica	0.58 MaxSensSpec	0.645 MaxSensSpec	0.23 PredPrev=Obs	0.12 MaxSensSpec
Stichopathes gravieri	0.57 MaxKappa	0.49 MaxSensSpec	0.47 MaxKappa	0.41 MaxKappa
Stichopathes m1	0.61 MaxKappa	0.6 MaxSensSpec	0.21 MaxKappa PredPrev=Obs	0.215 MaxKappa
Stichopathes m3	0.565 MaxSensSpec	0.49 MaxSensSpec	0.37 MaxKappa	0.02 MaxSensSpec

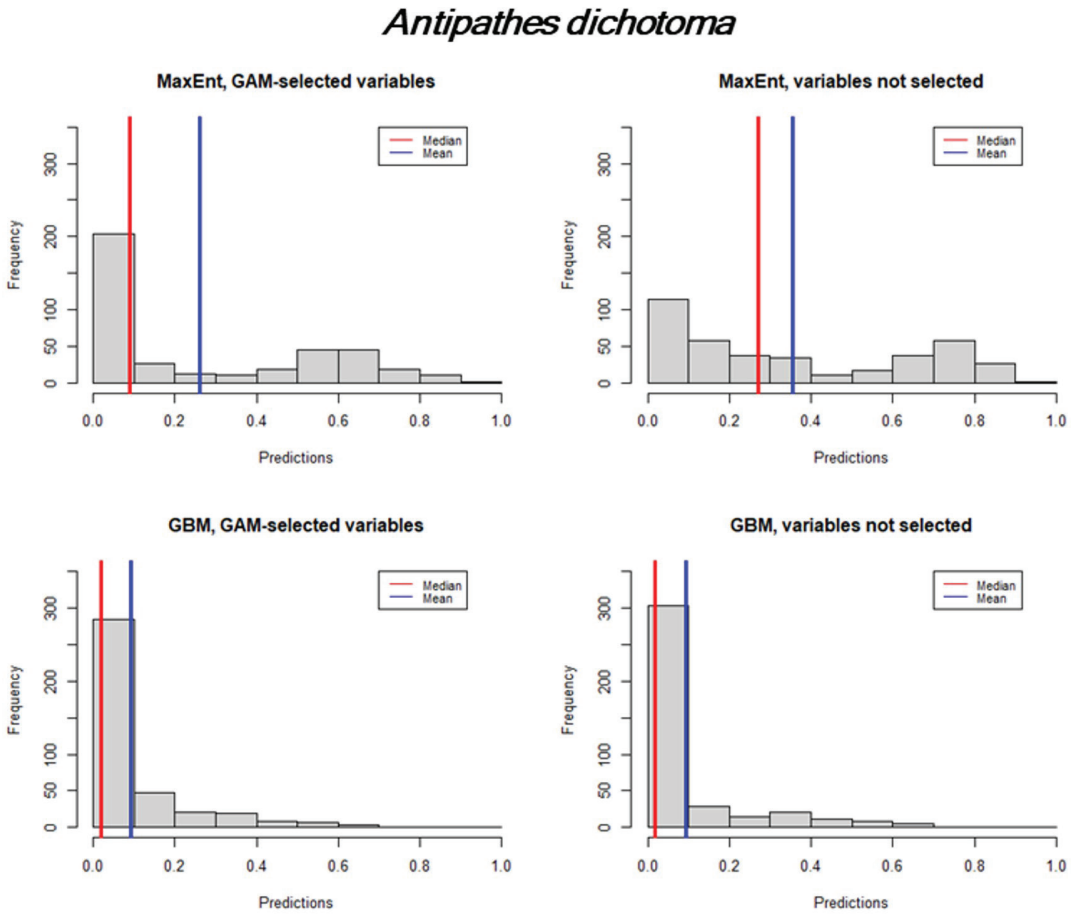

Fig. S5.1: Histograms showing the difference in the distribution of predicted occurrence probabilities between GBM and MaxEnt models built using all predictors and backward stepwise selected variables. Results are shown for each modelled morphospecies and are inclusive of mean (blue) and median (red) lines.

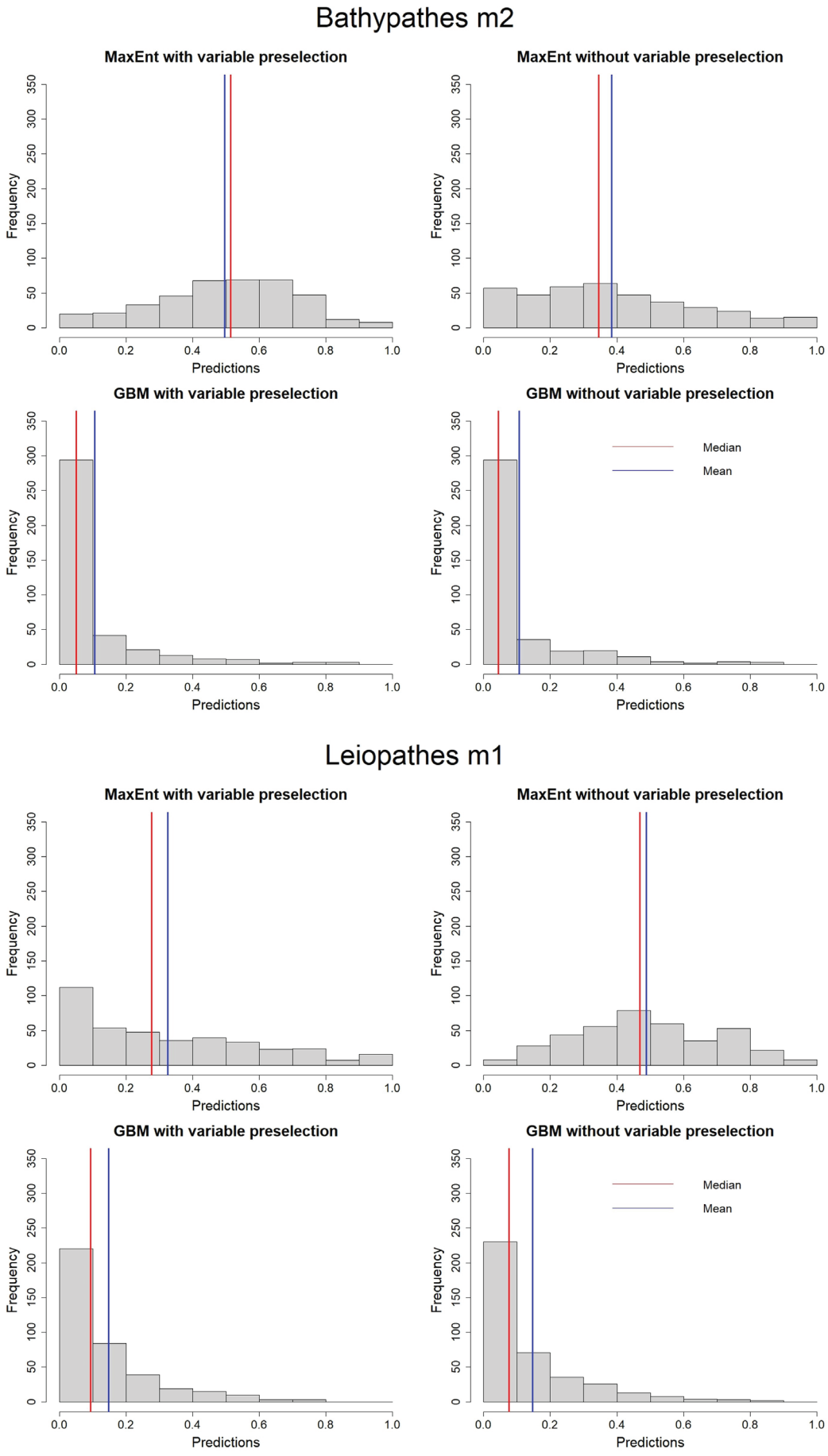

Fig. S5.2: Continue.

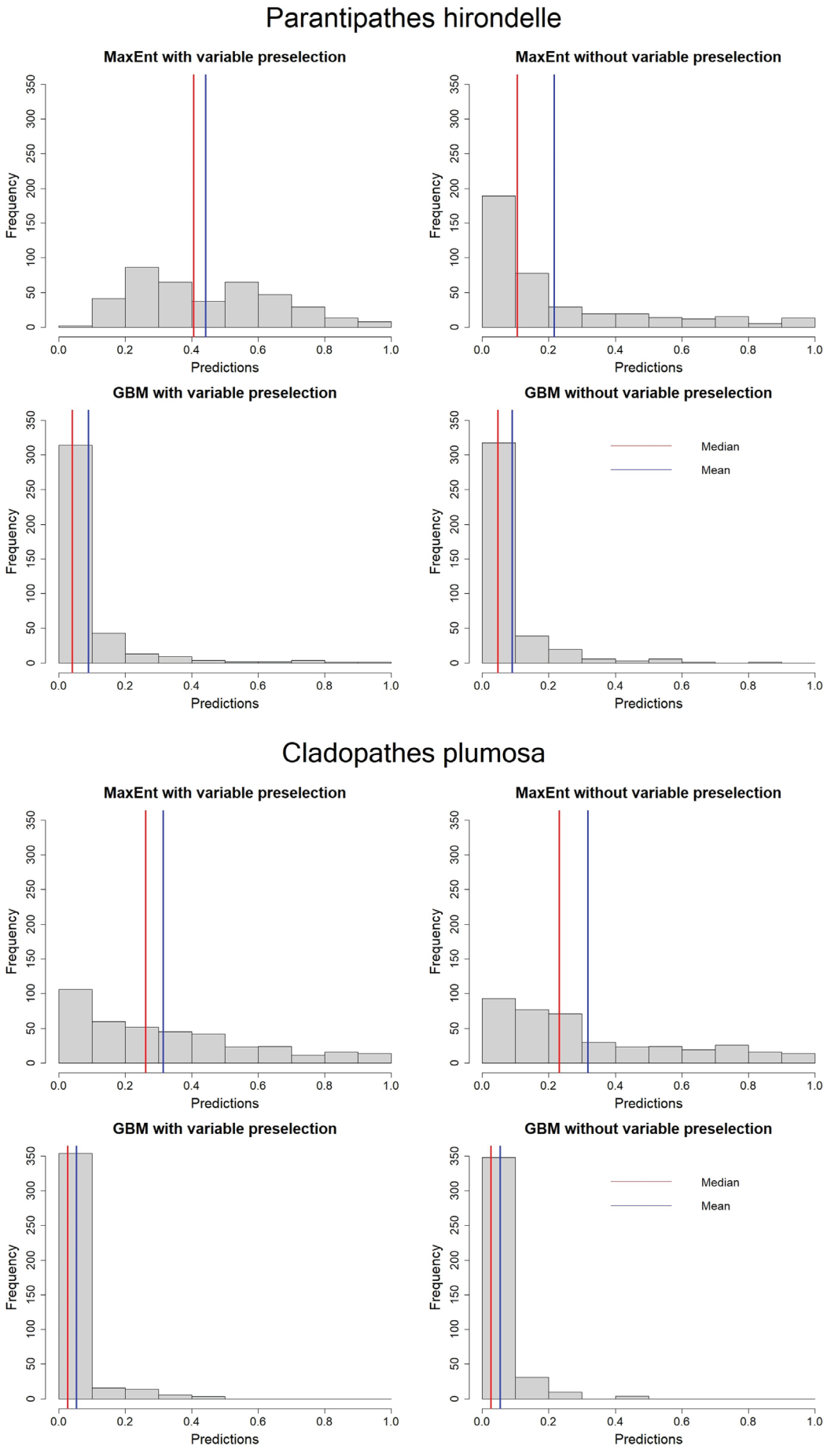

Fig. S5.3: Continue.

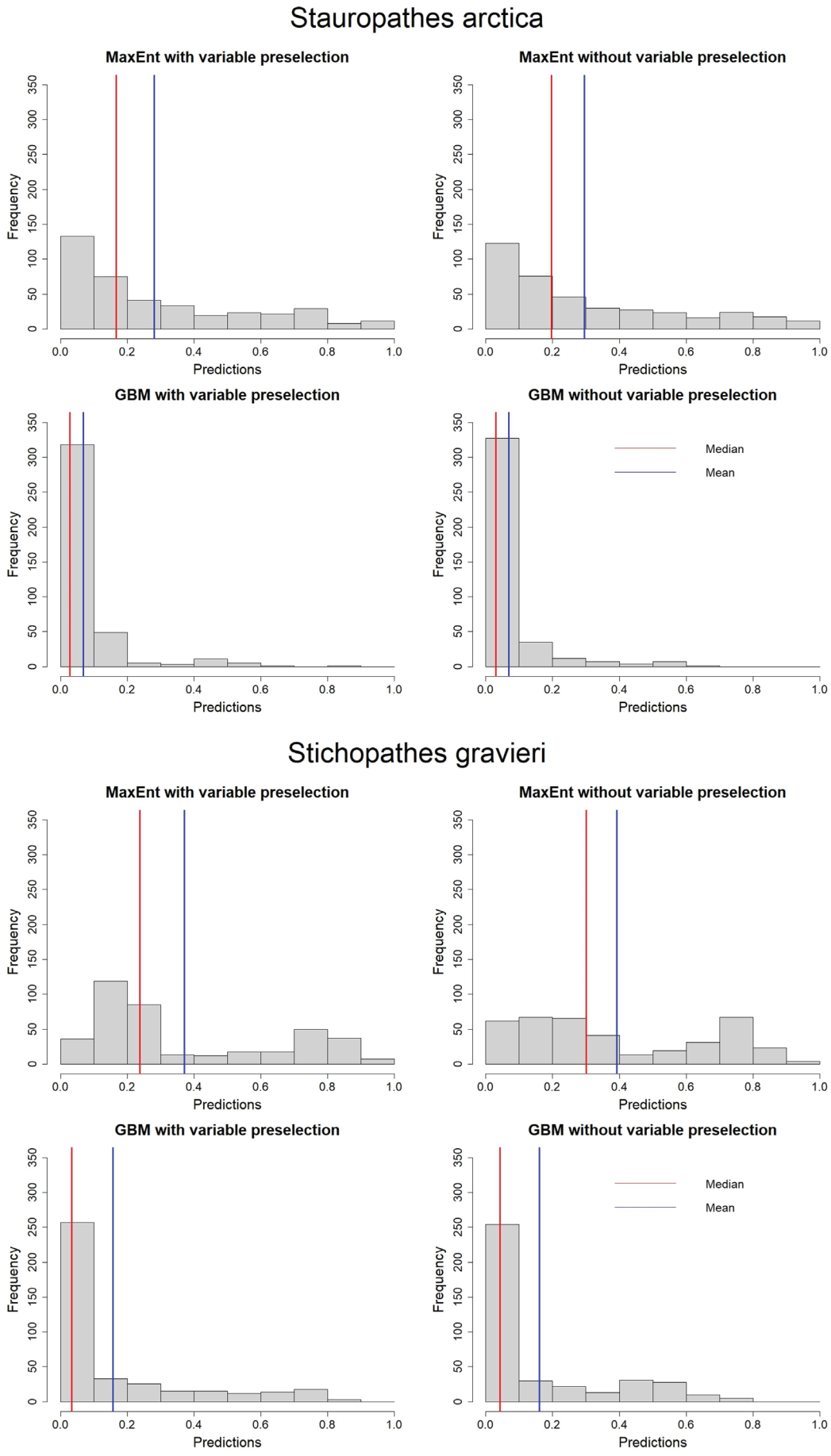

Fig. S5.4: Continue.

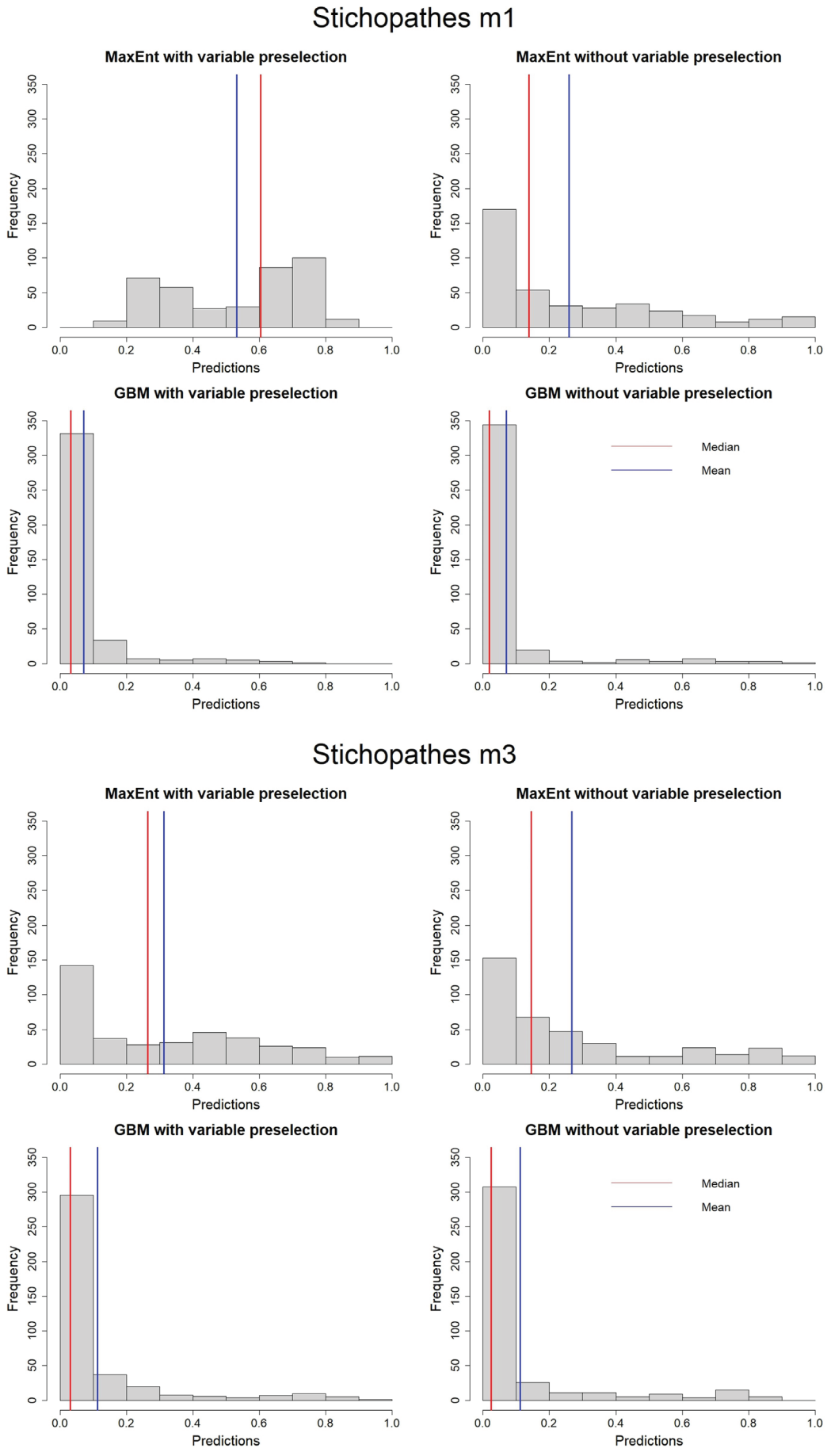

Fig. S5.5: Continue.

Ridgeline plots

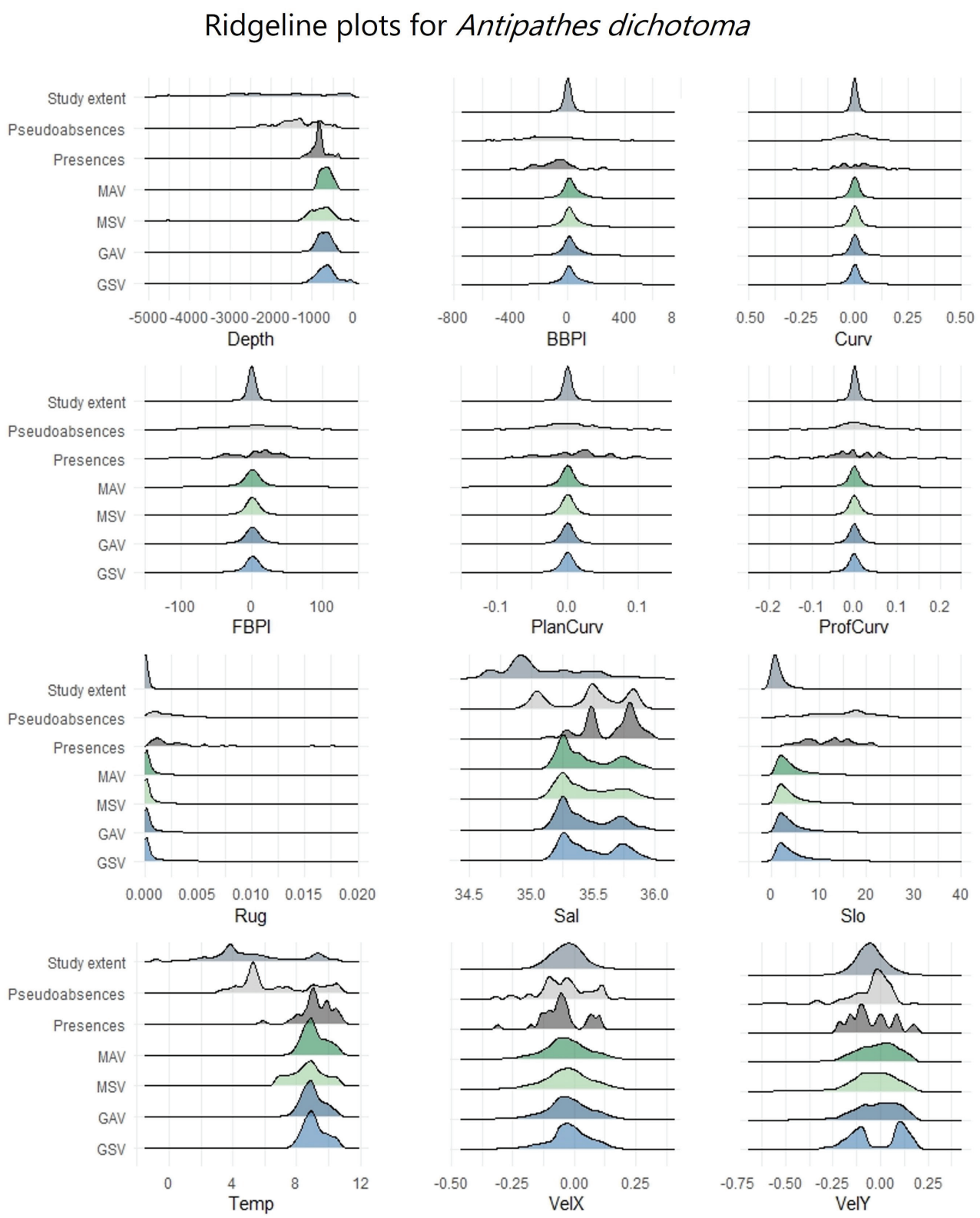

Fig. S6.1: For each predictor, the ridgeline plots show their distribution across the full extent of the study, presences, pseudoabsences, and thresholded probability values produced by MaxEnt models with all variables (MAV), MaxEnt models with pre-selected variables (MSV), MaxEnt models with all variables (GAV), MaxEnt models with pre-selected variables (GSV), masked for novel climates.

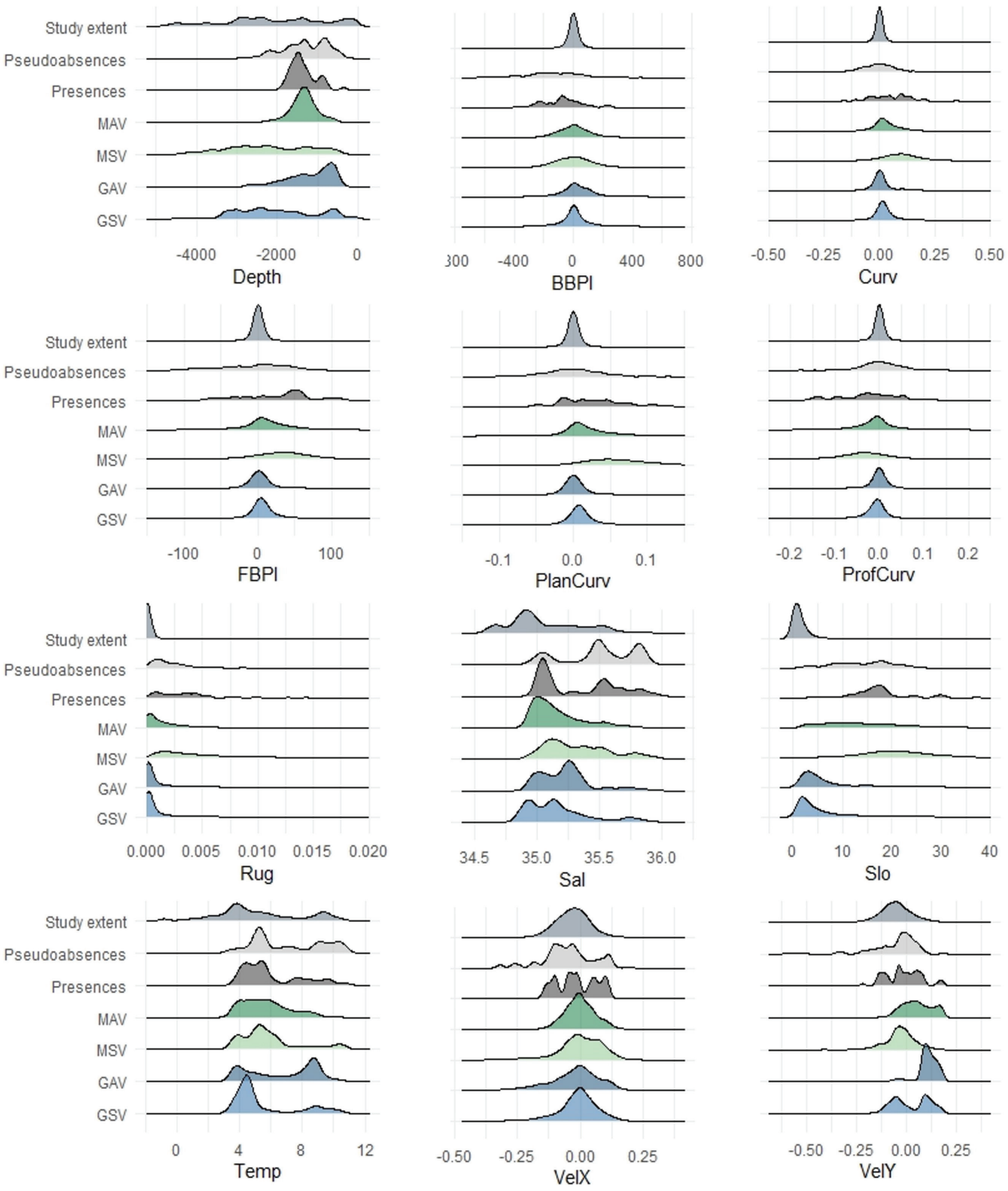

Fig. S6.2: Continue.

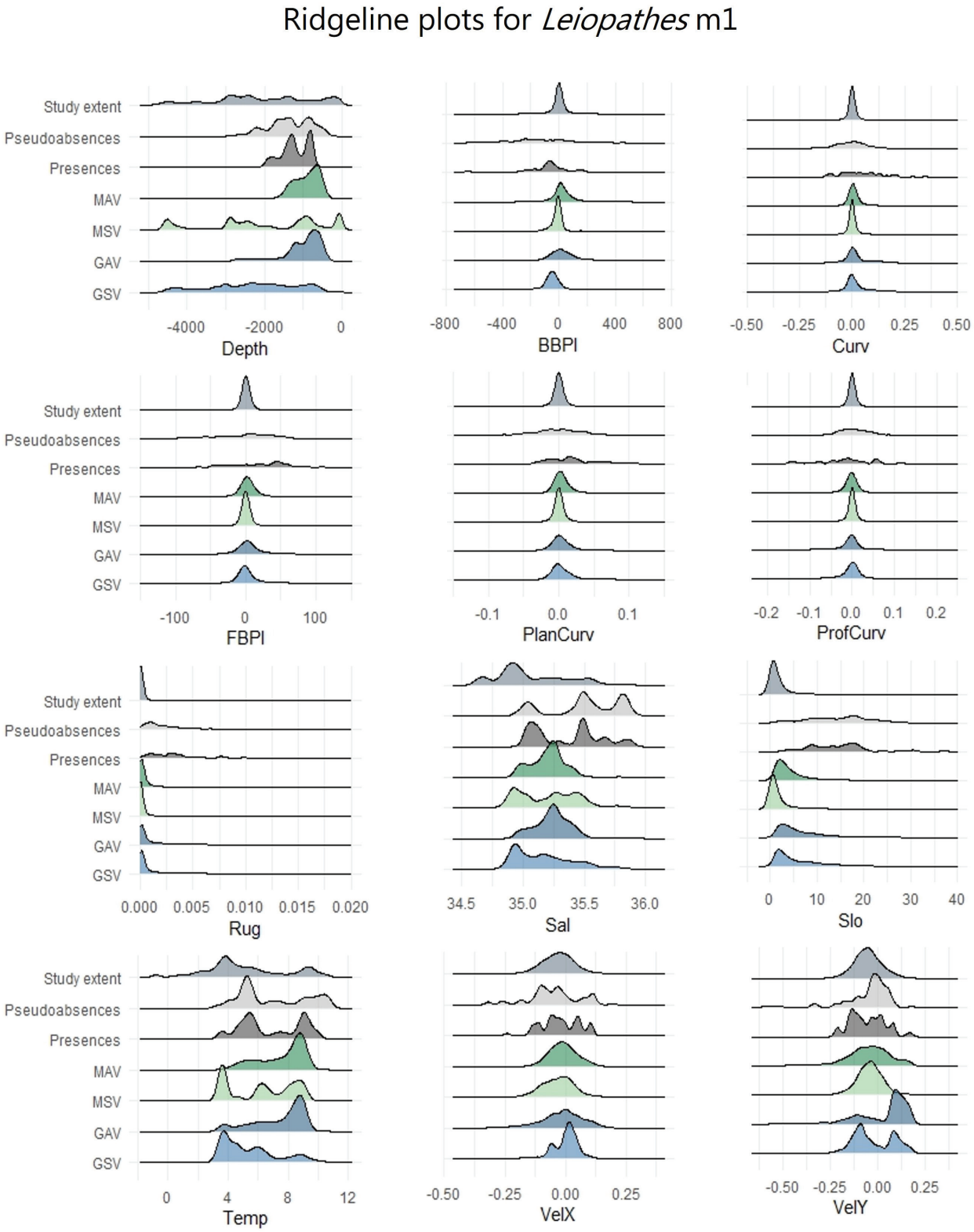

Fig. S6.3: Continue.

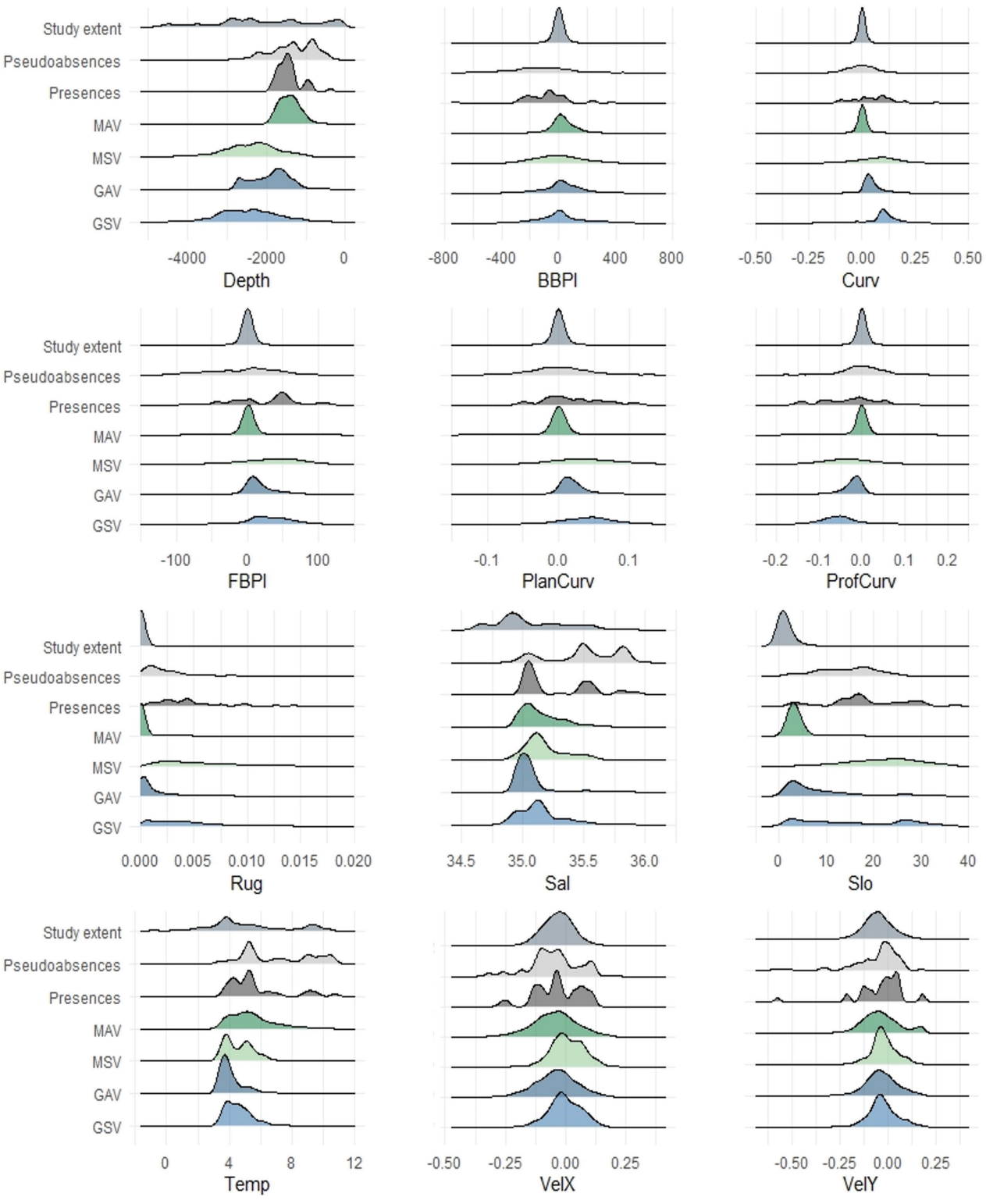

Fig. S6.4: Continue.

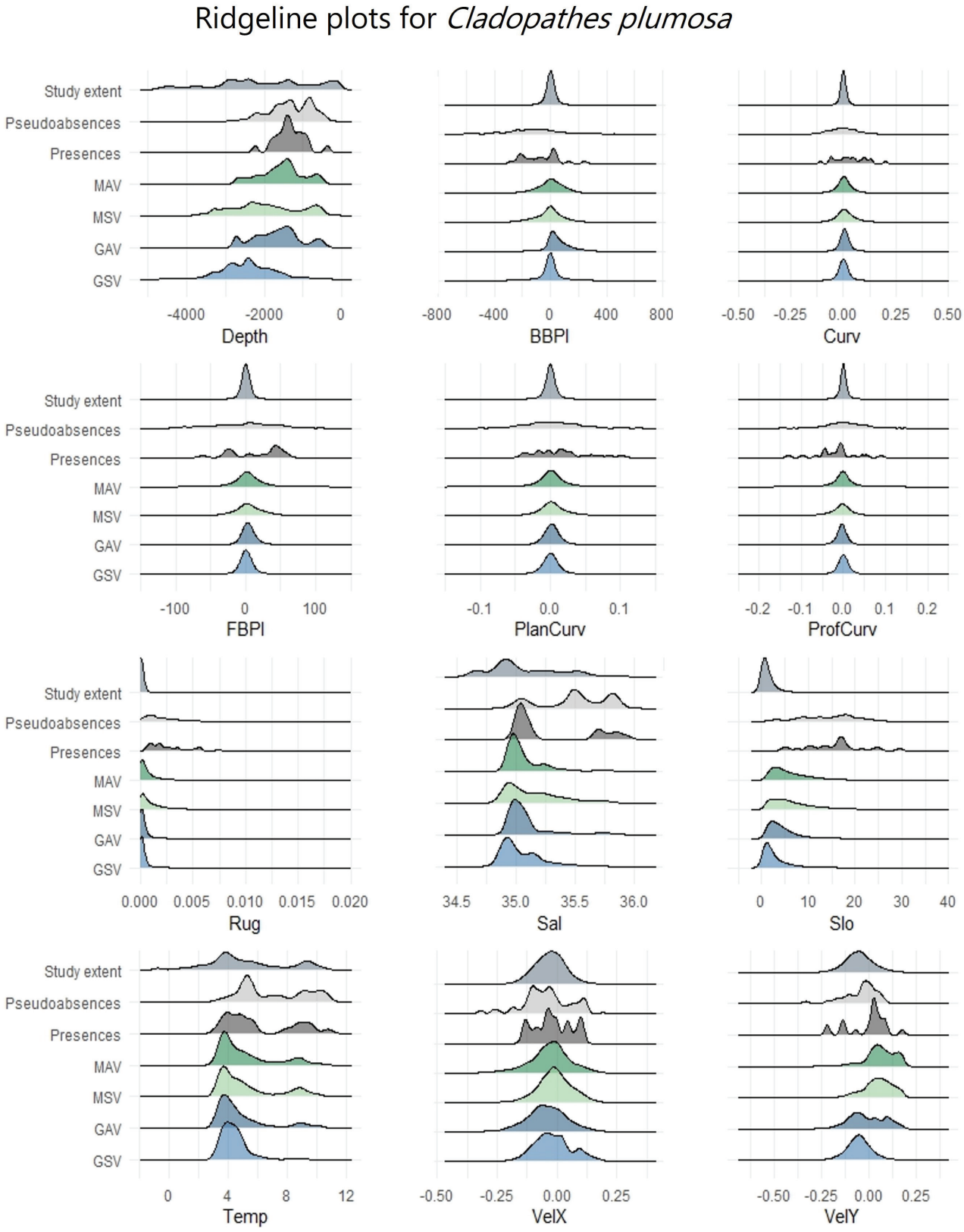

***Fig. S6.5**:* Continue.

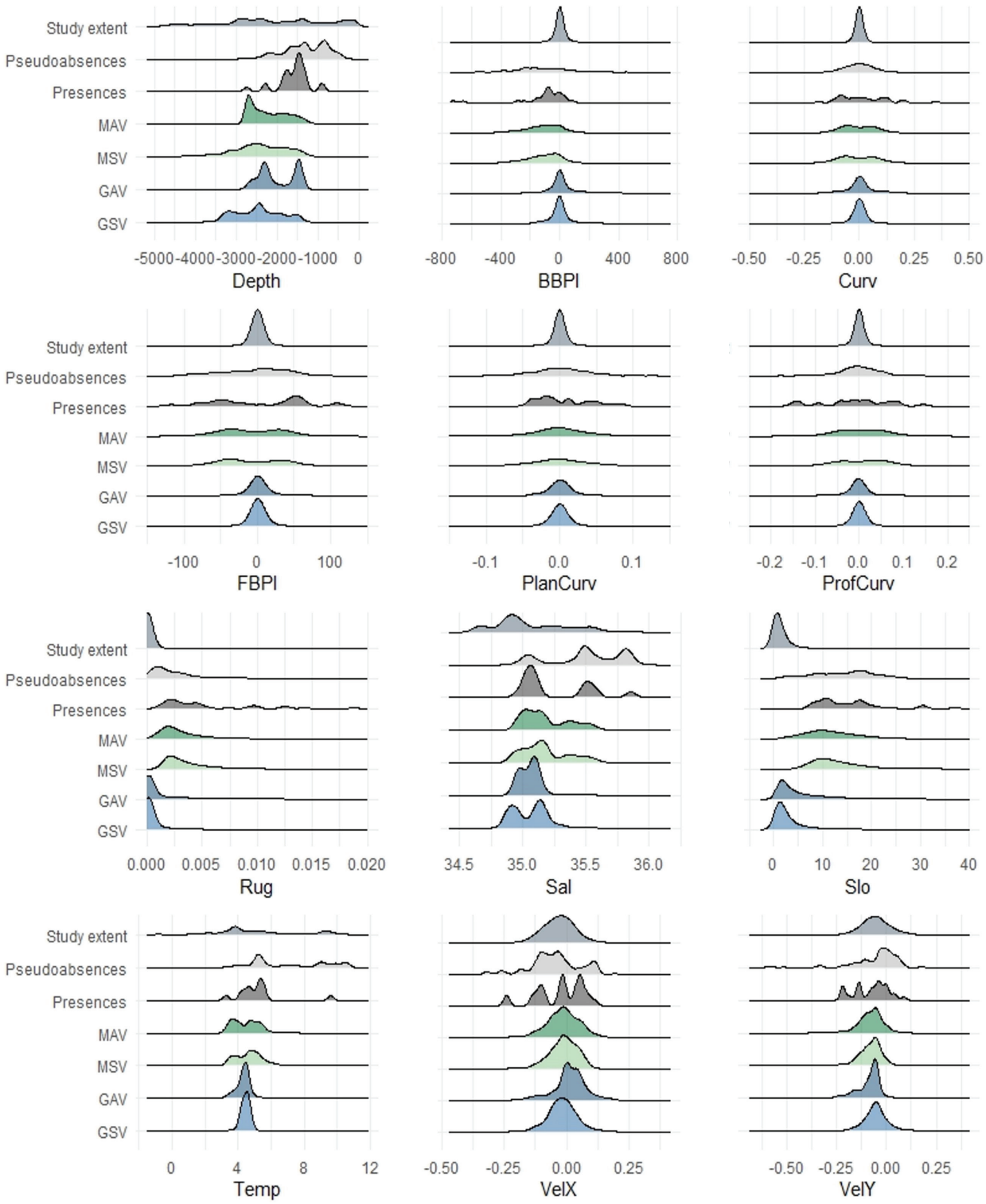

Fig.S6.6: Continue.

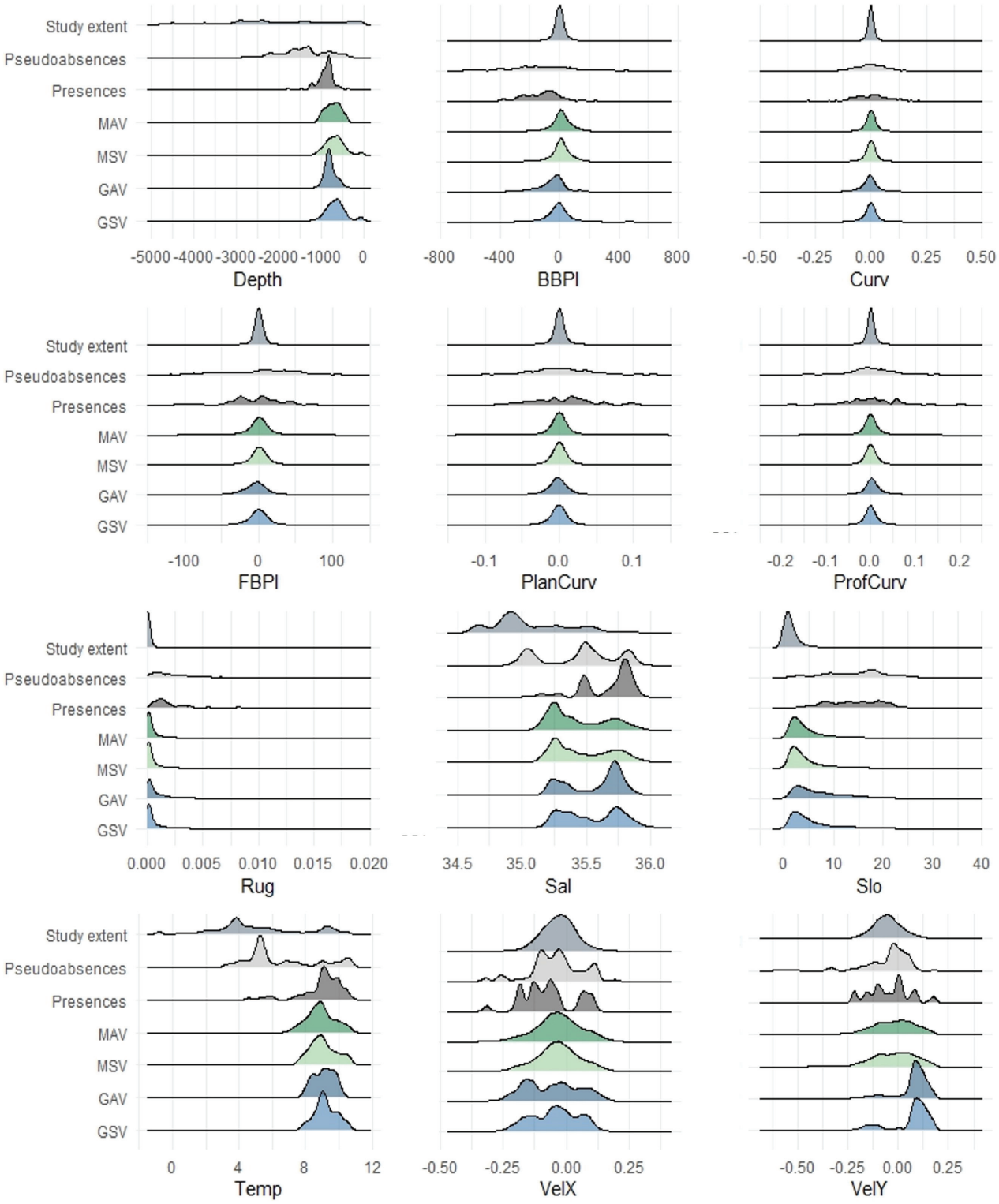

***Fig. S6.7**: Continue*

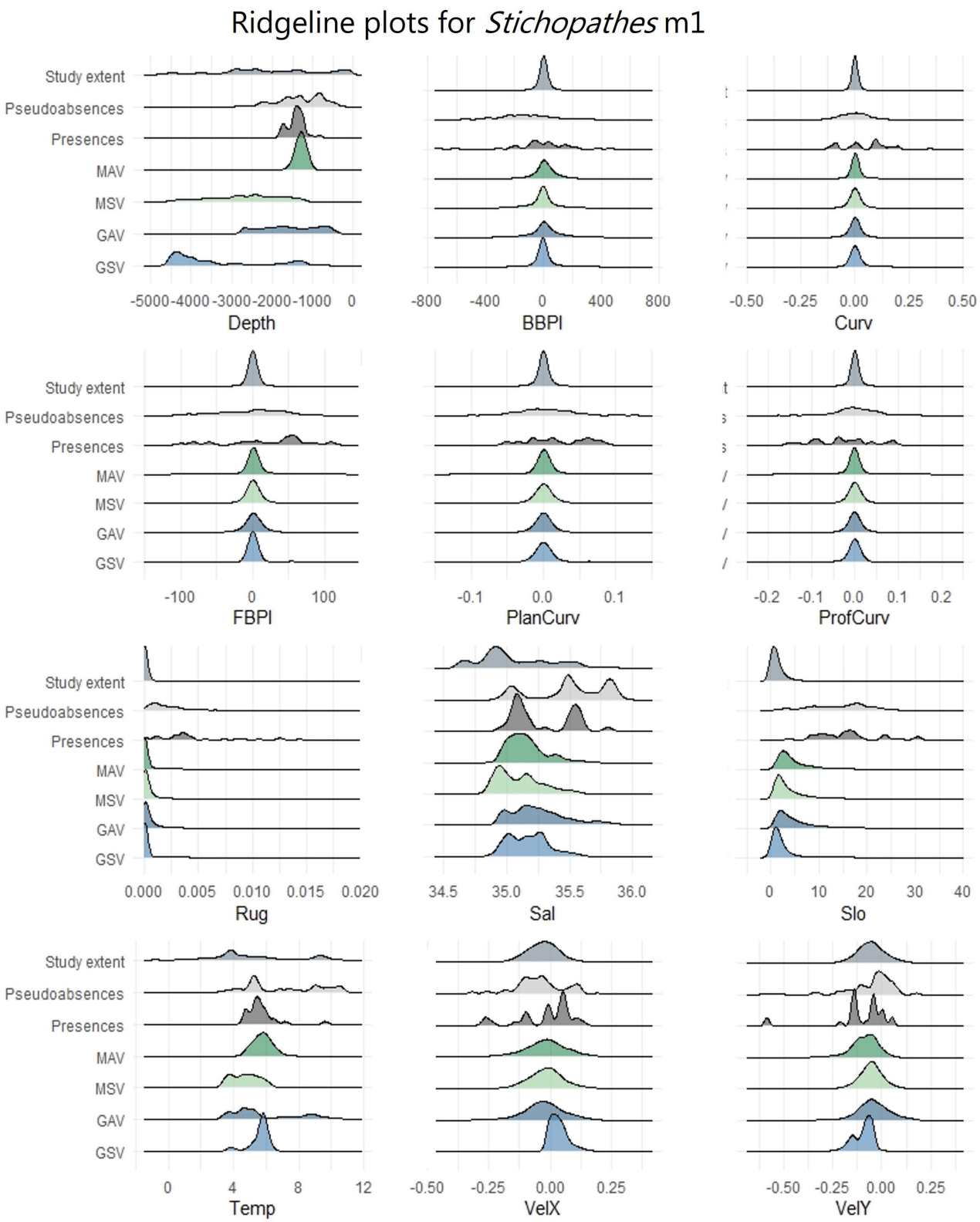

Fig. S6.8*:* Continue

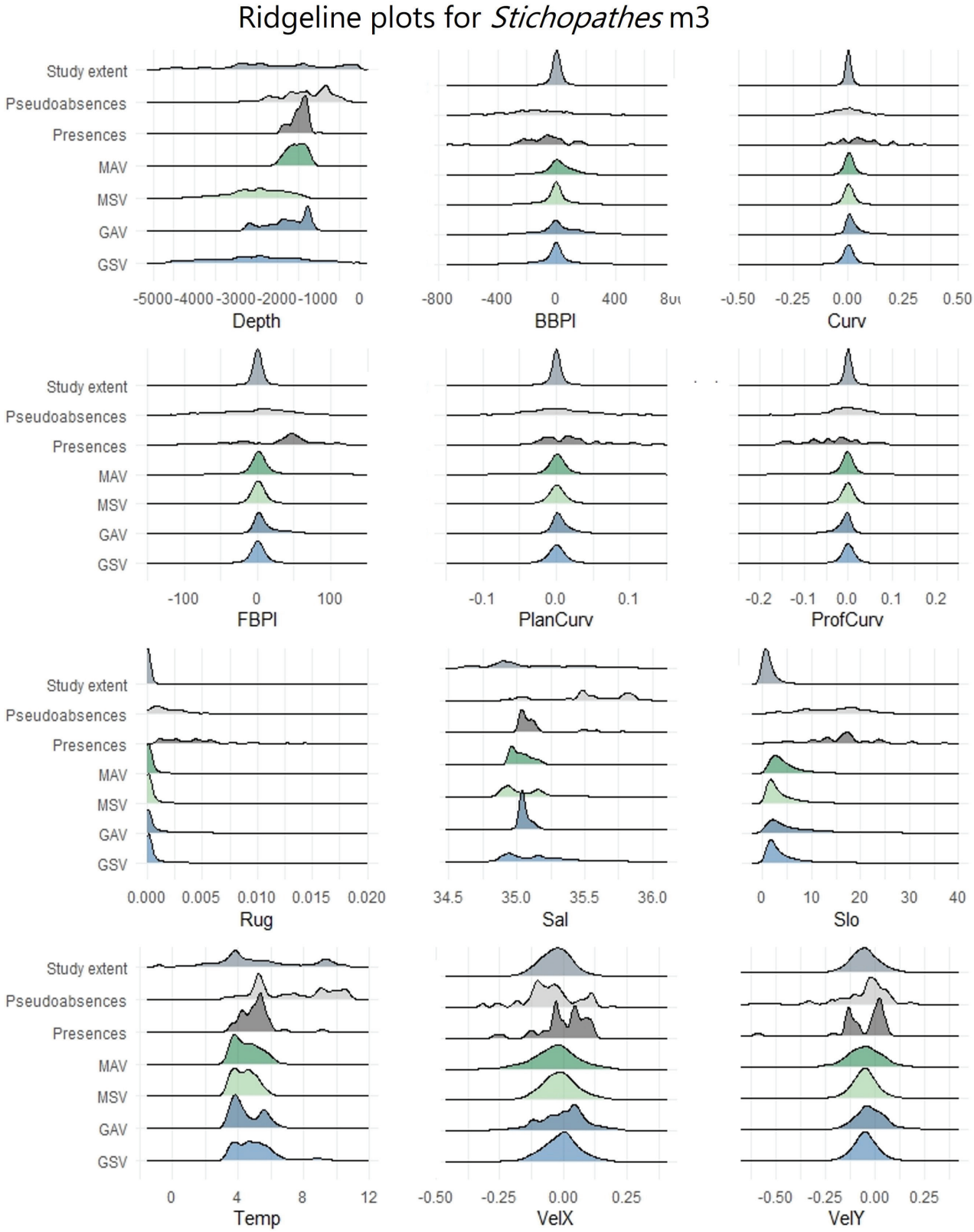

Fig. S6.9: Continue

Evaluation metrics

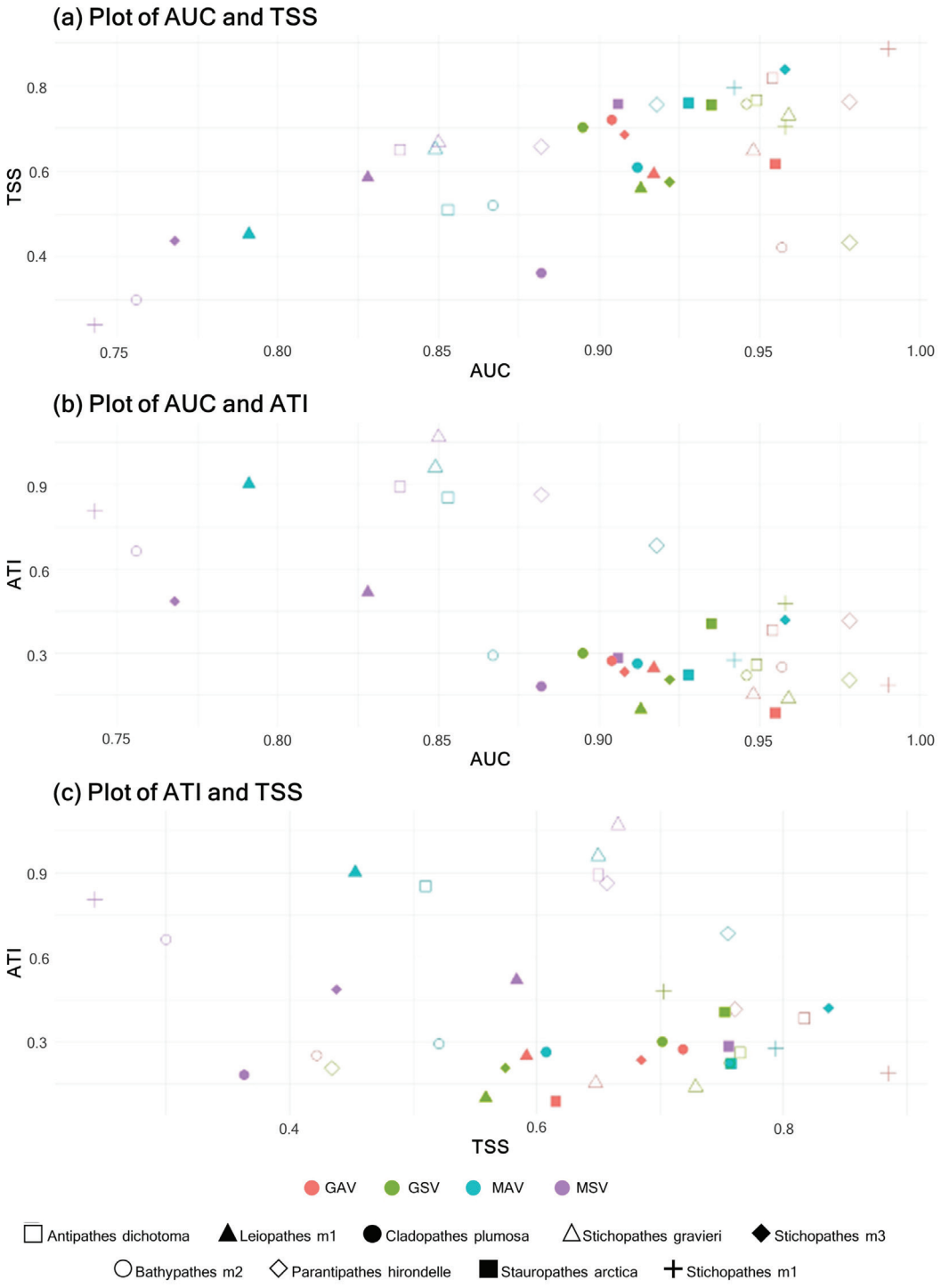

Fig. S7: Plot of AUC, TSS and ATI values of each modelling framework.

Table S13. Sensitivity and specificity values were calculated for each morphospecies and averaged for the modelling approach.

Morphospecies	Maximum Entropy				Gradient Boosting			
	Without variable preselection		With variable preselection		Without variable preselection		With variable preselection	
	Sensitivity	Specificity	Sensitivity	Specificity	Sensitivity	Specificity	Sensitivity	Specificity
Antipathes dichotoma	0.676	0.834	0.973	0.677	0.946	0.871	0.838	0.927
Bathypathes m2	0.595	0.926	0.357	0.943	1.000	0.422	0.833	0.923
Leiopathes m1	0.569	0.884	0.486	0.953	0.655	0.937	0.603	0.955
Parantipathes hirondelle	0.971	0.866	0.655	0.928	0.800	0.885	0.600	0.975
Parantipathes m2	0.667	0.941	1.000	0.363	0.762	0.957	0.810	0.892
Stauropathes arctica	0.889	0.869	0.852	0.904	0.630	0.986	0.852	0.902
Stichopathes gravieri	0.875	0.775	0.891	0.775	0.672	0.976	0.766	0.964
Stichopathes m1	0.857	0.937	0.357	0.885	0.893	0.992	0.714	0.989
Stichopathes m3	0.867	0.888	0.867	0.790	0.778	0.983	1.000	0.434
Average	0.774	0.880	0.872	0.533	0.793	0.890	0.780	0.885

Analysis of raster overlay

Table S14. Pearson's correlation analysis between the number of species presence and the model performance (AUC). The coefficients were calculated for each modelling method.

Modelling approach	Correlation coefficient	P-value
MaxEnt with all variables	-0.716	0.029
MaxEnt with pre-selected variables	-0.014	0.972
GBM with all variables	0.008	0.985
GBM with pre-selected variables	0.317	0.406

Table S15. Overlay proportion of presences in the final likelihood of morphospecies presence raster for each modelling approach (the highest counts are identified with a *).

Morphospecies	Maximum Entropy		Gradient Boosting	
	Without variable preselection	With variable preselection	Without variable preselection	With variable preselection
Antipathes dichotoma	267272	456864*	305012	161070
Bathypathes m2	19770	18878	68696	332775*
Leiopathes m1	254531	1966304	94620	214912
Parantipathes hirondelle	155768*	19270	70186	29554
Parantipathes m2	94573	280977	270674	1866324*
Stauropathes arctica	56281	55271	33577	675782*
Stichopathes gravieri	338617	338899*	32002	83720
Stichopathes m1	87717	2164874*	1261897	238948
Stichopathes m3	250859	1610415	61952	2426213*

Analysis with exchange of variables

To confirm that model variables should not be selected through a general step outside the model, but rather tailored to the algorithm being used, the analysis was replicated by using the variable set selected in GBM on the MaxEnt model, and vice versa. Due to time constraints, this analysis was only applied to the most occurring morphospecies: *Stichopathes gravieri* (64 occurrences). The results (see Table S16) indicate that, although the model's performance remains high, the ATI score in the MaxEnt model decreases noticeably.

These results suggest that, when the objective of habitat modelling is to predict to new locations, the variable selection step (if performed) should be incorporated into the modelling process to ensure optimal results.

This analysis resulted in a drop of the model generalization capability when the variable selection process was carried out using a different algorithm. Hence, using an improper set of variables increases the false positive and false negative rates, leading to incorrect predictions in environments otherwise considered unsuitable and contributing to high AUC values attributed to overfitting.

	MaxEnt			**GBM**		
	AUC	**TSS**	**ATI**	**AUC**	**TSS**	**ATI**
Original model	0.850	0.666	1.070	0.959	0.729	0.138
Exchanged variable array	0.836	0.688	0.784	0.942	0.745	0.149

Predictive distribution maps

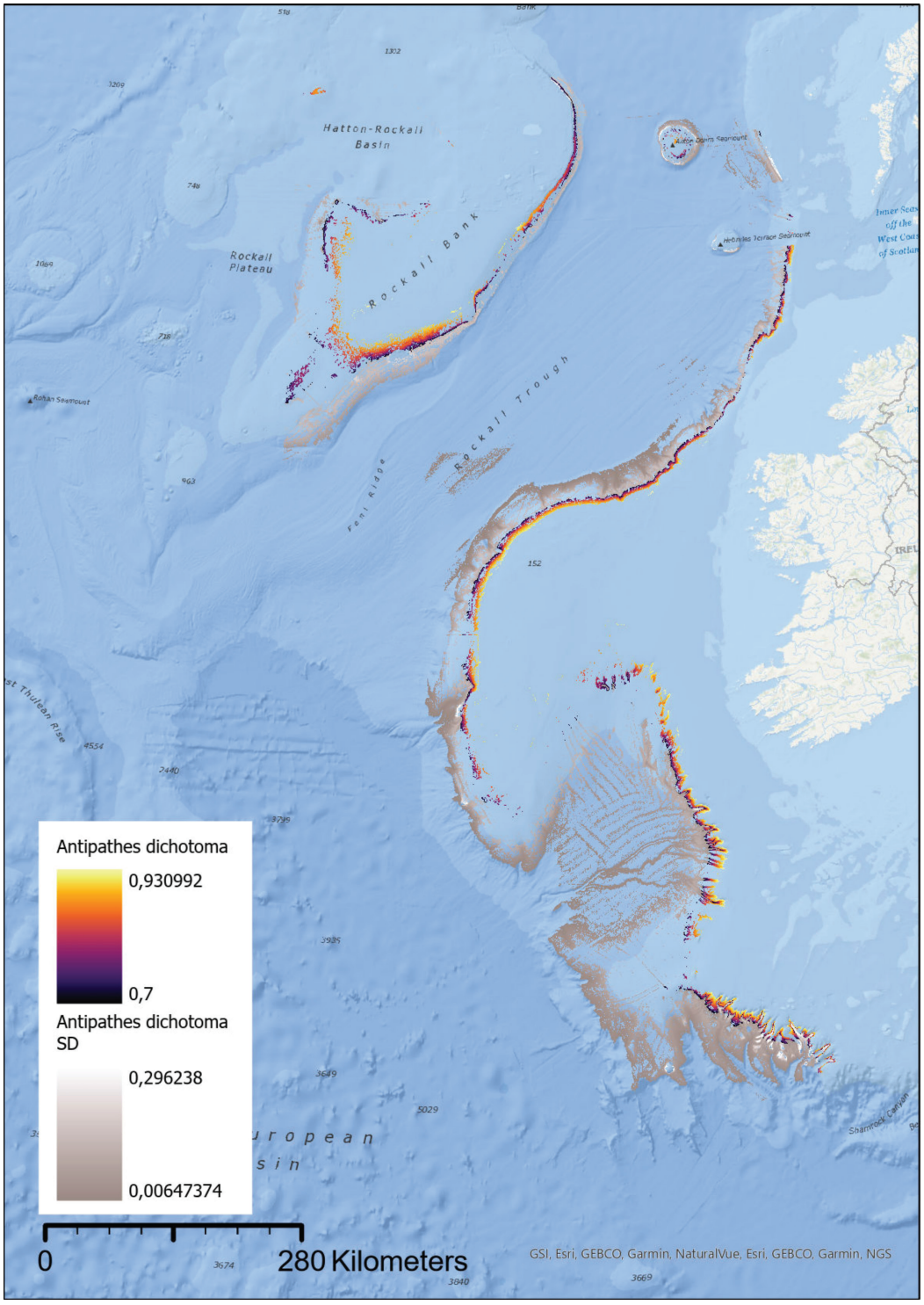

Fig. S8.1*:* Likelihood of presence and standard deviation of *Antipathes dichotoma*, when modelled with MaxEnt using all the available predictors.

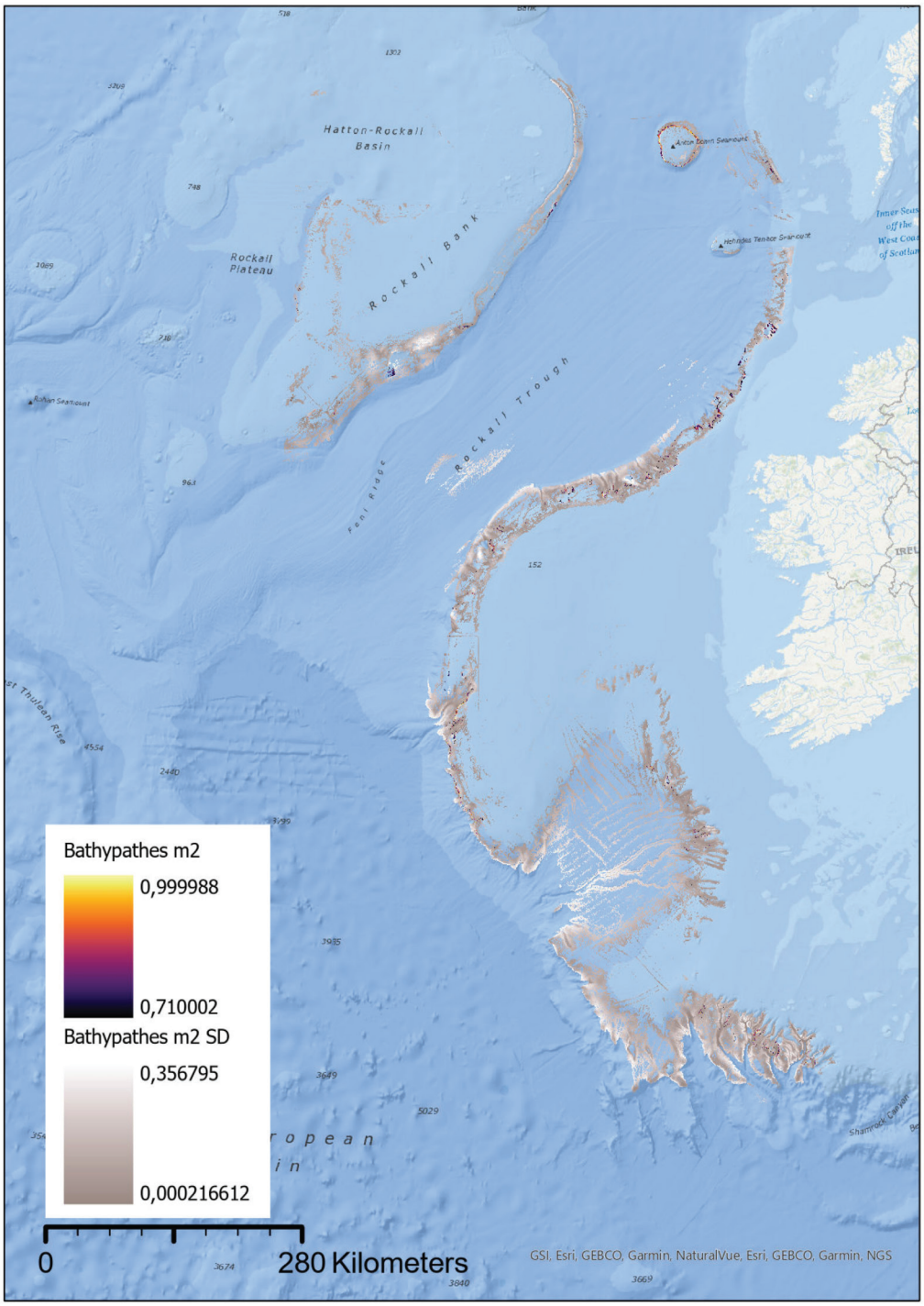

Fig. S8.2*:* Likelihood of presence and standard deviation of *Bathypathes* m2, when modelled with MaxEnt using all the available predictors.

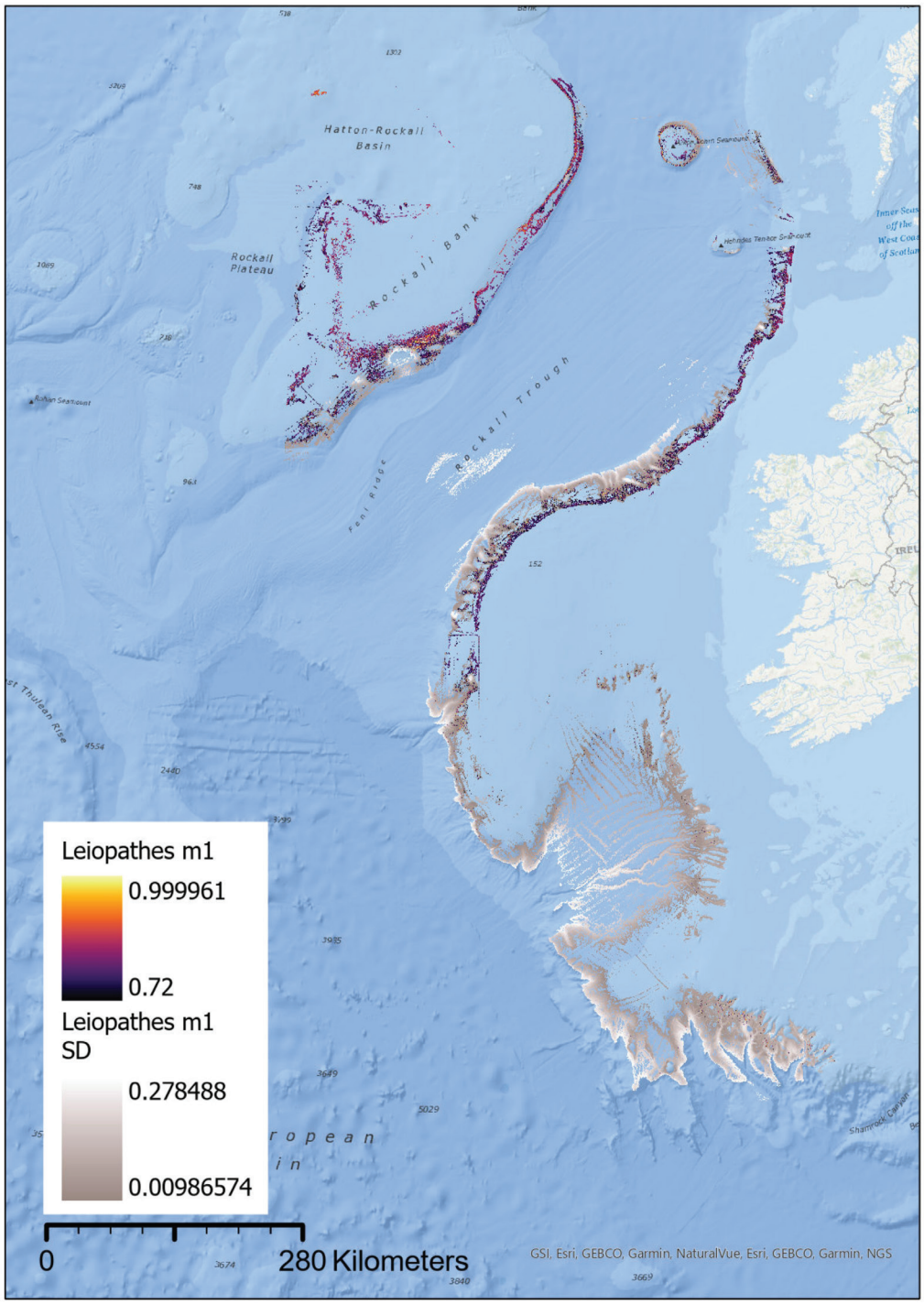

Fig. S8.3*:* Likelihood of presence and standard deviation of *Leiopathes* m1, when modelled with MaxEnt using all the available predictors.

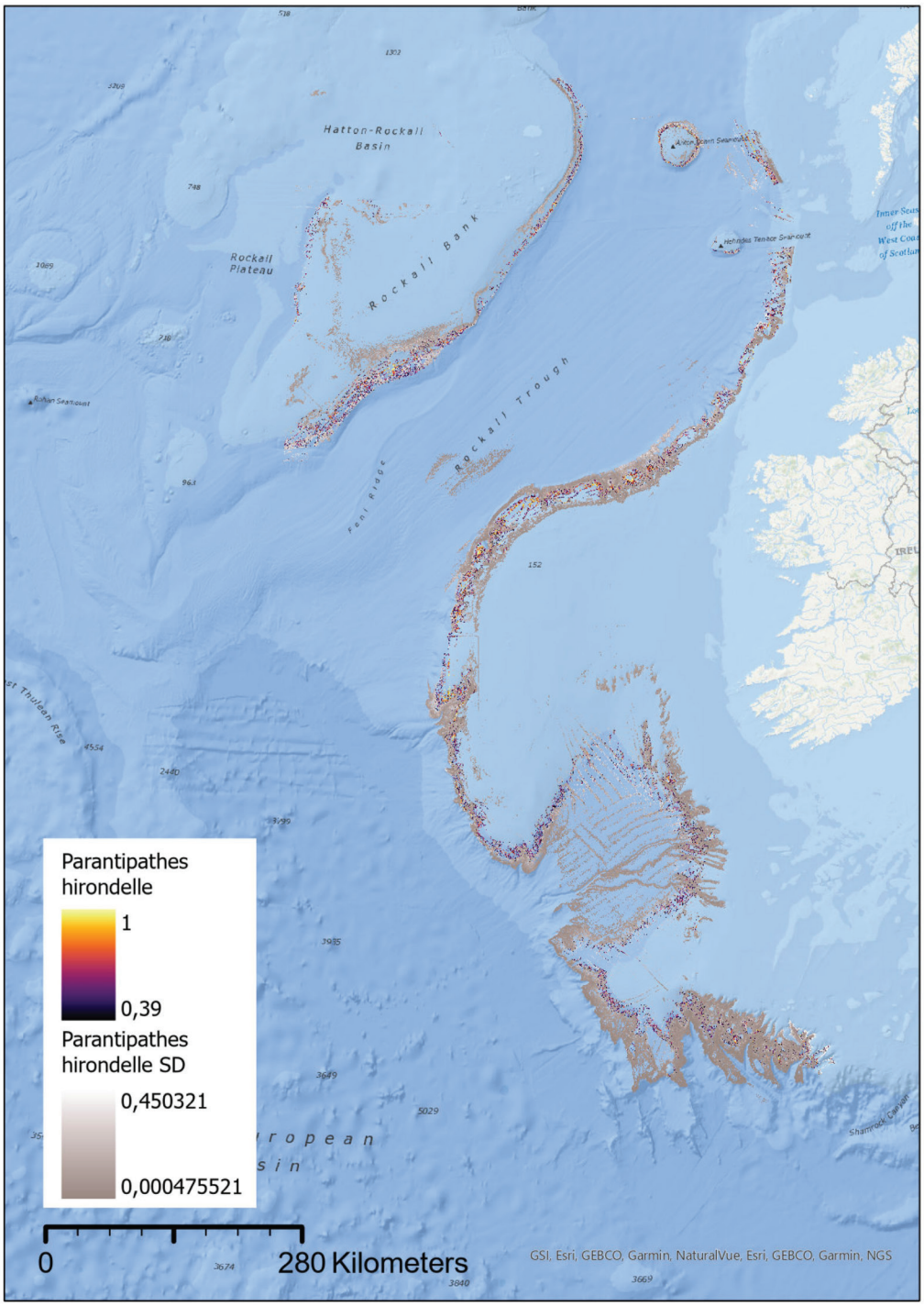

Fig. S8.4*:* Likelihood of presence and standard deviation of *Parantipathes hirondelle*, when modelled with MaxEnt using all the available predictors.

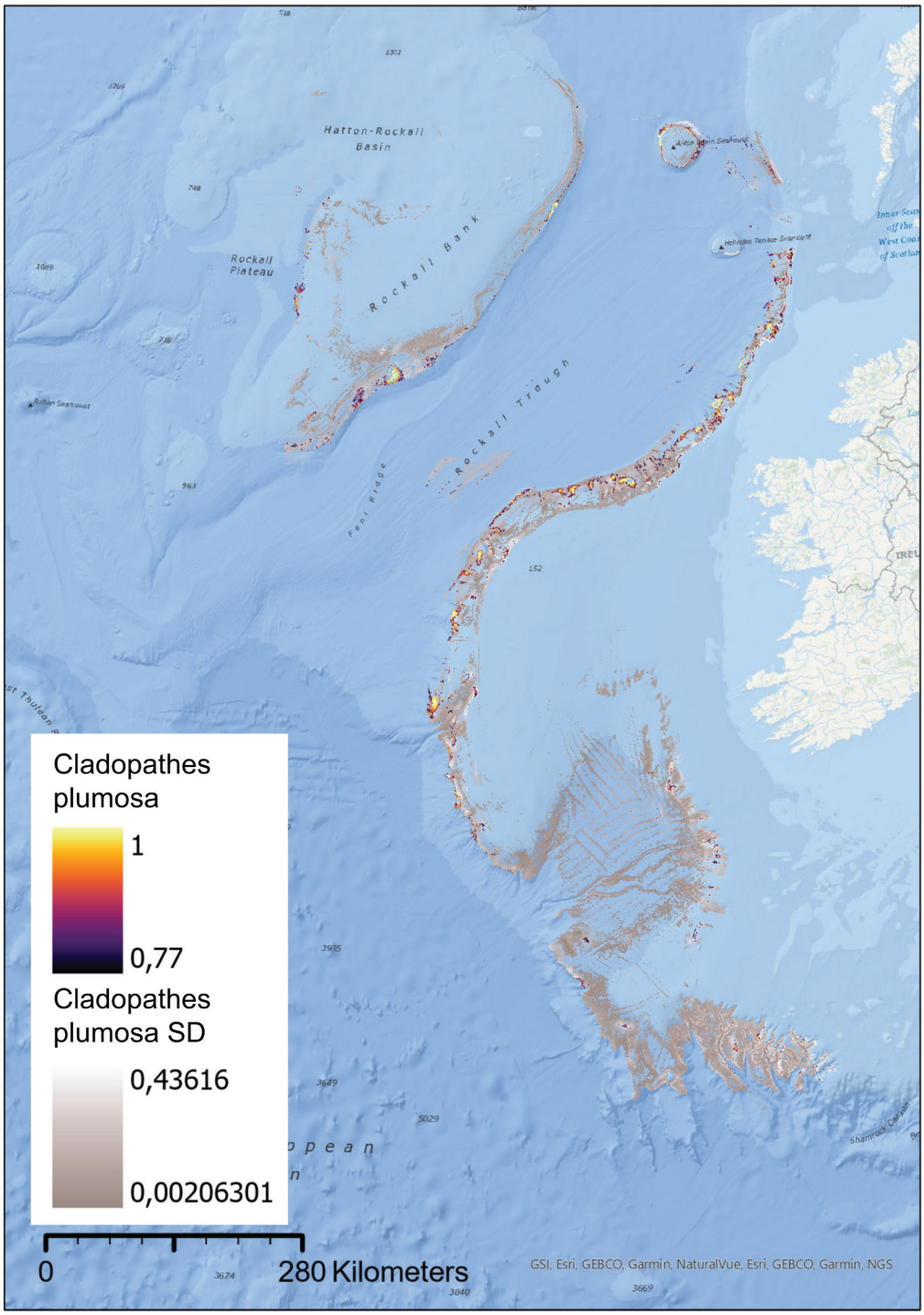

***Fig. S8.5**:* Likelihood of presence and standard deviation of *Cladopathes plumosa*, when modelled with MaxEnt using all the available predictors.

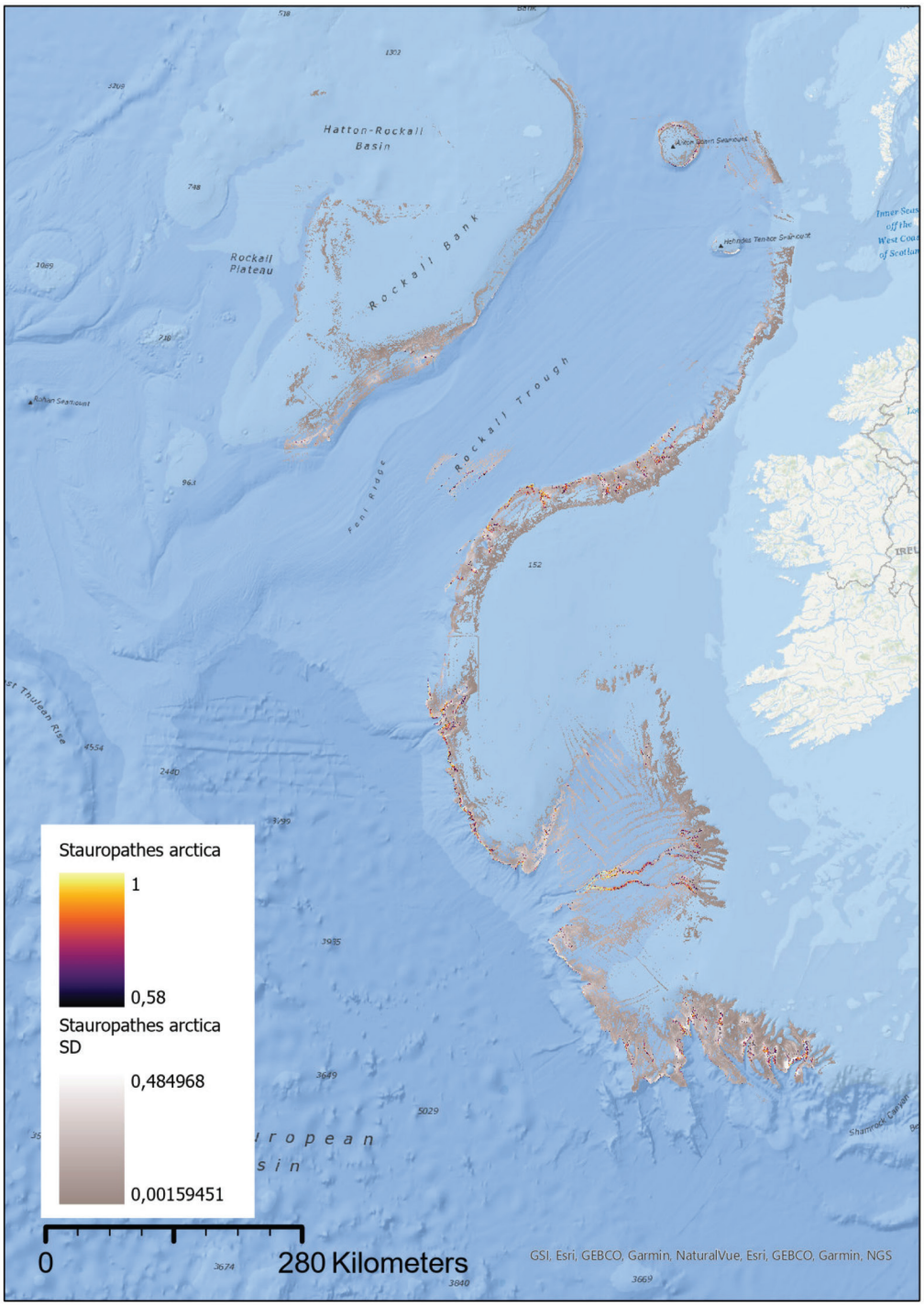

Fig. S8.6*:* Likelihood of presence and standard deviation of *Stauropathes arctica*, when modelled with MaxEnt using all the available predictors.

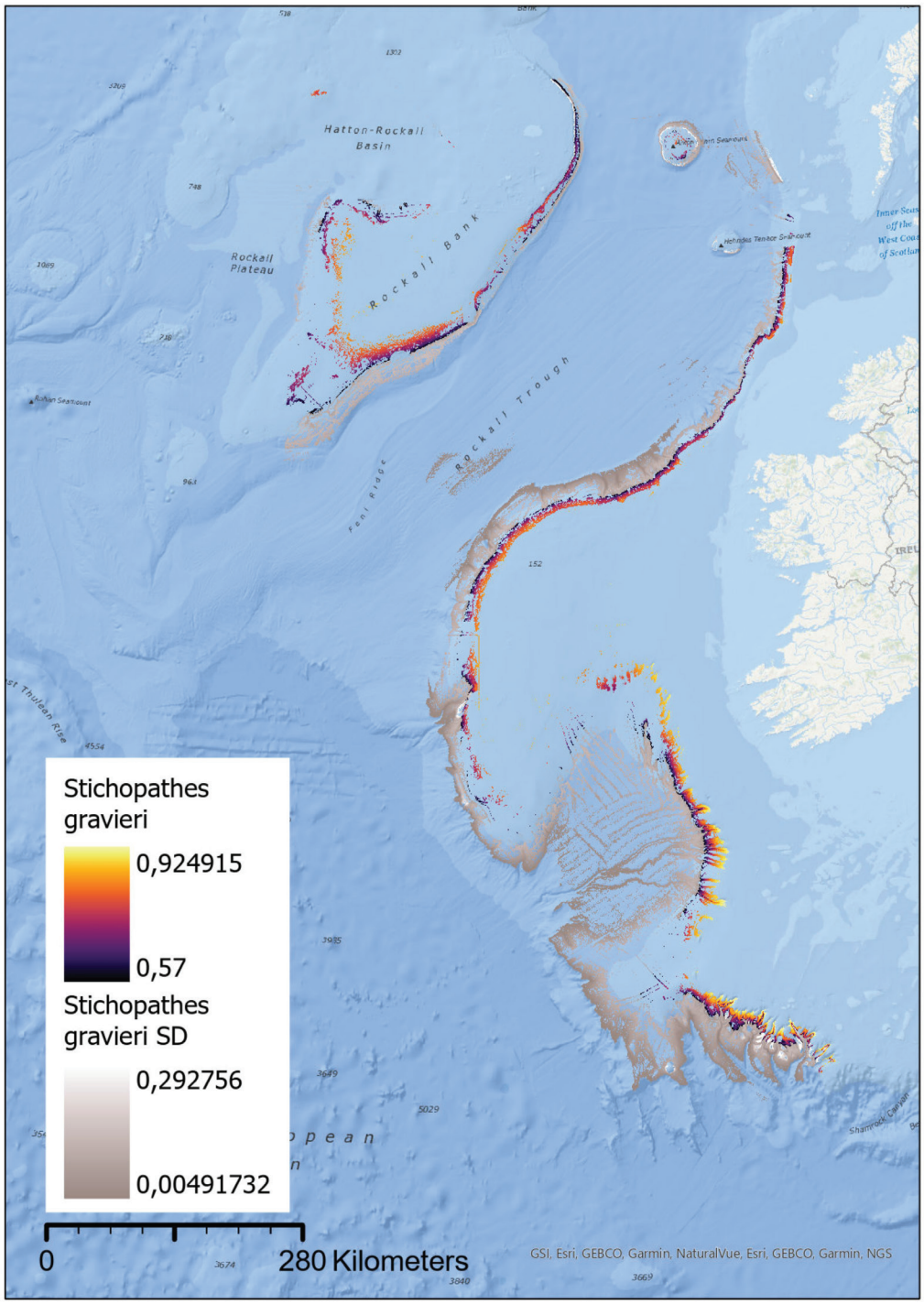

***Fig. S8.7**:* Likelihood of presence and standard deviation of *Stichopathes gravieri*, when modelled with MaxEnt using all the available predictors.

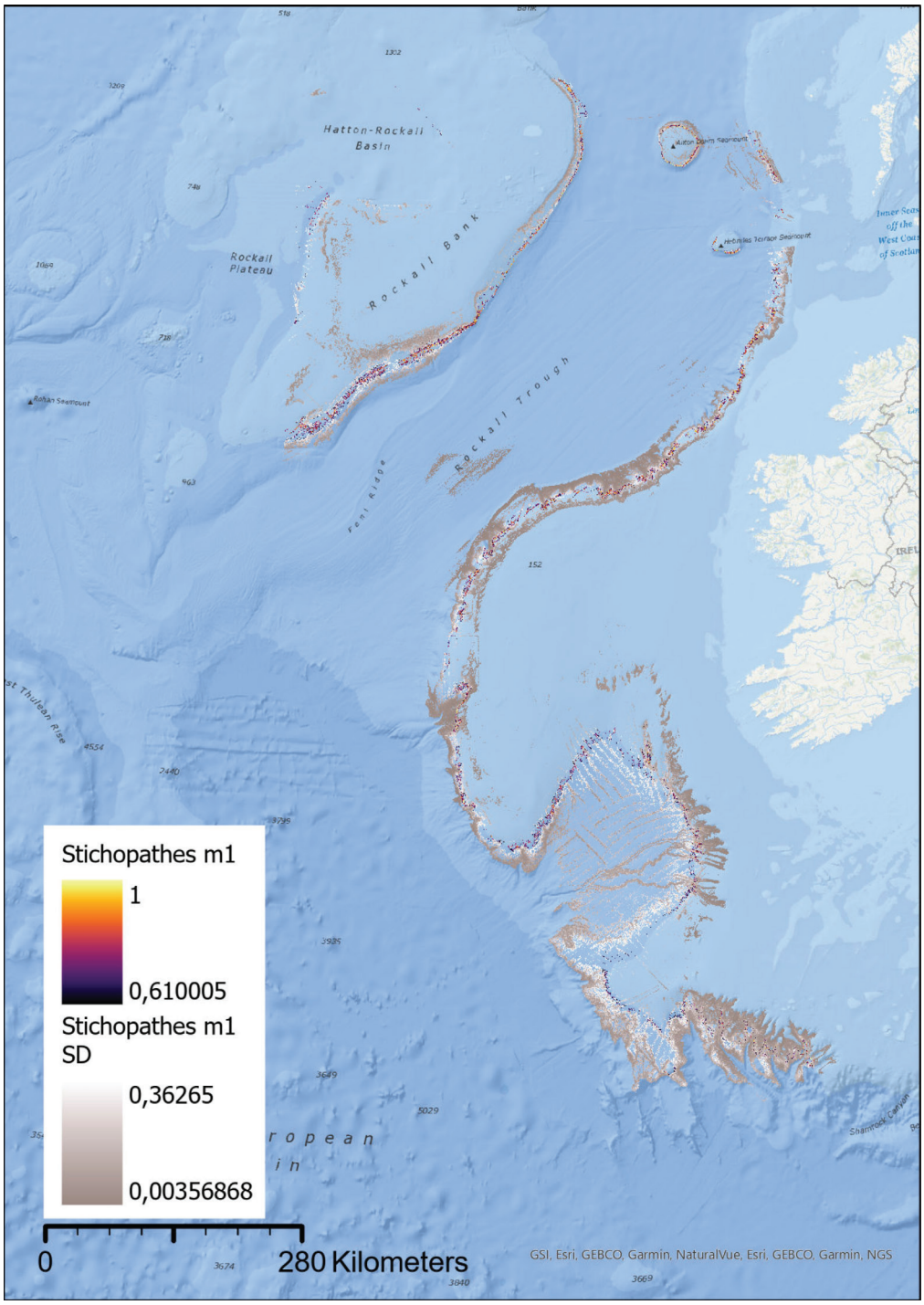

***Fig. S8.8**:* Likelihood of presence and standard deviation of *Stichopathes* m1, when modelled with MaxEnt using all the available predictors.

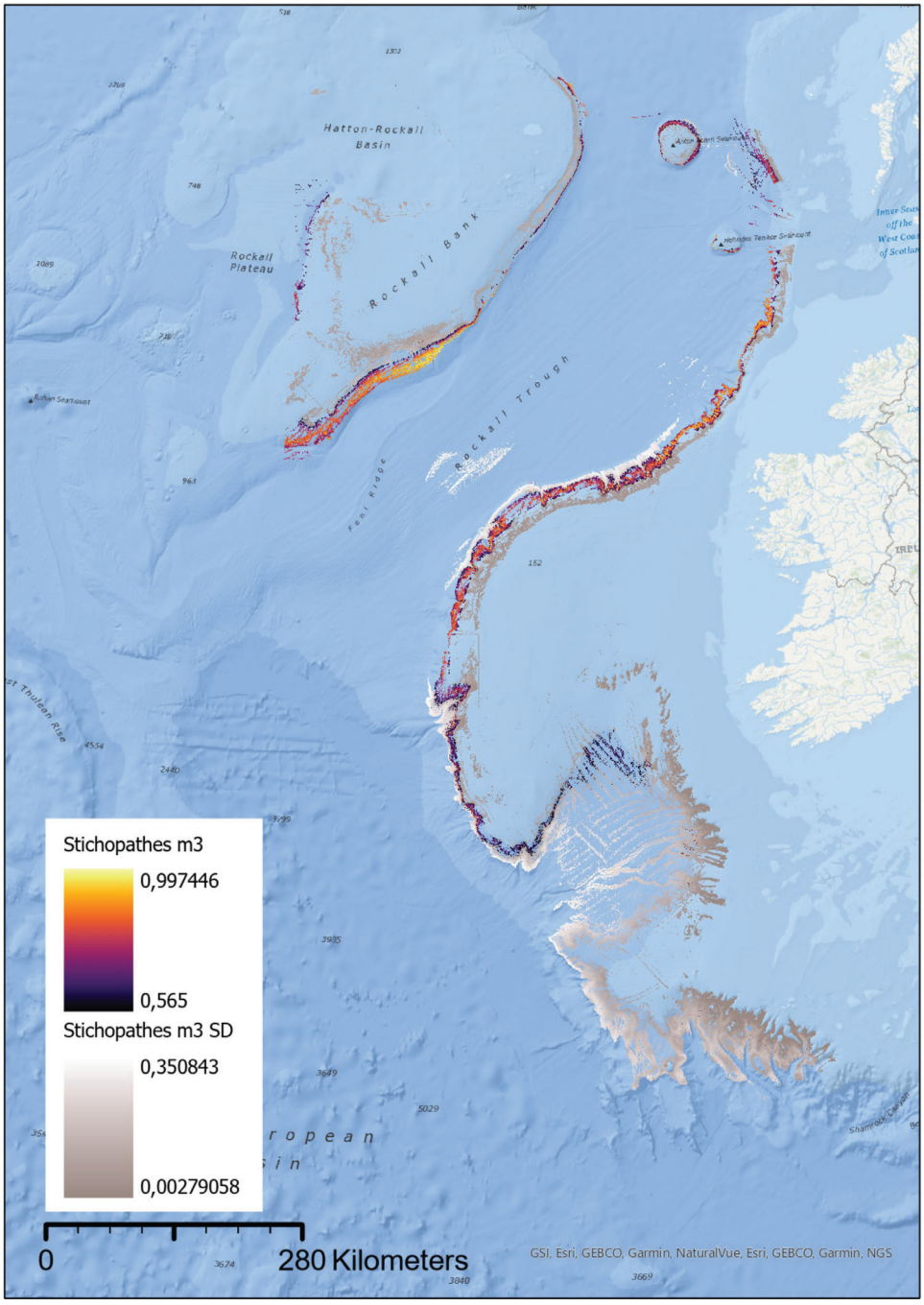

Fig. S8.9*:* Likelihood of presence and standard deviation of *Stichopathes* m3, when modelled with MaxEnt using all the available predictors.

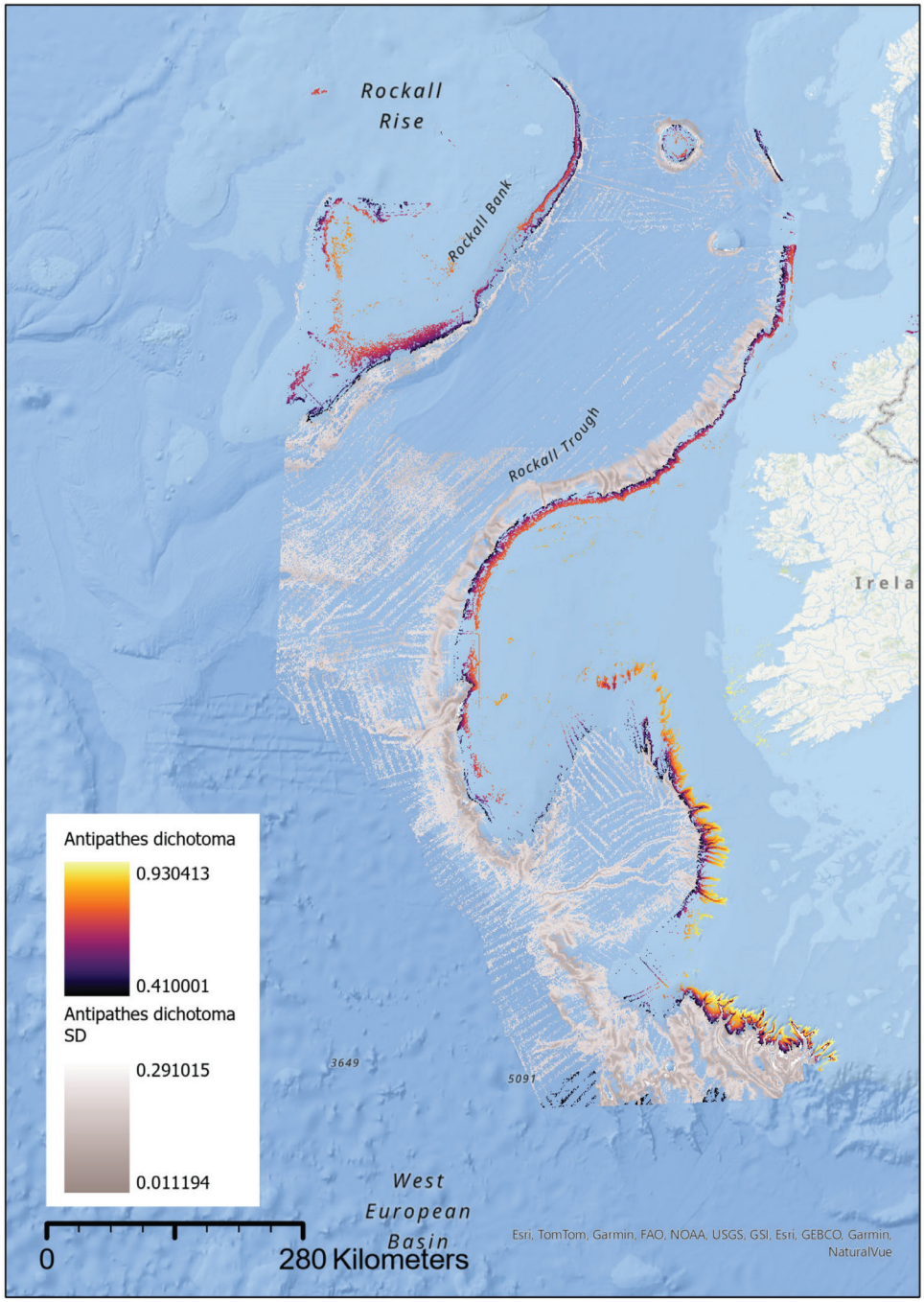

Fig. S9.1*:* Likelihood of presence and standard deviation of *Antipathes dichotoma*, when modelled with MaxEnt using parsimonious backward stepwise variable selection.

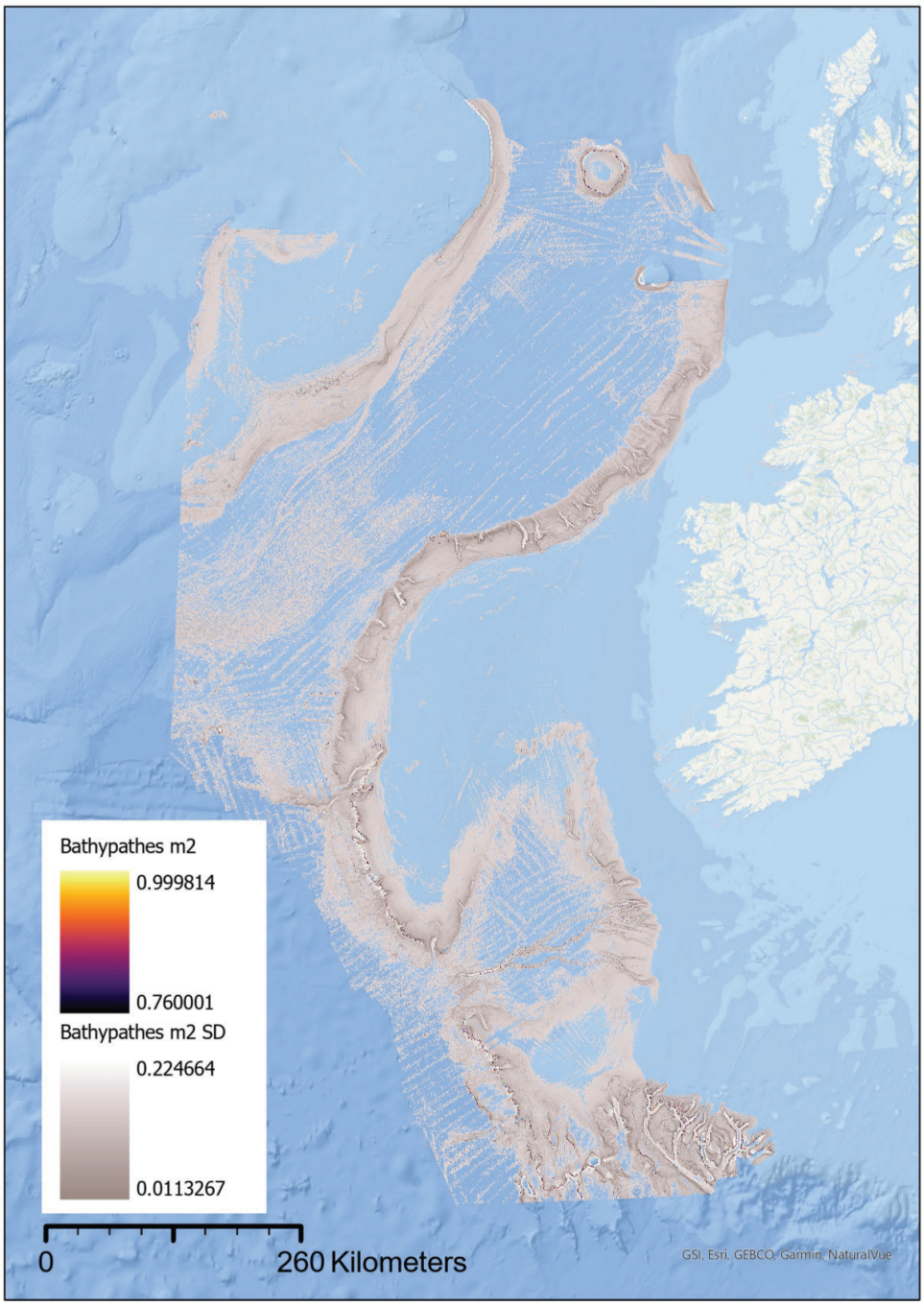

***Fig. S9.2**:* Likelihood of presence and standard deviation of *Bathypathes* m2, when modelled with MaxEnt using parsimonious backward stepwise variable selection.

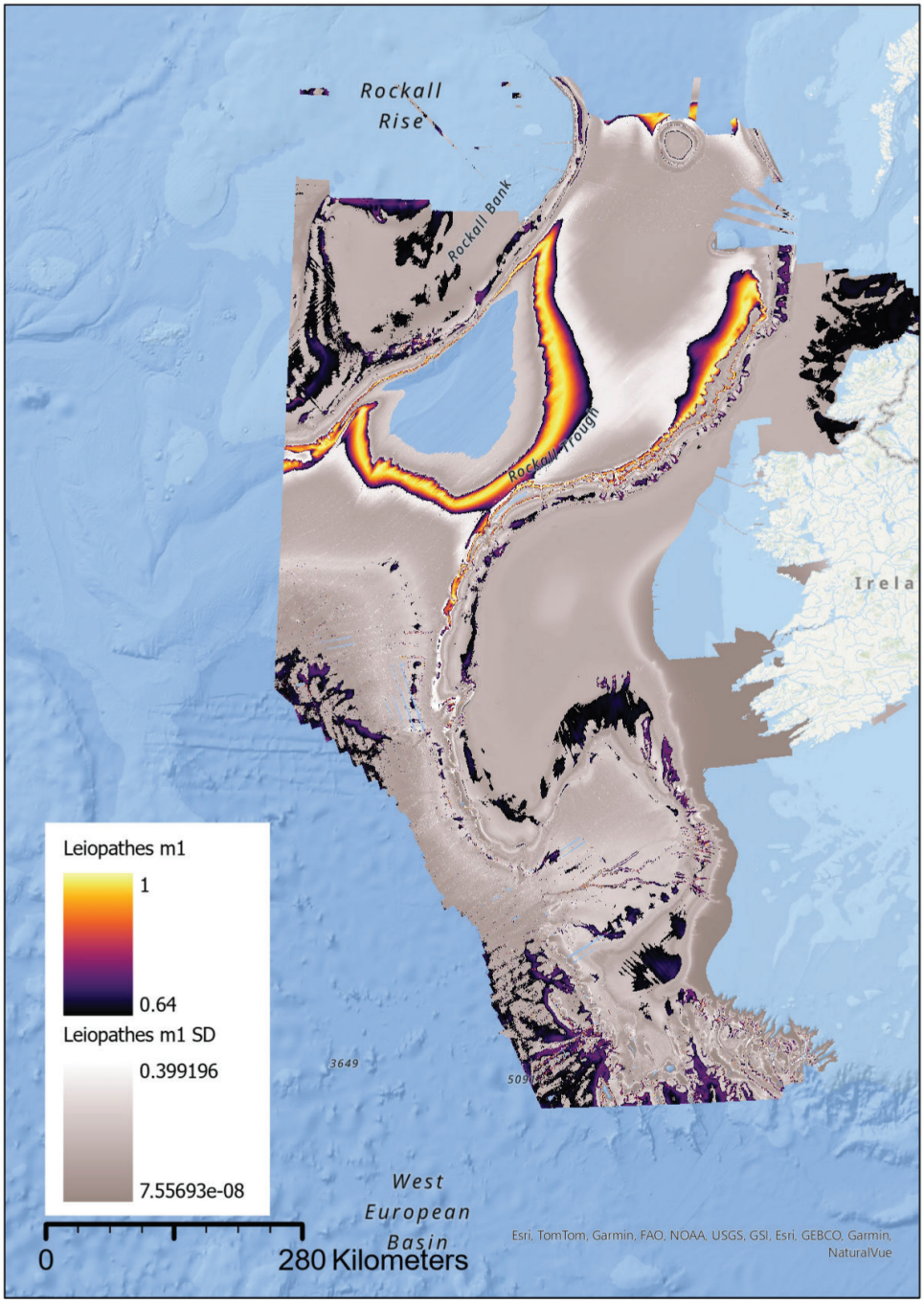

Fig. S9.3*:* Likelihood of presence and standard deviation of *Leiopathes* m1, when modelled with MaxEnt using parsimonious backward stepwise variable selection.

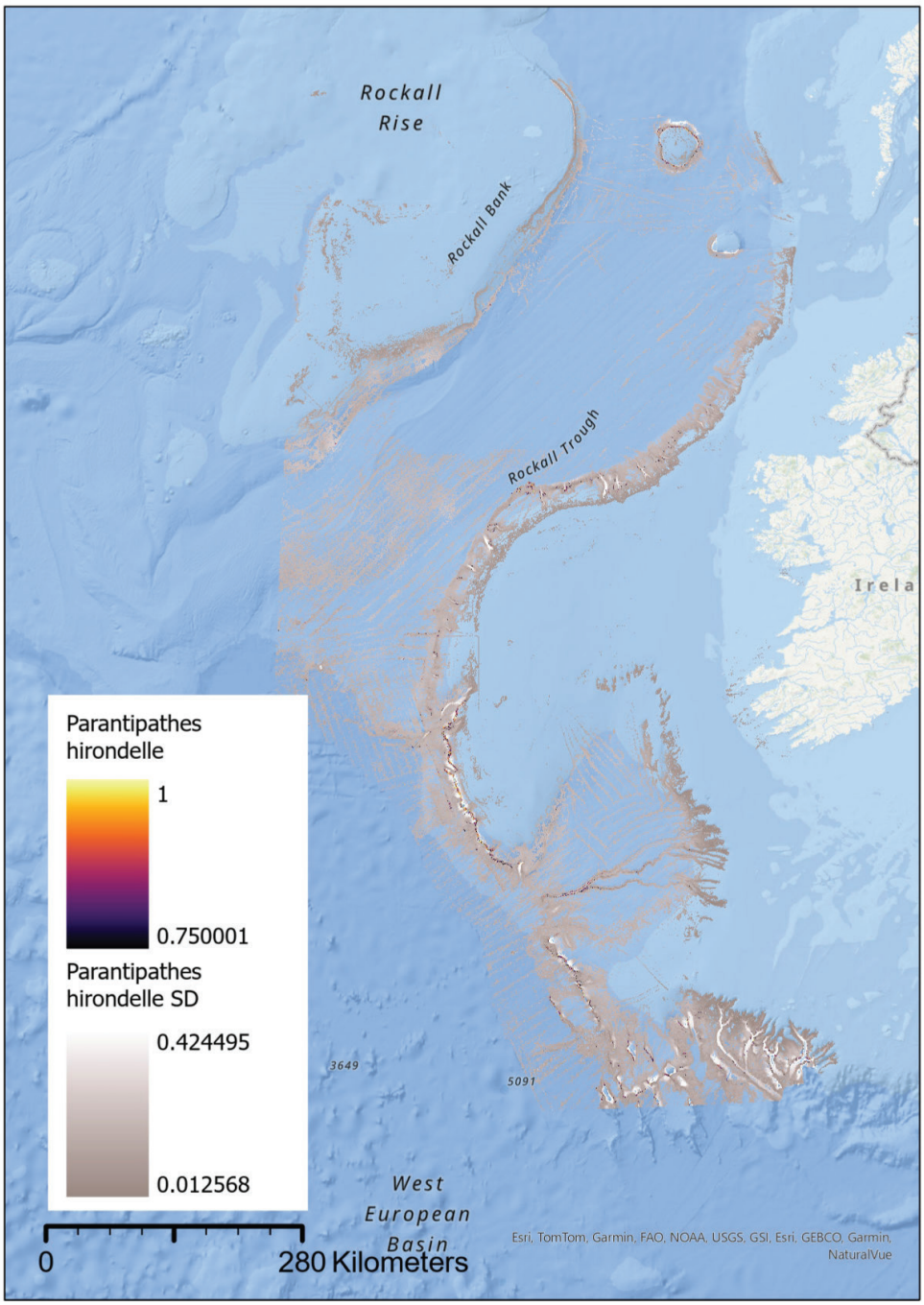

Fig. S9.4*:* Likelihood of presence and standard deviation of *Parantipathes hirondelle*, when modelled with MaxEnt using parsimonious backward stepwise variable selection.

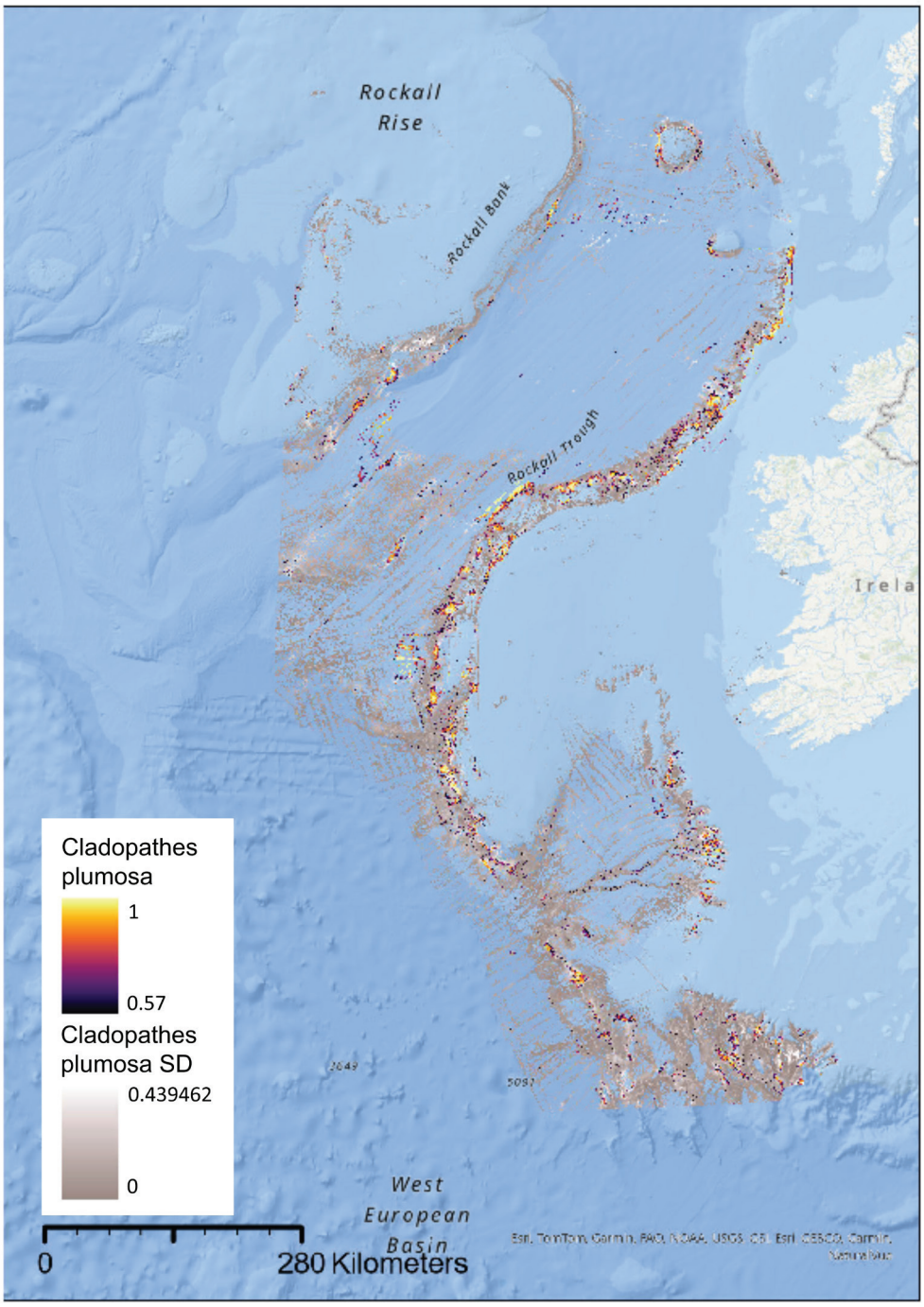

***Fig. S9.5**:* Likelihood of presence and standard deviation of *Cladopathes plumosa*, when modelled with MaxEnt using parsimonious backward stepwise variable selection.

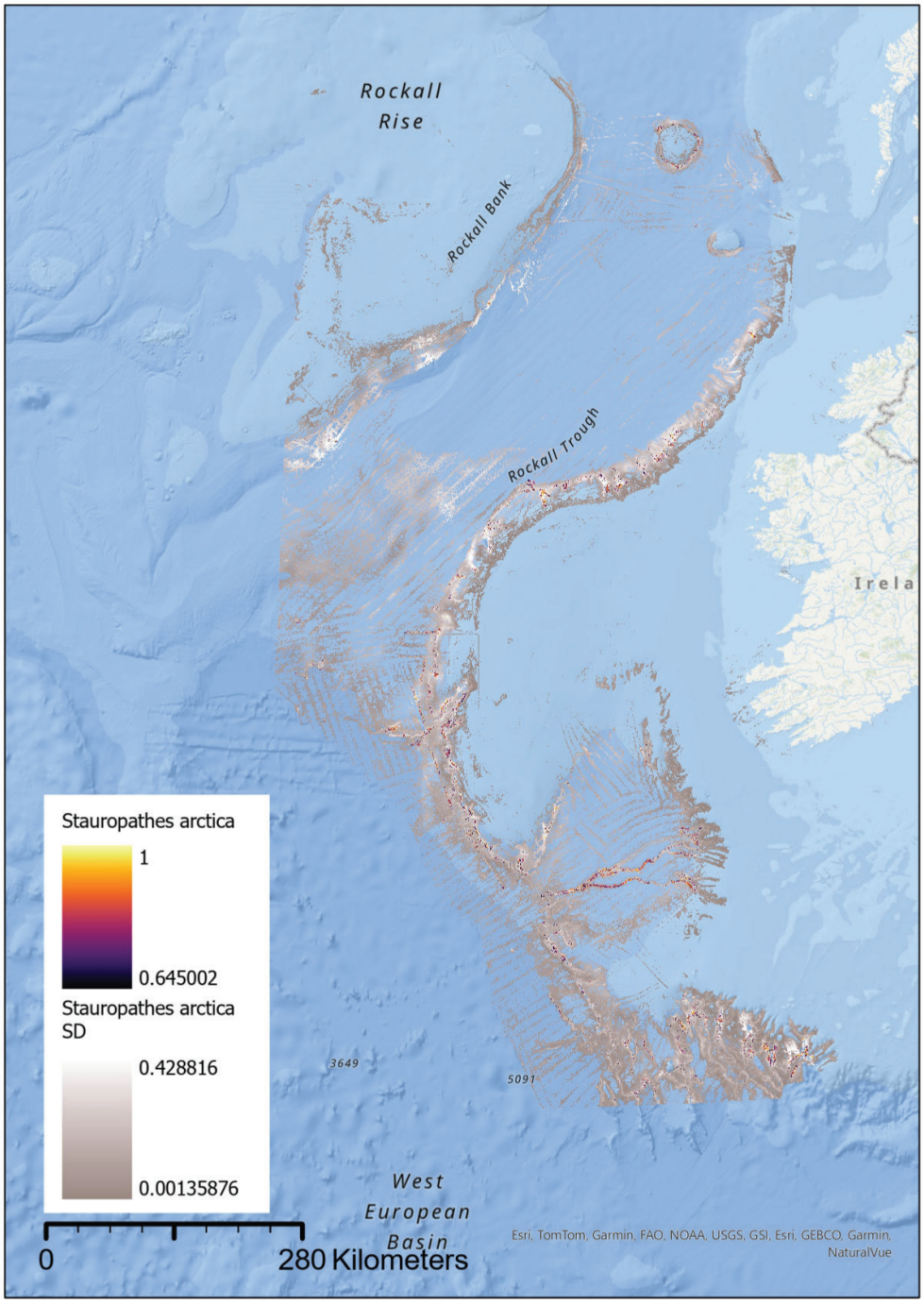

***Fig. S9.6**:* Likelihood of presence and standard deviation of *Stauropathes arctica*, when modelled with MaxEnt using parsimonious backward stepwise variable selection.

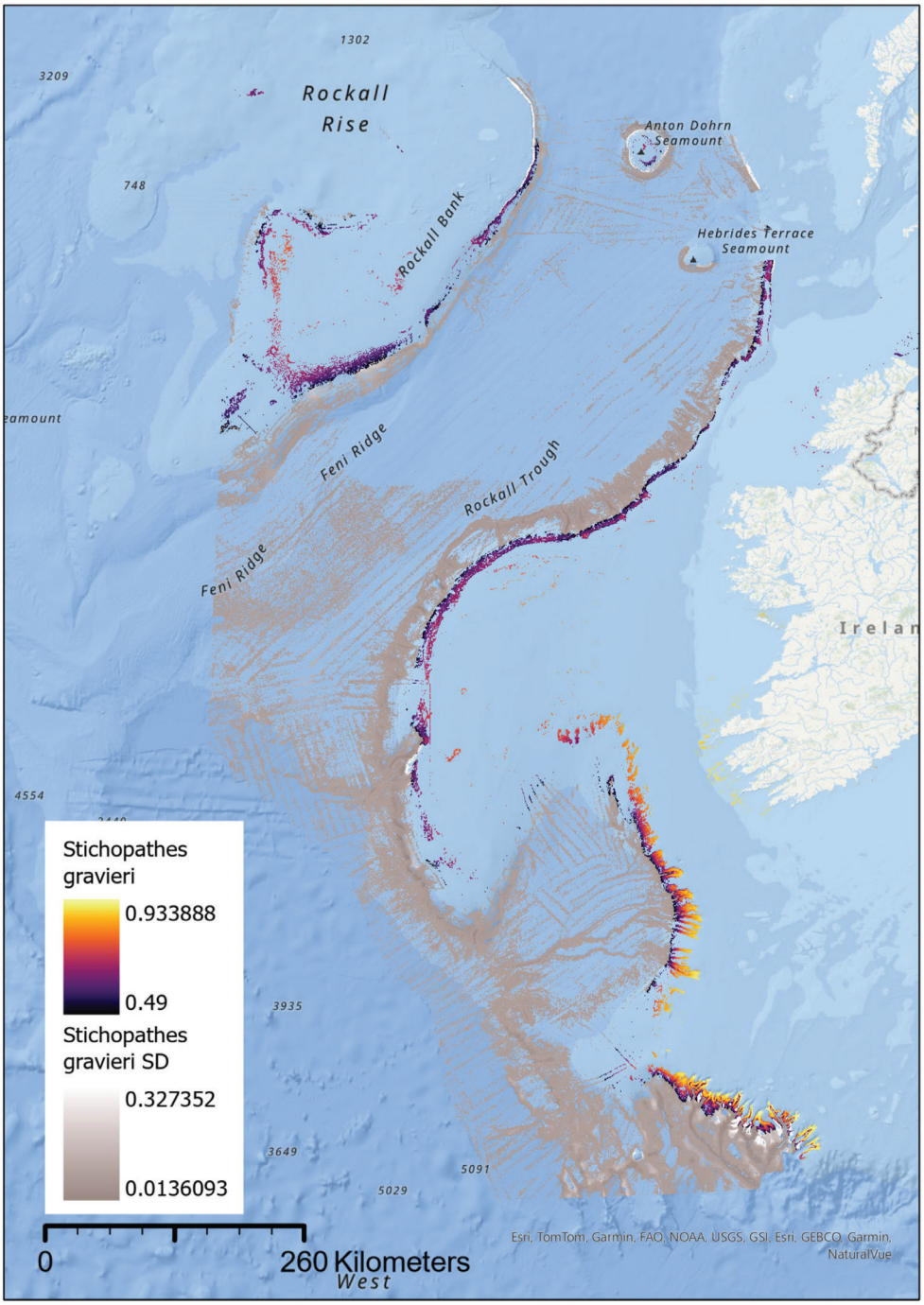

***Fig. S9.7**:* Likelihood of presence and standard deviation of *Stichopathes gravieri*, when modelled with MaxEnt using parsimonious backward stepwise variable selection.

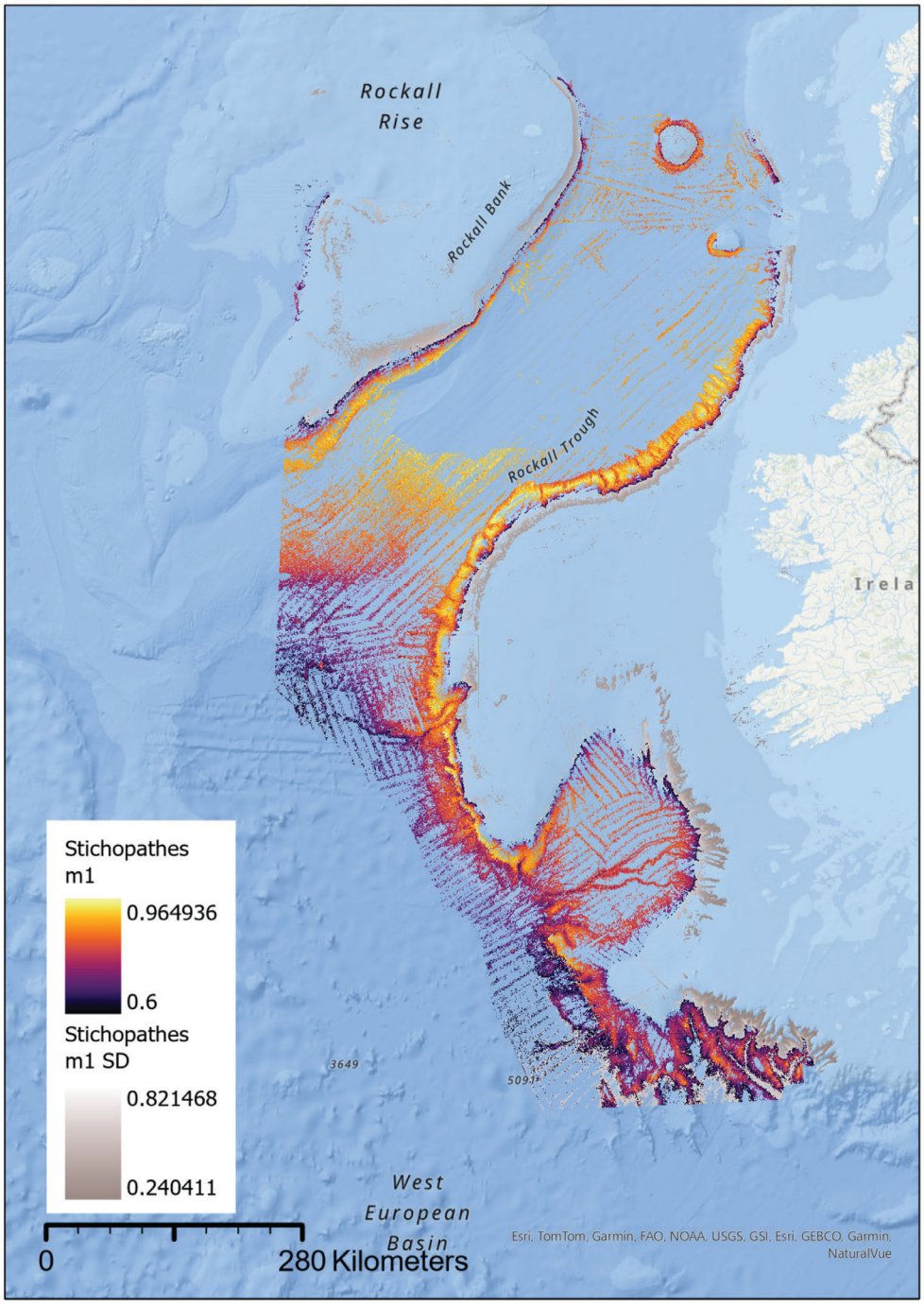

***Fig. S9.8**:* Likelihood of presence and standard deviation of *Stichopathes* m1, when modelled with MaxEnt using parsimonious backward stepwise variable selection.

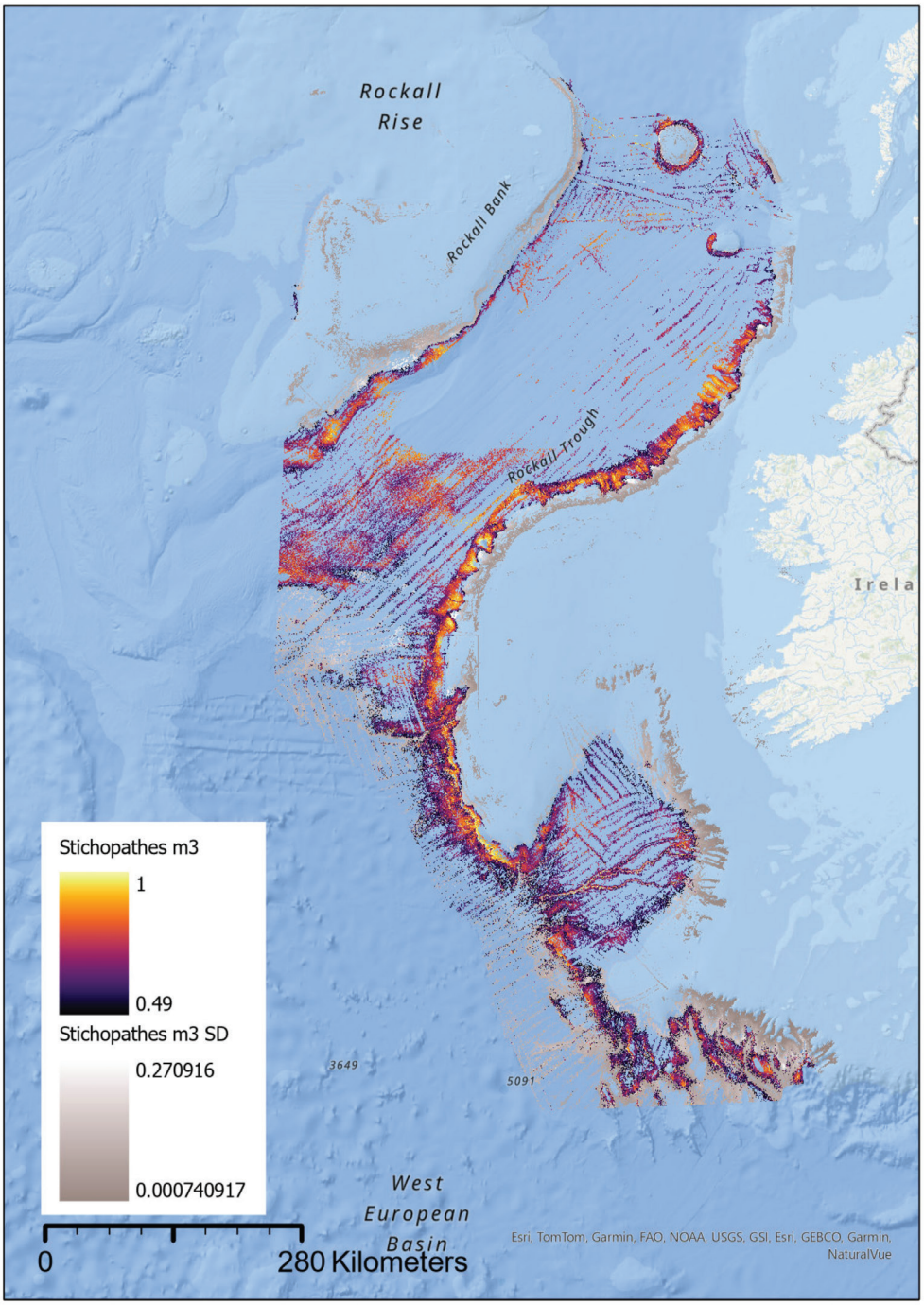

***Fig. S9.9**:* Likelihood of presence and standard deviation of *Stichopathes* m3, when modelled with MaxEnt using parsimonious backward stepwise variable selection.

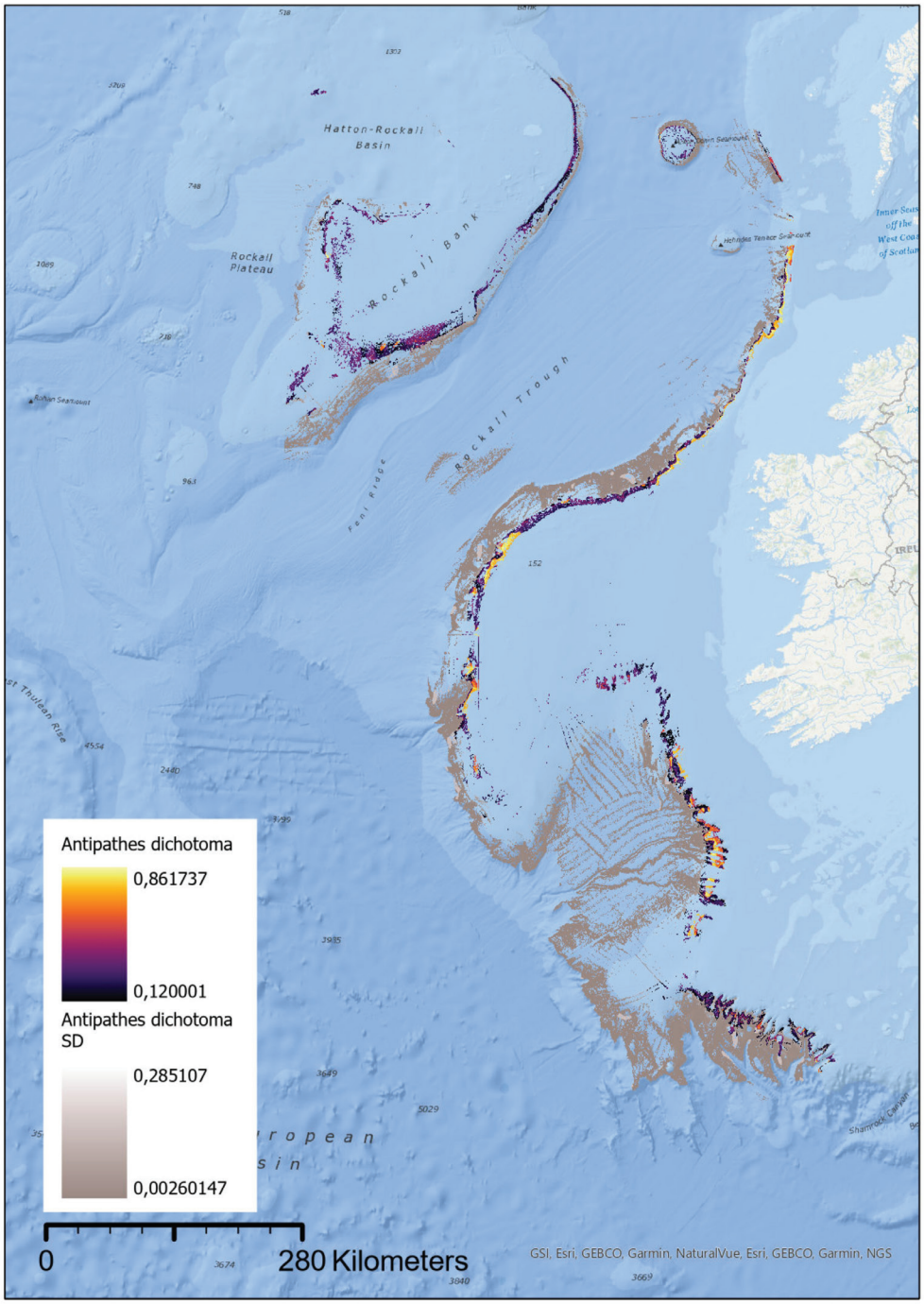

Fig. S10.1*:* Likelihood of presence and standard deviation of *Antipathes dichotoma*, when modelled with GBM using all the available predictors.

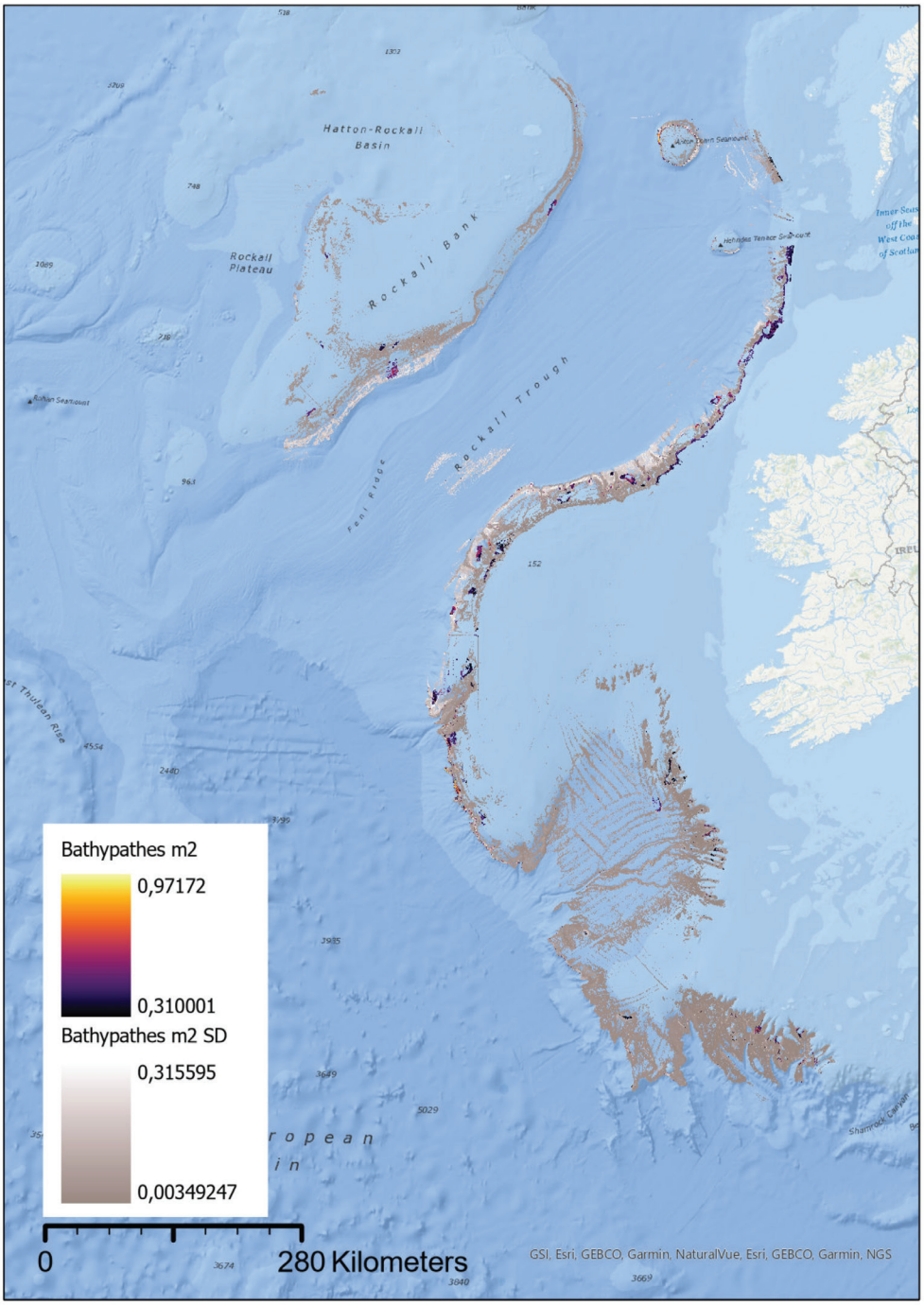

***Fig. S10.2**:* Likelihood of presence and standard deviation of *Bathypathes* m2, when modelled with GBM using all the available predictors.

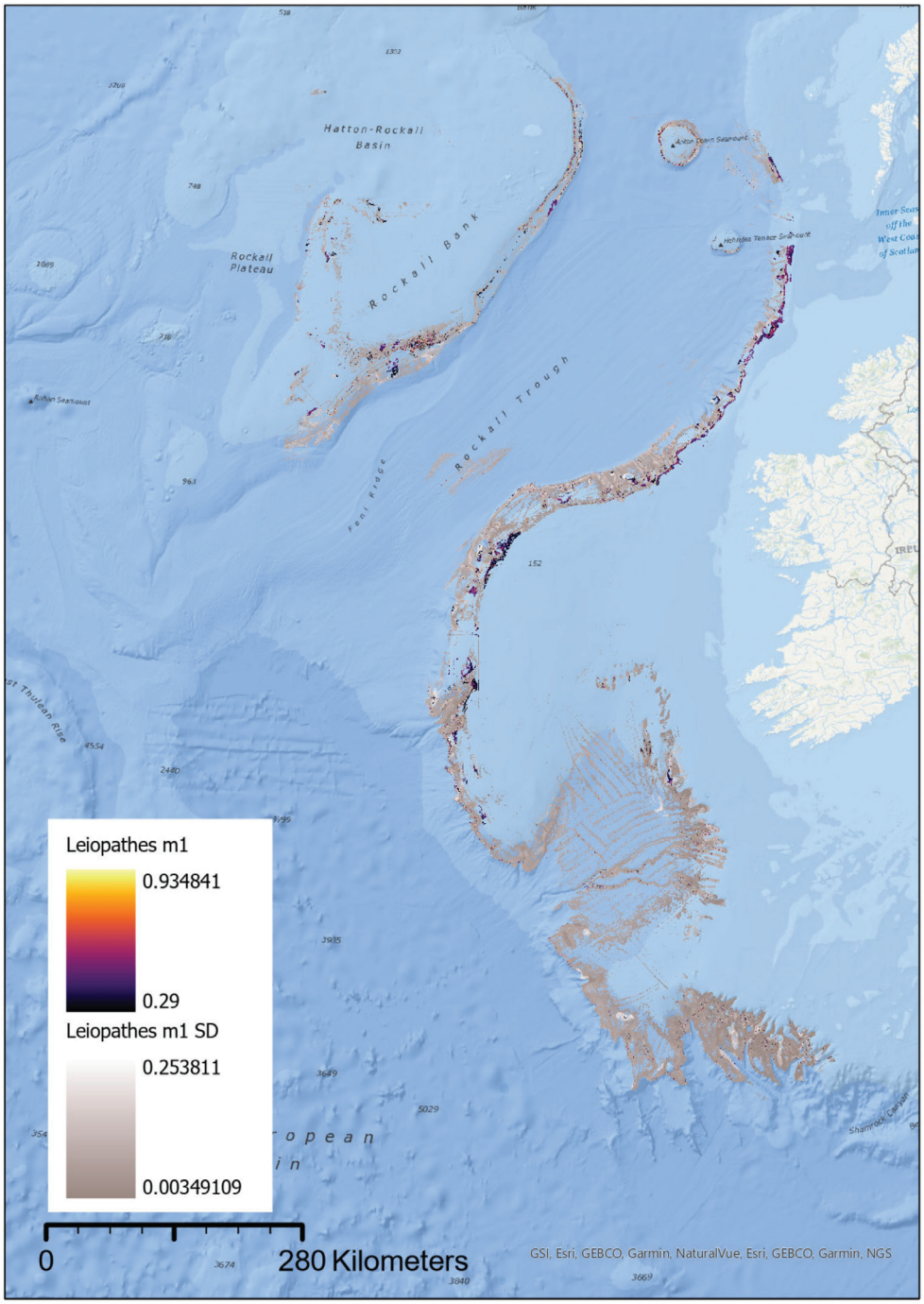

Fig. S10.3*:* Likelihood of presence and standard deviation of *Leiopathes* m1, when modelled with GBM using all the available predictors.

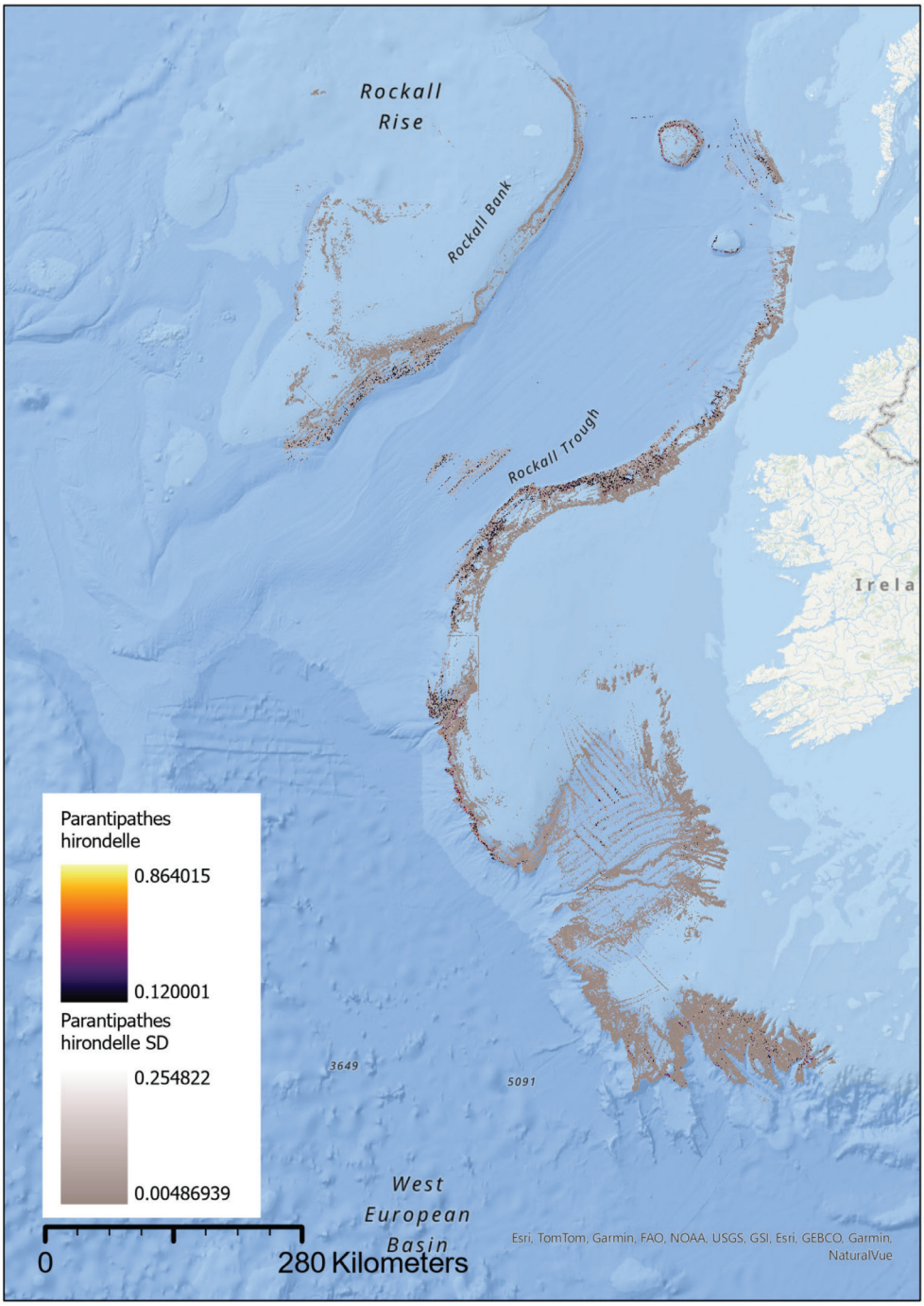

Fig. S10.4*:* Likelihood of presence and standard deviation of *Parantipathes hirondelle*, when modelled with GBM using all the available predictors.

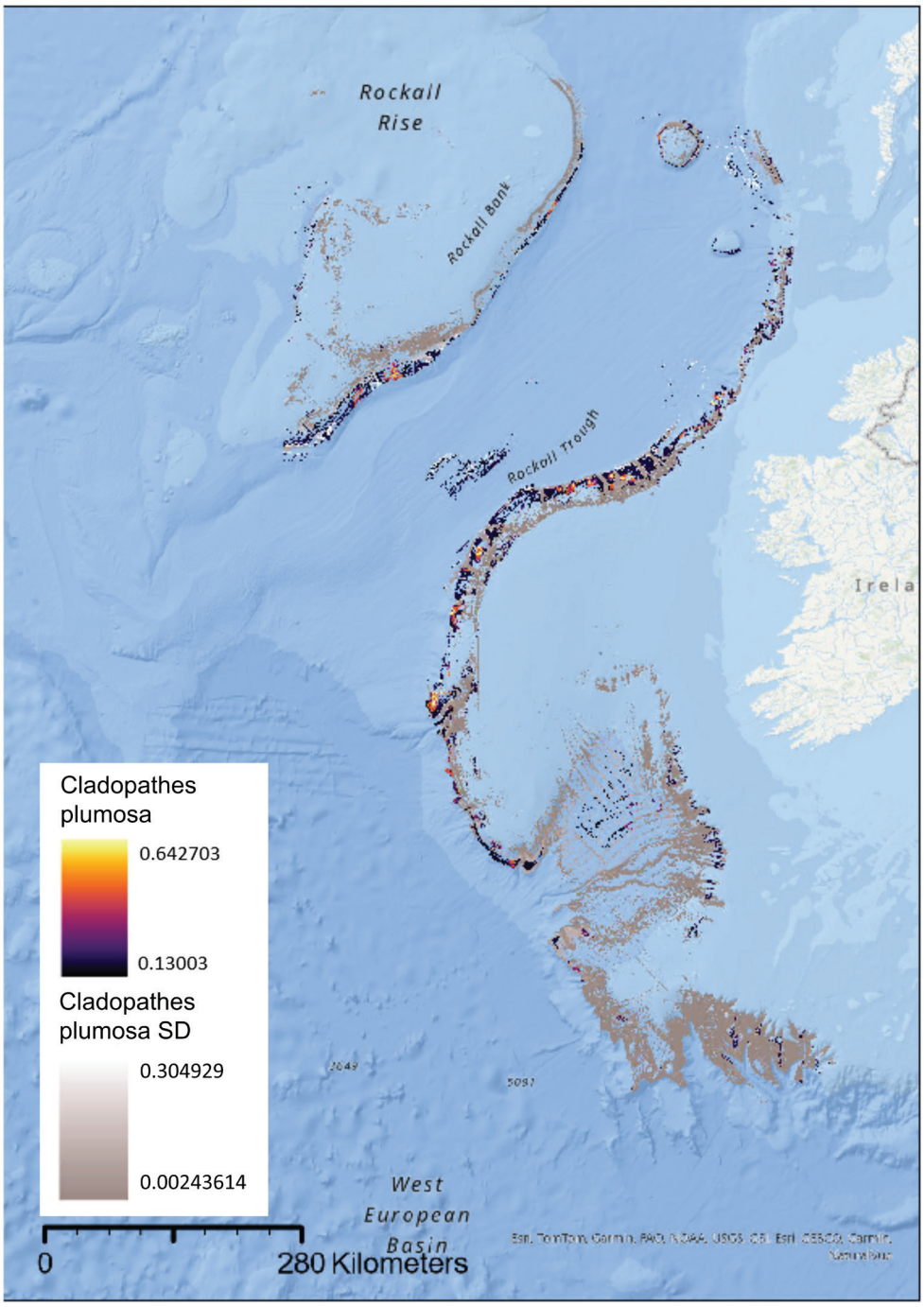

***Fig. S10.5**:* Likelihood of presence and standard deviation of *Cladopathes plumosa*, when modelled with MaxEnt GBM using all the available predictors.

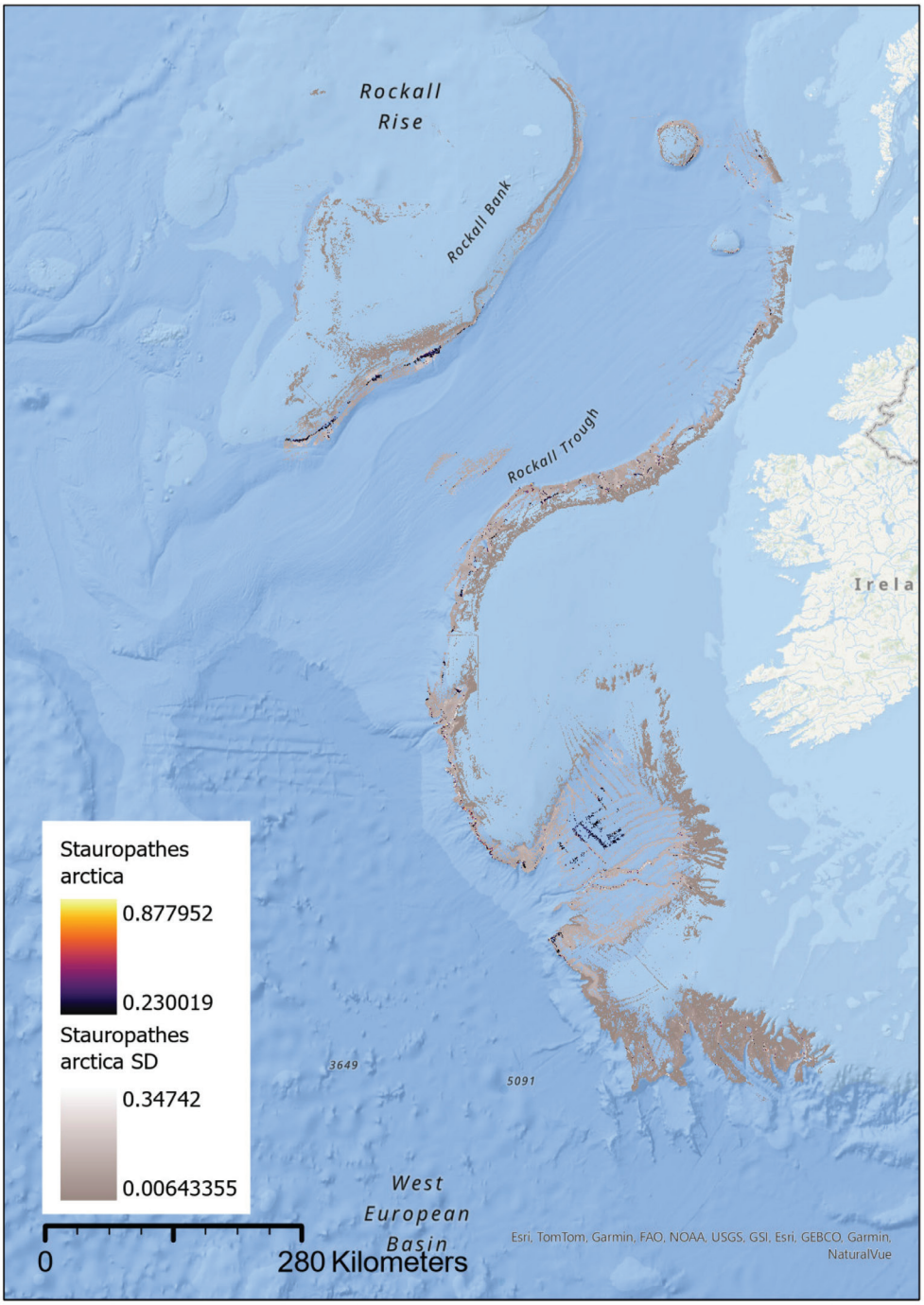

Fig. S10.6: Likelihood of presence and standard deviation of *Stauropathes arctica*, when modelled with GBM using all the available predictors.

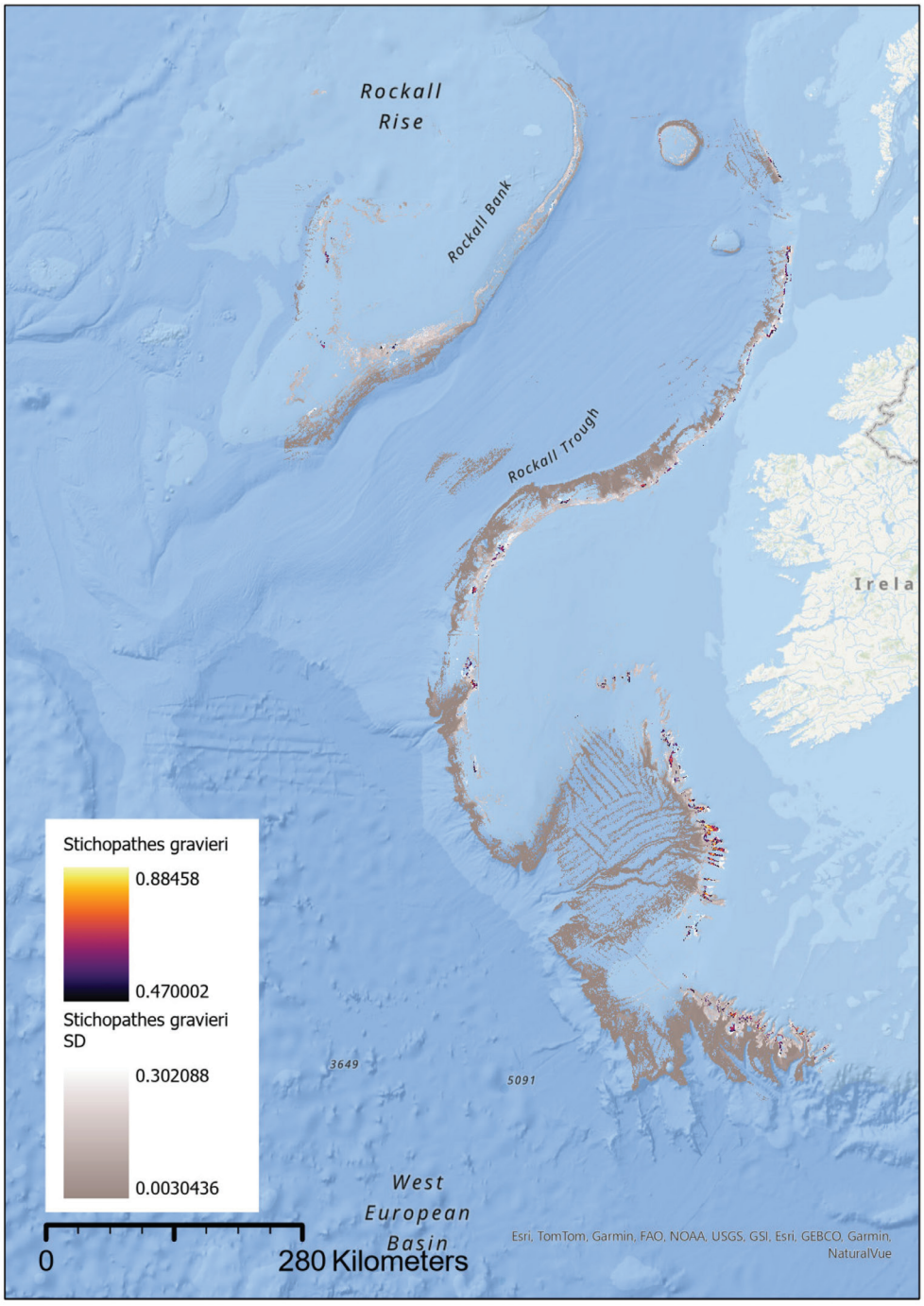

Fig. S10.7*:* Likelihood of presence and standard deviation of *Stichopathes gravieri*, when modelled with GBM using all the available predictors.

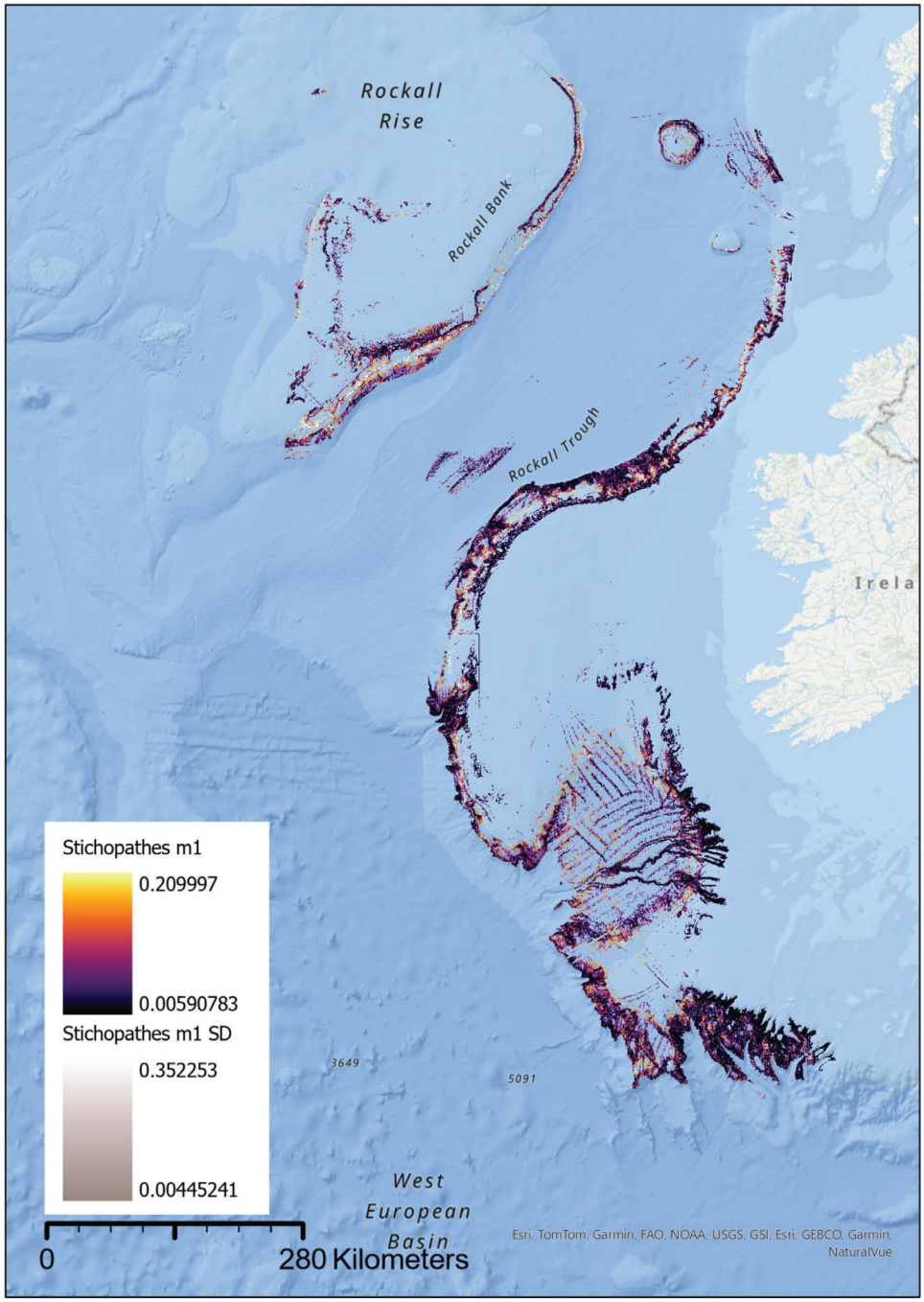

Fig. S10.8*:* Likelihood of presence and standard deviation of *Stichopathes* m1, when modelled with GBM using all the available predictors.

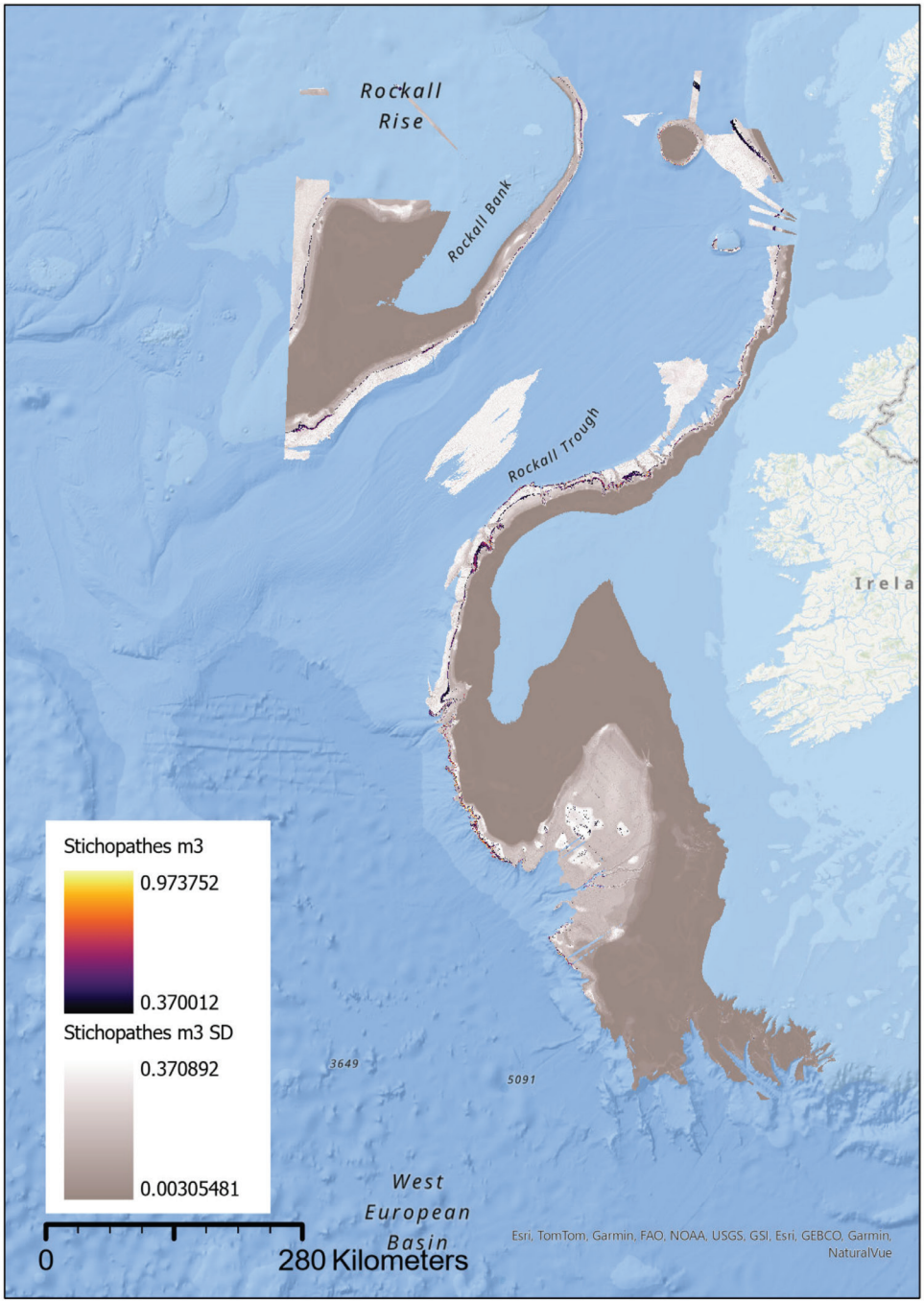

Fig. S10.9*:* Likelihood of presence and standard deviation of *Stichopathes* m3, when modelled with GBM using all the available predictors.

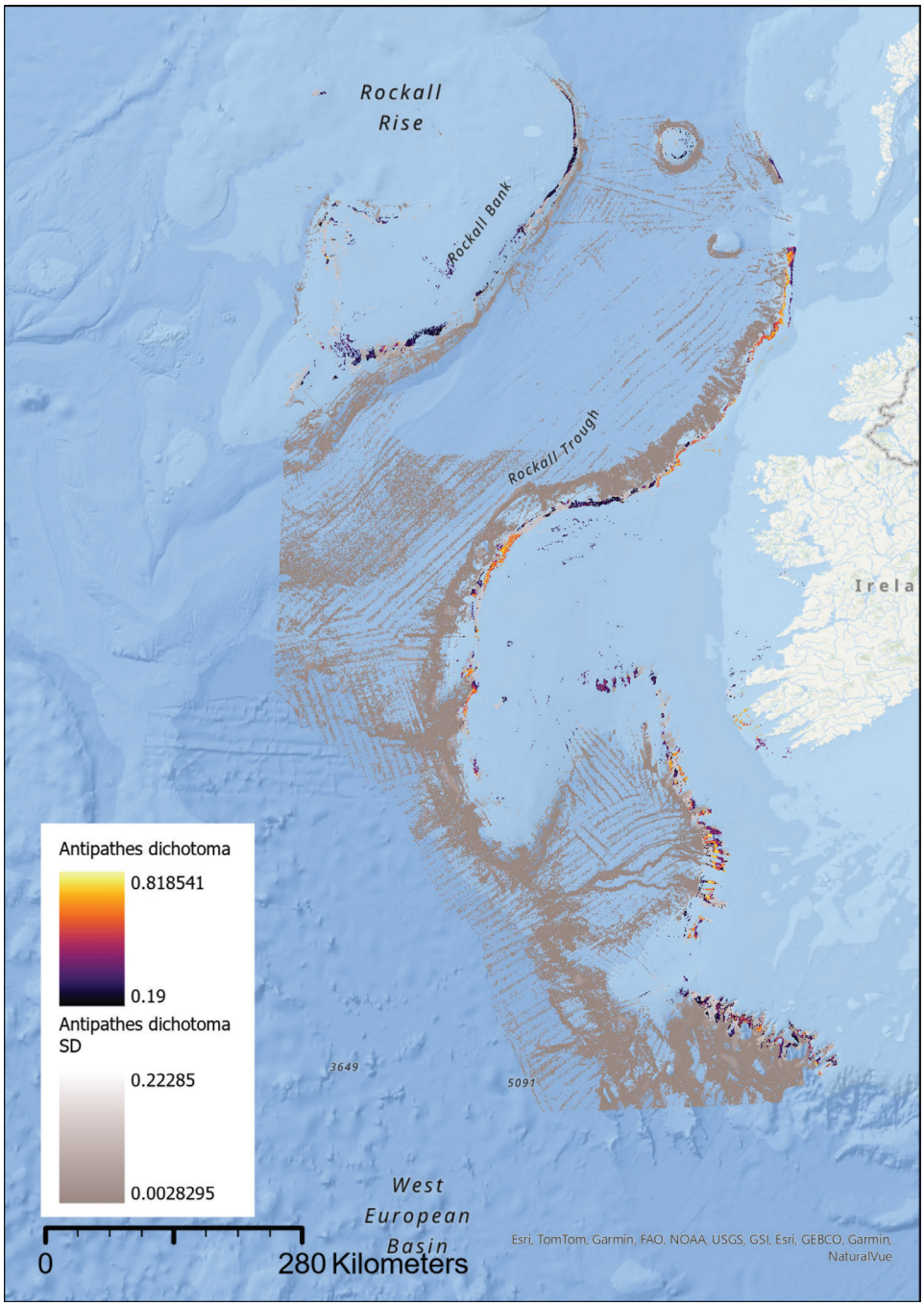

Fig. S11.1*:* Likelihood of presence and standard deviation of *Antipathes dichotoma*, when modelled with GBM using parsimonious backward stepwise variable selection.

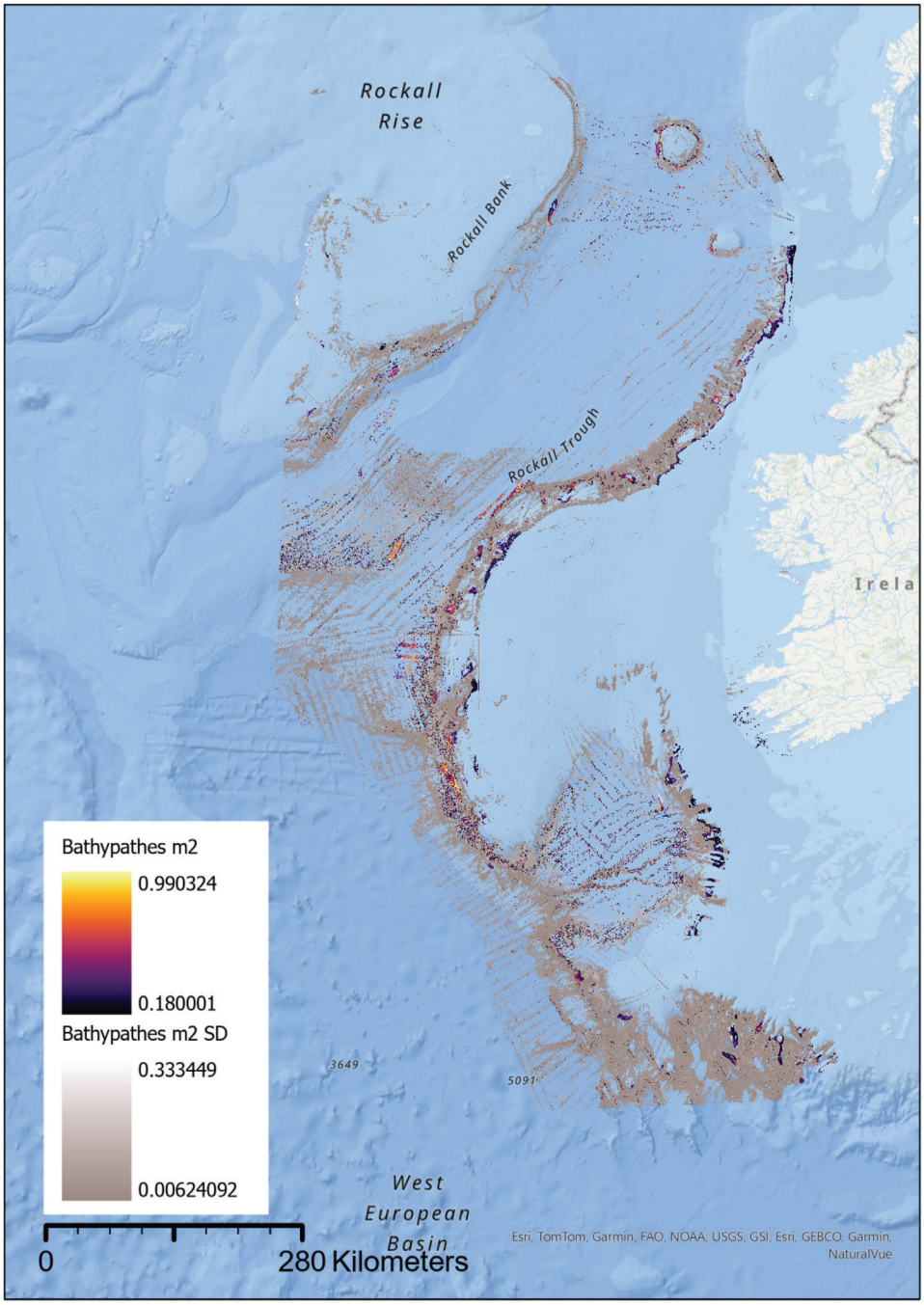

***Fig. S11.2**:* Likelihood of presence and standard deviation of *Bathypathes* m2, when modelled with GBM using parsimonious backward stepwise variable selection.

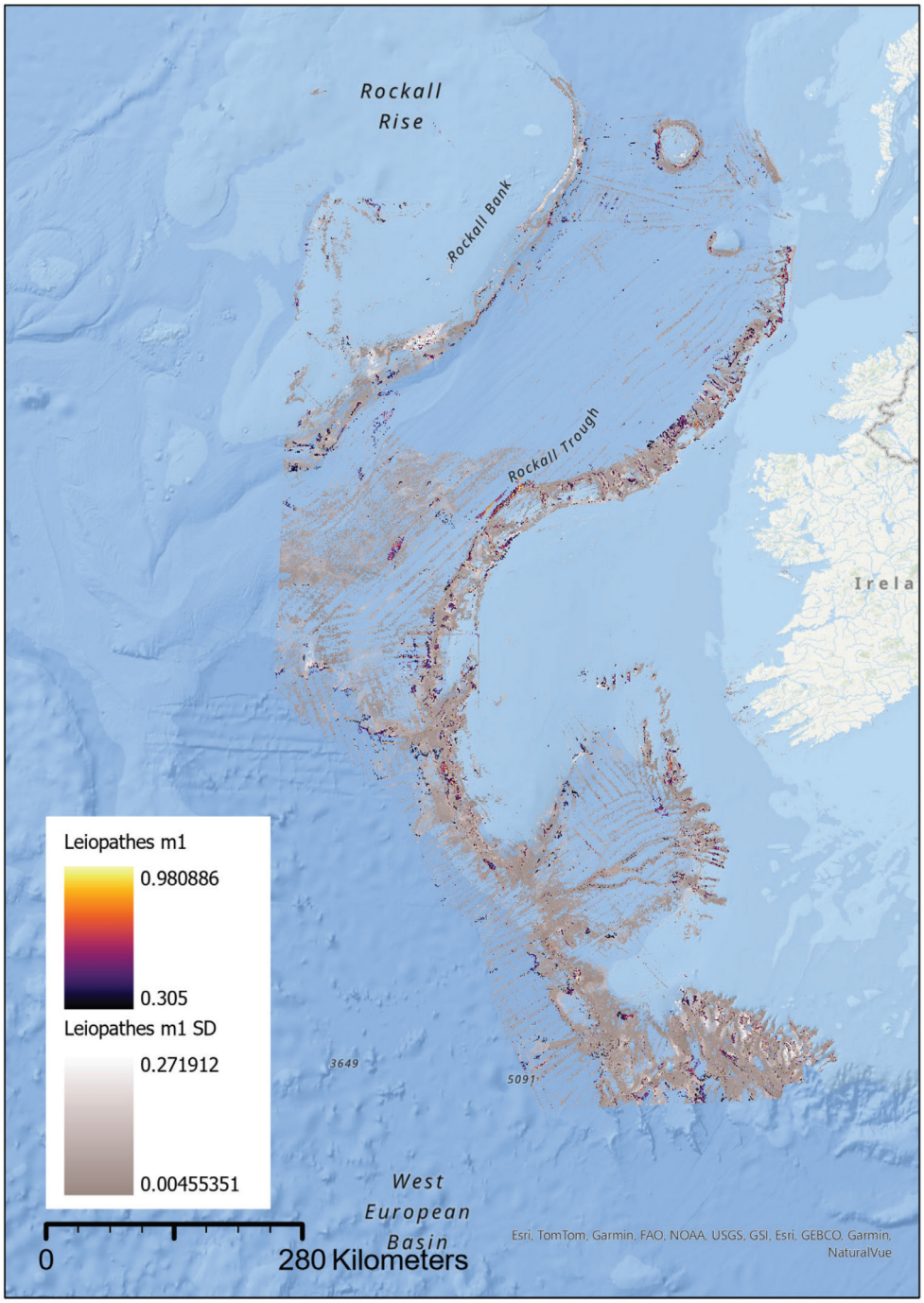

***Fig. S11.3**:* Likelihood of presence and standard deviation of *Leiopathes* m1, when modelled with GBM using parsimonious backward stepwise variable selection.

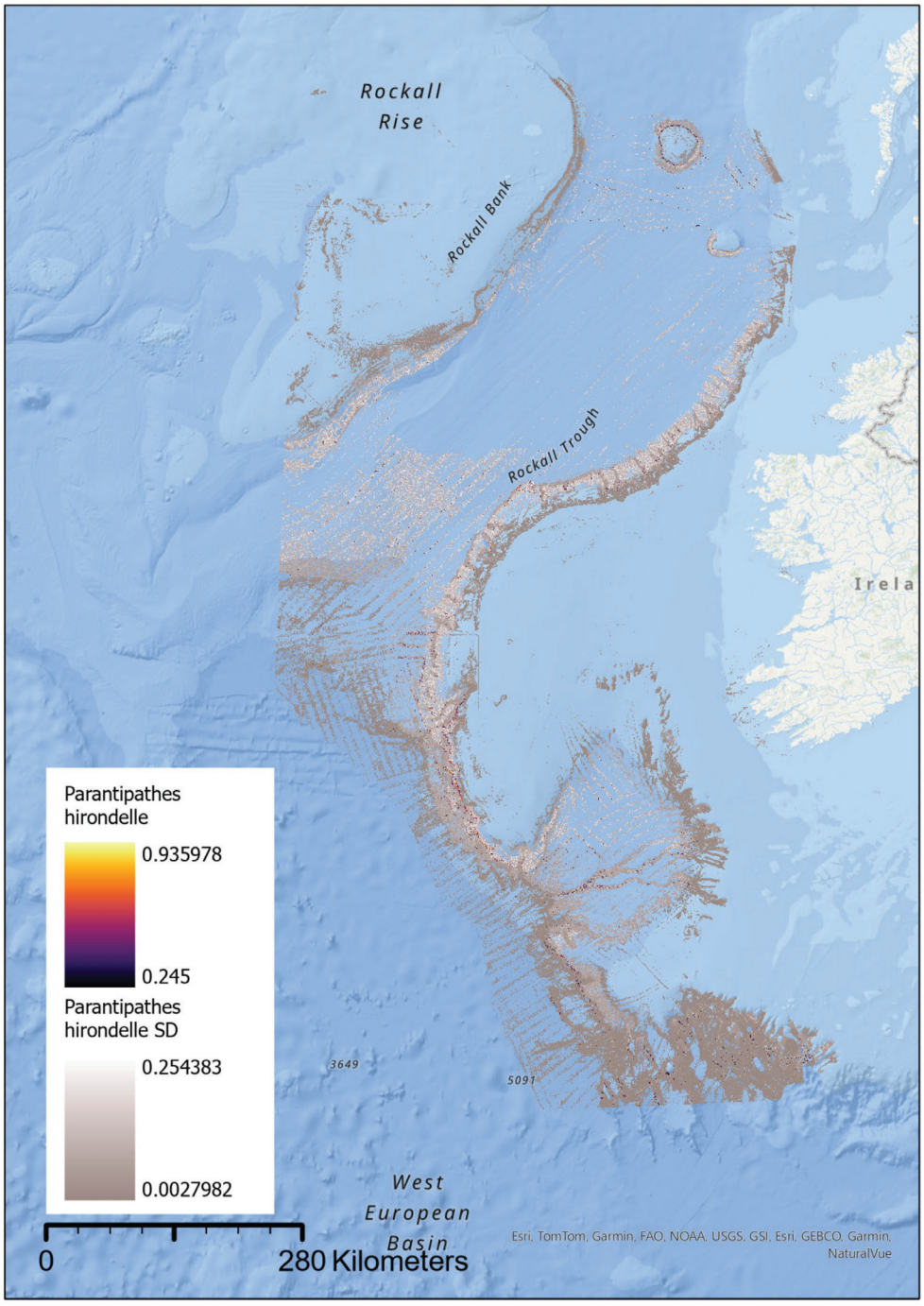

***Fig. S11.4**:* Likelihood of presence and standard deviation of *Parantipathes hirondelle*, when modelled with GBM using parsimonious backward stepwise variable selection.

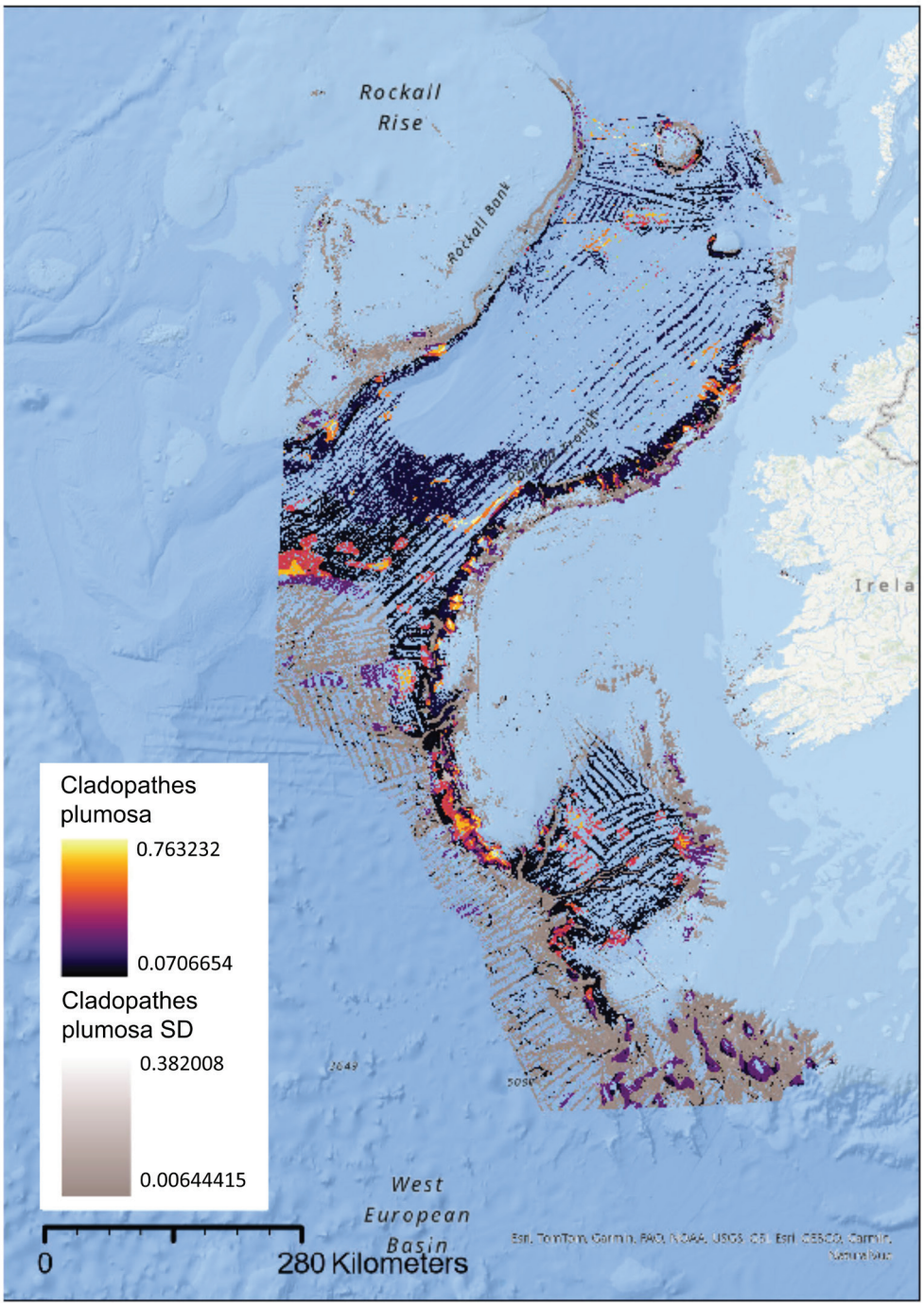

***Fig. S11.5**:* Likelihood of presence and standard deviation of *Cladopathes plumosa*, when modelled with MaxEnt GBM parsimonious backward stepwise variable selection.

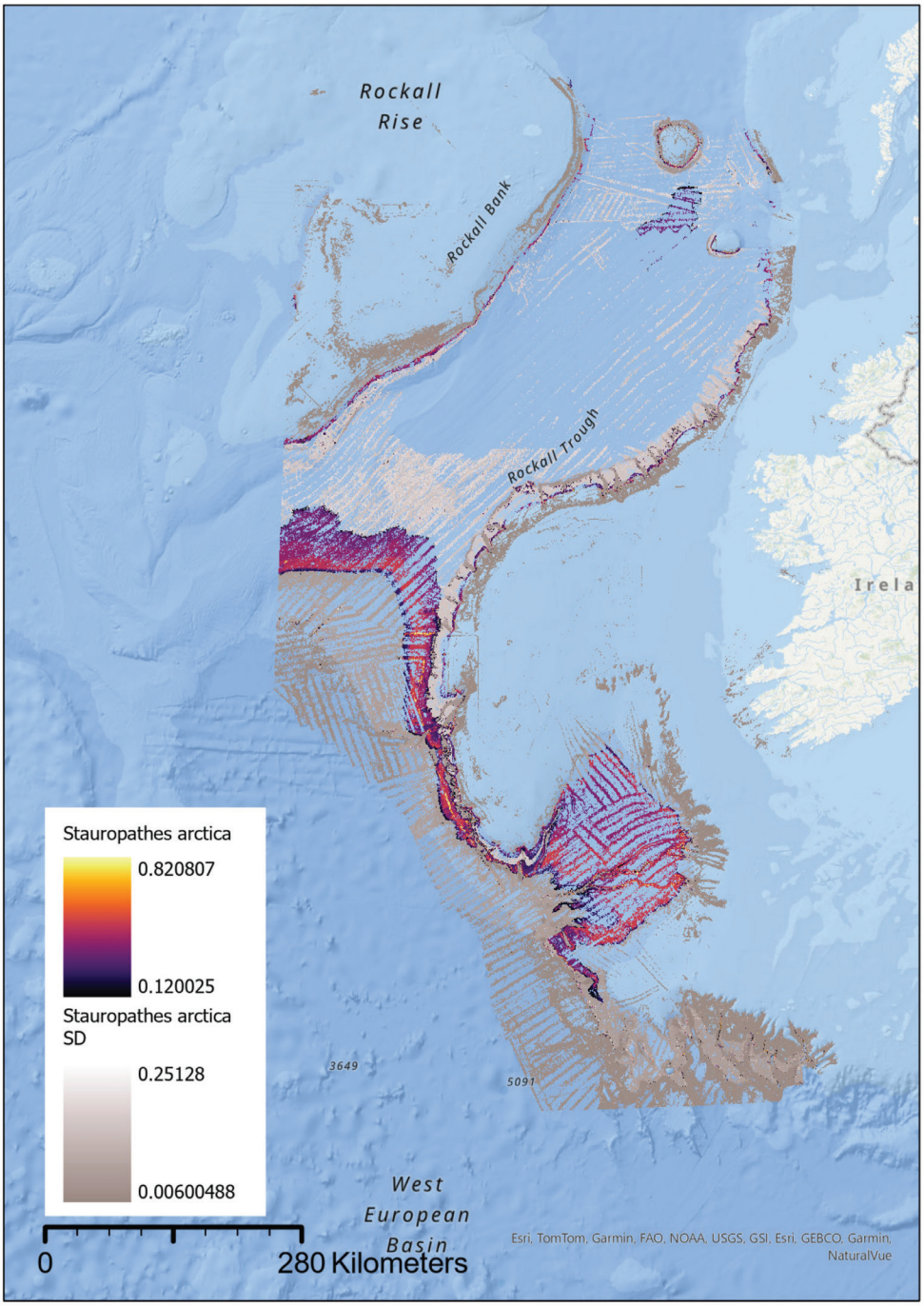

***Fig. S11.6**:* Likelihood of presence and standard deviation of *Stauropathes arctica*, when modelled with GBM using parsimonious backward stepwise variable selection.

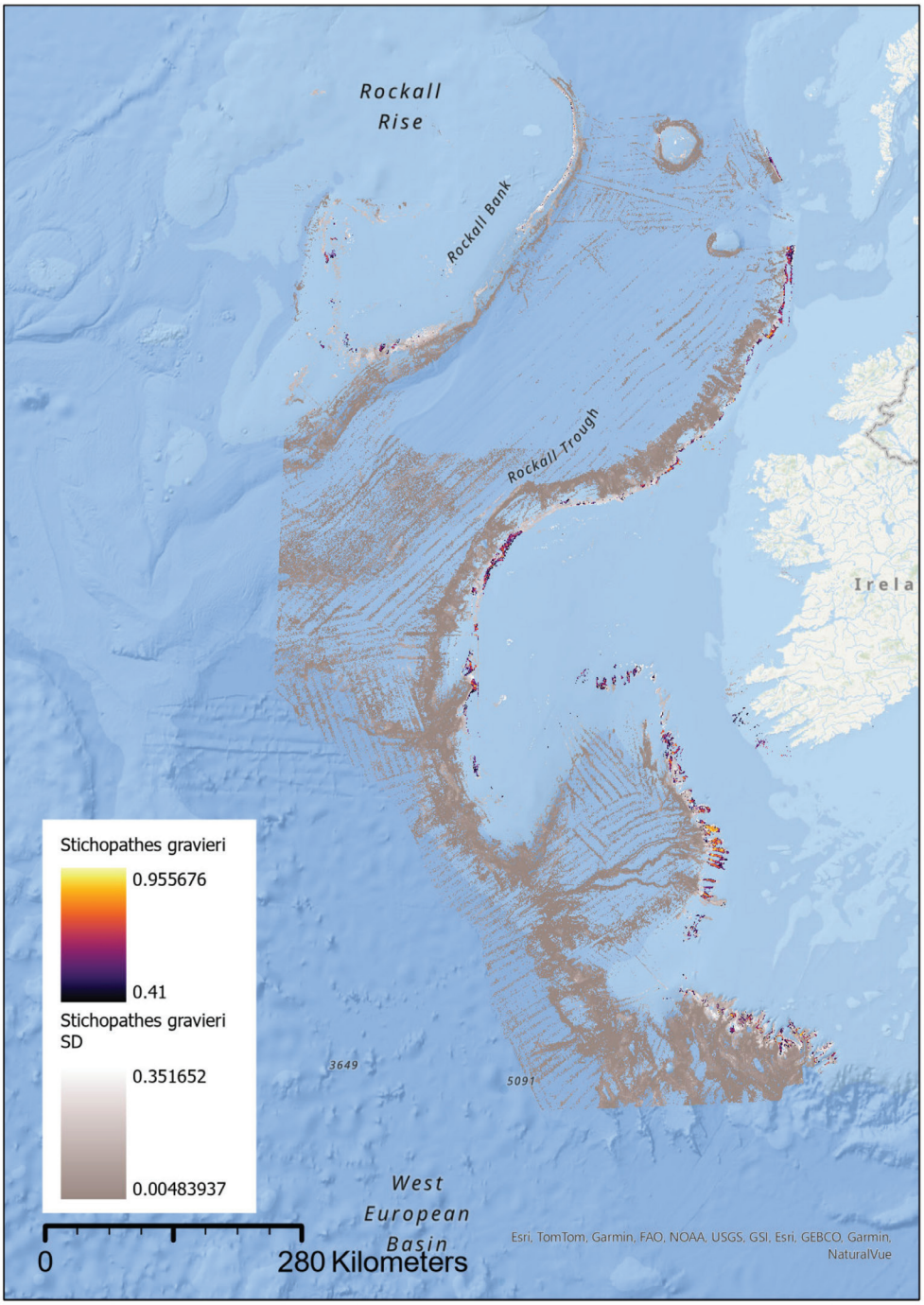

***Fig. S11.7**:* Likelihood of presence and standard deviation of *Stichopathes gravieri*, when modelled with GBM using parsimonious backward stepwise variable selection.

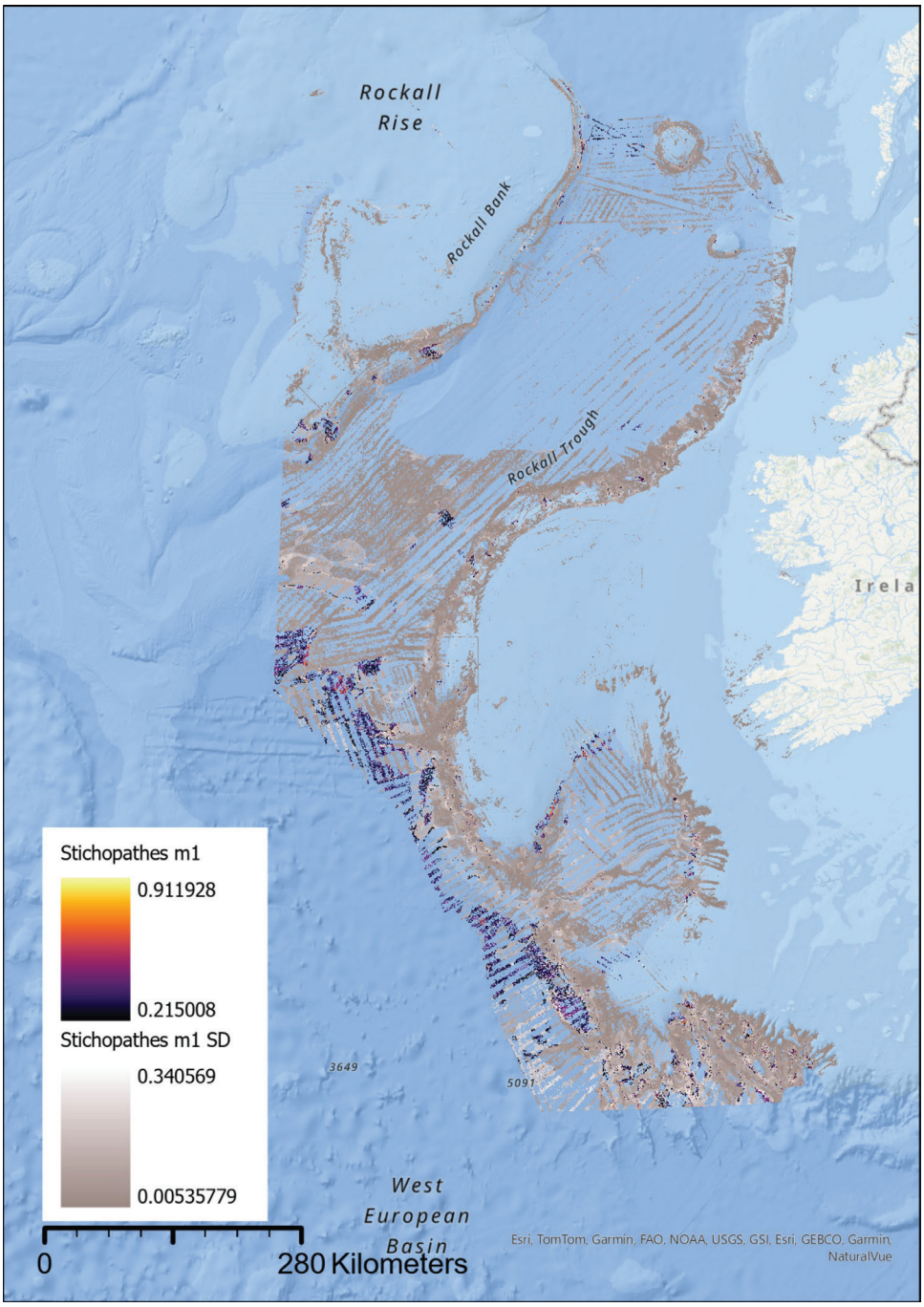

Fig. S11.8*:* Likelihood of presence and standard deviation of *Stichopathes* m1, when modelled with GBM using parsimonious backward stepwise variable selection.

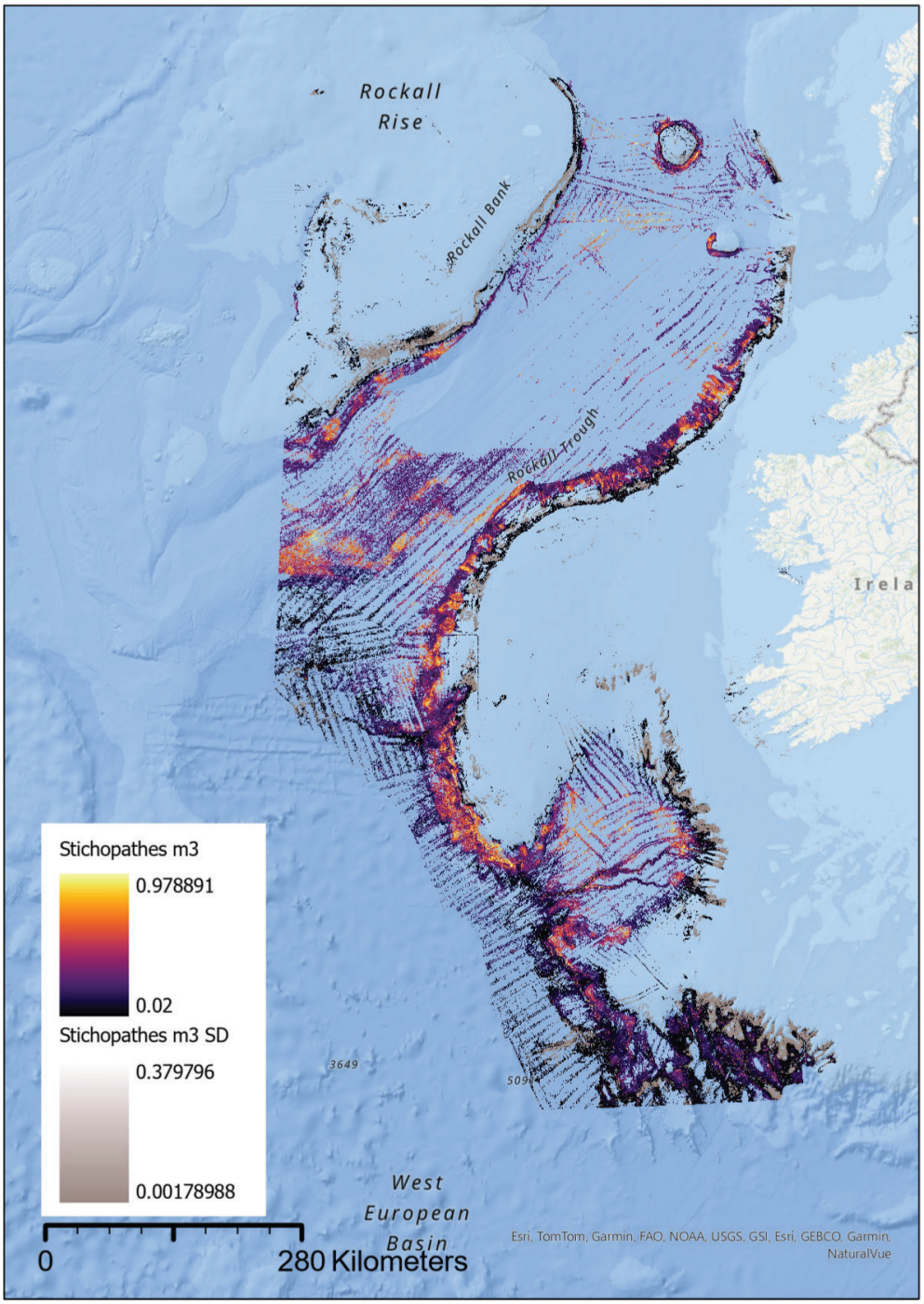

***Fig. S11.9**:* Likelihood of presence and standard deviation of *Stichopathes* m3, when modelled with GBM using parsimonious backward stepwise variable selection.